

**Ocean circulation and climate variability
in the western South Atlantic and eastern South America
during the last deglaciation**

Dissertation zur Erlangung
des Doktorgrades am
Fachbereich Geowissenschaften
der Universität Bremen

vorgelegt von
Cristiano Mazur Chiessi
Bremen, April 2008

Tag des Kolloquiums:

25. Juli 2008

Gutachter:

Prof. Dr. Gerold Wefer

Prof. Dr. Dierk Hebbeln

Prüfer:

Prof. Dr. Katrin Huhn

Dr. André Paul

Table of contents

Abstract	iii
Chapter 1 Introduction	1
1.1 Motivation	1
1.2 Objectives	4
1.3 Outline	5
Chapter 2 Environmental setting	7
2.1 Oceanic circulation	7
2.2 Atmospheric circulation	10
2.3 Geology	12
Chapter 3 Methods	15
3.1 Mg/Ca paleothermometry	15
3.2 Stable isotopes	16
3.3 X-ray fluorescence core scanner	20
3.4 Radiocarbon dating	21
3.5 The University of Victoria Earth System Climate Model	23
Chapter 4 Signature of the Brazil-Malvinas Confluence (Argentine Basin) in the isotopic composition of planktonic foraminifera from surface sediments	25
<i>C. M. Chiessi, S. Ulrich, S. Mulitza, J. Pätzold, G. Wefer</i>	
4.1 Abstract	25
4.2 Introduction	26
4.3 Regional setting	27
4.4 Materials and methods	31
4.5 Results	35
4.6 Discussion	38
4.7 Paleoceanographic implications and conclusions	42
Chapter 5 South Atlantic interocean exchange as the trigger for the Bølling warm event	45
<i>C. M. Chiessi, S. Mulitza, A. Paul, J. Pätzold, J. Groeneveld, G. Wefer</i>	
5.1 Abstract	45
5.2 Introduction	46
5.3 Material and methods	46

5.4	Results and discussion	48
5.5	Conclusions	53
5.6	Supplementary material	55
Chapter 6 Impact of the Atlantic Multidecadal Oscillation in the South American summer monsoon		63
<i>C. M. Chiessi, S. Mulitza, J. Pätzold, G. Wefer</i>		
6.1	Abstract	63
6.2	Introduction	64
6.3	Environmental setting and methods	64
6.4	Results	66
6.5	Discussion	68
6.6	Conclusions	71
6.7	Supplementary material	73
Chapter 7 Final remarks		77
7.1	Summary and conclusions	77
7.2	Future studies	79
Acknowledgments		83
References		85

Abstract

The growing impact of human activities on the climate system adds a new dimension of complexity and urgency to climate change research. Human activities may have the potential to push key components of the climate system past critical states into qualitatively different modes of operation, i.e. to exceed a tipping point. This possibility requires additional efforts from the many branches of climate change research in order to improve the accuracy of climate change projections. The examination of past climate records has proven to be a very useful area of climate change research, allowing, for instance, the verification of outputs from climate models, as well as an evaluation of the range of responses from the climate system to different forcings, the timing of these responses and the feedback mechanisms involved.

This thesis tackles two elements of the climate system whose tipping points are currently considered very critical: the Atlantic meridional overturning circulation (AMOC) and South American precipitation. The major goal of this work is to better understand and work out a detailed reconstruction of ocean circulation and climate variability in the western South Atlantic and eastern South America during the last deglaciation, with special emphasis on abrupt climate change.

Marine sediment samples from the western South Atlantic were used as archives of oceanic and climatic signals. The methods applied included radiocarbon dating of planktic foraminifera, stable isotopes and Mg/Ca ratios of planktic and benthic foraminifera, and Ti intensities in bulk sediment. Exceptionally high sedimentation rates in the study area during the last deglaciation, allowed sub-decadal-scale temporal resolution on the analyses. Additionally, outputs from an Earth system climate model of intermediate-complexity have been used to validate the physical coherence of the suggested mechanisms for paleoceanographic changes.

This investigation first determined how different species of planktic foraminifera record the present-day properties of the upper water column of the western South Atlantic (focused on the Brazil-Malvinas Confluence (BMC)) in their isotopic compositions. For this purpose, the oxygen and carbon isotopic compositions of *Globigerinoides ruber* (pink and white varieties analyzed separately), *Globigerinoides trilobus*, *Globigerina bulloides*, *Globorotalia inflata* and *Globorotalia truncatulinoides* (left- and right-coiling forms analyzed separately) were measured. A latitudinal

transect of 56 surface sediment samples from the continental slope off Brazil, Uruguay and Argentina between 20 and 48°S were used. Lowest oxygen isotopes values were found in *G. ruber* (pink), followed by *G. ruber* (white) and *G. trilobus* reflecting the highly stratified near surface water conditions north of the BMC. *Globigerina bulloides* was present mainly south of the BMC and records subsurface conditions supporting earlier plankton tow studies. *Globorotalia inflata* and *G. truncatulinoides* (left and right) were both available over the whole transect and calcify in the depth level with the steepest temperature change across the BMC. Accordingly, the oxygen isotopic compositions of these species depict a sharp gradient of 2 ‰ at the confluence with remarkably stable values north and south of the BMC. The data show that the oxygen isotopic composition of *G. inflata* and *G. truncatulinoides* (left and right) are the most reliable indicators for the present position of the BMC.

As a second step, changes in the upper water column of the western South Atlantic during the last deglaciation were addressed, and the implications for abrupt climate change were discussed. The high latitudes of the North Atlantic experienced an abrupt temperature increase of 9°C within a couple of decades during the transition from Heinrich event 1 (H1) to the Bølling warm event (at ~14.7 cal kyr BP). Nevertheless, the mechanism responsible for this warming remains uncertain. Records presented in this thesis show that during the transition from H1 to the Bølling, the western South Atlantic experienced a warming of ~6.5°C and an increase in the oxygen isotopic composition of seawater ($\delta^{18}\text{O}_{\text{sw}}$) of 1.2 ‰ at the permanent thermocline. Simultaneously, a warming of ~3.5°C with no significant change in $\delta^{18}\text{O}_{\text{sw}}$ was determined for intermediate depths. Most of the warming can be explained by tilting the South Atlantic east-west isopycnals from a flattened towards a steepened position, associated with a collapsed (H1) and strong (Bølling) AMOC, respectively. However, this zonal seesaw explains an increase of just 0.3 ‰ in permanent thermocline $\delta^{18}\text{O}_{\text{sw}}$. Considering that $\delta^{18}\text{O}_{\text{sw}}$ of the South Atlantic permanent thermocline is strongly influenced by the inflow of salty Indian Ocean upper waters, the data suggest that a strengthening in the Agulhas Leakage took place at the transition from H1 to the Bølling, and that this is responsible for the change in $\delta^{18}\text{O}_{\text{sw}}$ recorded in the western South Atlantic. The temperature anomalies between the “Heinrich-like” and the “Bølling-like” climate states simulated with the University of Victoria Earth System Climate Model were consistent with the proxy-based reconstructions. Taken together, these results highlight the important role played by Indian-Atlantic interocean exchange as the trigger for the resumption of the AMOC and the Bølling warm event.

Finally, the multidecadal variability in precipitation over eastern South America was reconstructed. More specifically, the impact of the Atlantic Multidecadal Oscillation (AMO) on the

South American Summer Monsoon (SASM) was investigated, using marine records of the La Plata River drainage basin (PRDB) discharge. The records are based on stable oxygen isotopic composition of shallow-dwelling planktic foraminifera (controlled by the PRDB plume) and Ti intensity in bulk sediment (controlled by the source of the terrigenous sediments), and cover a period of approximately 4500 years of the last deglaciation. Spectral and wavelet analyses of the records indicate a periodic oscillation of about 60 years in both the extension of the PRDB plume and the source of the terrigenous sediments. The observed oscillation most probably reflects variability in the SASM activity associated to the AMO. During negative (positive) AMO phase, the anomalously warm (cold) South Atlantic would increase (decrease) SACZ activity and displace the main belt of SASM precipitation to the south (north). Amplified (reduced) SACZ activity would increase (decrease) rainfall over the PRDB and the basin's isotopically low discharge into the western South Atlantic, affecting the composition of the upper water column above the core site. The southward (northward) displacement of the SACZ would increase (decrease) rainfall and erosion on the southern Ti-rich half of the PRDB, eventually increasing (decreasing) the Ti content of the terrigenous fraction of the sediments delivered to the core site. The results point out to a clear impact of the AMO on the SASM.

Chapter 1

Introduction

1.1 Motivation

In recent decades, the attention focused on the science of climate change has increased substantially. Instrumental, historical and proxy climate records from the most diversified archives along with the outputs from climate models of different complexities have been intensively investigated. The examination of past climate records has proven to be a very useful area of climate change research, allowing: (i) the assessment of the impact of climate change on past civilizations; (ii) the verification of outputs from climate models; and (iii) the evaluation of the range of responses from the climate system to different forcings, the timing of these responses and the feedback mechanisms involved. In this context, the unifying goal between past climate reconstructions and climate modeling efforts lies on improving our ability to project the impacts of future climate change, an issue of utmost importance to society.

Besides glacial-interglacial mainly astronomically forced climate cycles, the late Quaternary has shown some high-amplitude abrupt climate changes. Previous reviews (e.g. Lockwood, 2001; Alley et al., 2003; Rial et al., 2004) have defined “abrupt climate change” as occurring when the climate system is forced to cross some threshold, triggering a transition to a new state at a rate determined by the climate system itself and faster than the cause. For instance, rapid climate shifts occurred during the transition from the last glaciation to the Holocene (from ~19 to 10 cal kyr BP) and were first described from sites of the Northern Hemisphere (NH) as the Oldest, Older and Younger Dryas. A wide range of records from the terrestrial (e.g. Wohlfarth, 1996; Brauer et al., 1999; Renssen and Isarin, 2001), polar (e.g. Dansgaard et al., 1993; NGRIP members, 2004; Rasmussen et al., 2006), and marine realms (e.g. Boyle and Keigwin, 1987; Bond et al., 1993; Sarnthein et al., 2001) reflect the climate evolution in the NH mid- and high-latitudes during the last deglaciation. In the most widely accepted view, the primary trigger for abrupt changes on a global scale is located in the NH. Sudden increases in deglacial freshwater influx from melting of the NH continental ice-sheets, and as a consequence the drastic reduction of North Atlantic Deep Water (NADW) formation, disrupted the Atlantic meridional overturning circulation (AMOC) (Fig. 1.1) (e.g. Broecker et al., 1988; Rahmstorf, 2002; McManus et al., 2004). After the last glacial maximum, a first short-lived meltwater pulse around 19 cal kyr BP delivered to the

Nordic Seas (Clark et al., 1996) and subsequent melting of icebergs from the Laurentide ice sheet (Heinrich event 1 (H1)) (Bond et al., 1992) generated a dramatic quasi-cessation of the AMOC (McManus et al., 2004). The AMOC and ultimately NADW formation has been described as a sensitive part of the global ocean circulation, and consequently of global climate. By decreasing the AMOC strength, the transport of heat and salt towards the NH also diminishes, leading to the accumulation of heat and salt in the Southern Hemisphere (SH), a process described as the bipolar seesaw (e.g. Manabe and Stouffer, 1988; Crowley, 1992; Broecker, 1998). The synchronization of ice-cores from Antarctica and Greenland provides further evidence for the anti-correlated pattern of temperature changes between both hemispheres (e.g. Blunier and Brook, 2001; EPICA Community Members, 2006).

In the western tropical Atlantic Ocean and over eastern South America, the events of AMOC disruption during the last deglaciation were expressed with a warming of surface and intermediate depth waters (Rühlemann et al., 1999; Rühlemann et al., 2004), an increase in sea surface salinity (Weldeab et al., 2006), a strong positive precipitation anomaly over NE Brazil (Arz et al., 1998; Behling et al., 2000; Jennerjahn et al., 2004; Wang et al., 2004; Jaeschke et al., 2007), and an increased inflow of Amazon moisture towards South American subtropical latitudes (Fig. 1.1) (Cruz et al., 2005; Wang et al., 2007).

While some modeling studies suggest that the interhemispheric seesaw pattern is largely induced by changes in AMOC strength triggered by variability in NH salinity (e.g. Manabe and Stouffer, 1988; Rahmstorf, 2002), other models propose that changes in temperature, sea ice extent and/or salinity around Antarctica could influence the strength of the AMOC (e.g. Knorr and Lohmann, 2003; Shin et al., 2003), and therefore trigger abrupt events in the North Atlantic realm as well. These different results show that the ultimate mechanism behind abrupt climate variability and the seesaw pattern still remains uncertain and high-resolution paleoceanographic and paleoclimatic records from the SH can potentially contribute in solving some of the open questions, especially considering the lack of SH records.

The growing impact of human activities on the climate system adds a new dimension of complexity and urgency to climate change research, and requires additional efforts in order to make more accurate projections of future climate change. Human activities may have the potential to push key components of the climate system past critical states into qualitatively different modes of operation, i.e. to exceed a tipping point (e.g. Hansen et al., 2007; Lenton et al., 2008). For instance, high-complexity climate models and field observations have shown that a significant

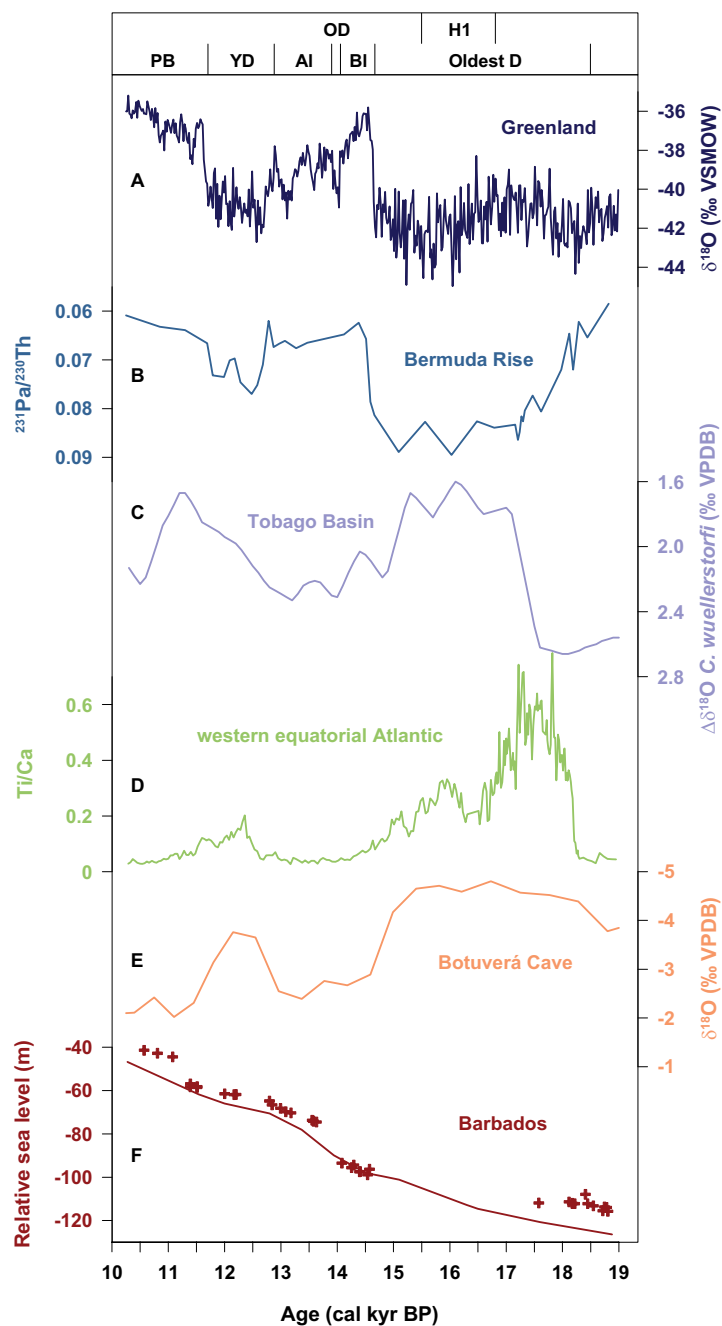


Figure 1.1. Last deglaciation paleoclimatic and paleoceanographic records from the Atlantic Ocean and adjacent continents. A: North Greenland Ice Core Project (NGRIP) $\delta^{18}\text{O}$ (NGRIP members, 2004) plotted versus the Greenland Ice Core Chronology 2005 (GICC05) (Rasmussen et al., 2006). B: GGC5 $^{231}\text{Pa}/^{230}\text{Th}$ (McManus et al., 2004). C: M35003-4 continental ice volume corrected benthic foraminiferal $\delta^{18}\text{O}$ (Hüls, 2000; Rühlemann et al., 2004), calculated by subtracting the global $\delta^{18}\text{O}$ ice effect (Fairbanks, 1989; Fairbanks et al., 1992) from foraminiferal $\delta^{18}\text{O}$. D: GeoB3910-2 Ti/Ca ratios in bulk sediment (Jaeschke et al., 2007). E: Botuverá Cave BT2 stalagmite $\delta^{18}\text{O}$ (Cruz et al., 2005). F: Barbados relative sea level exclusively based on *Acropora palmata* U/Th ages and depths corrected for a rate of vertical tectonic uplift of 0.34 mm yr^{-1} (crosses) (Peltier and Fairbanks, 2006), and an updated version of the sea level curve of Lambeck and Chappell (2001) (curve). Periods are labeled as follows (Vidal et al., 1997; Rasmussen et al., 2006): AI-Allerød, BI-Bølling, H1-Heinrich event 1, OD-Older Dryas, Oldest D-Oldest Dryas, PB-Preboreal, YD-Younger Dryas. VPDB-Vienna Pee Dee belemnite. VSMOW-Vienna standard mean ocean water.

reduction on the AMOC is very likely to occur in the near future, due to anthropogenic increases in greenhouse gases, global warming and intensification of the hydrological cycle (e.g. Cubasch et al., 2001; Bryden et al., 2005; Meehl et al., 2007). However, model results and the sparse field observations bring along a considerable degree of uncertainty that would require further evidence to be additionally relied upon (e.g. Cunningham et al., 2007; Randall et al., 2007). The fidelity of climate models can be evaluated if their ability to reproduce past abrupt climate change could be proved (e.g. Clark et al., 2002; Shukla et al., 2006; Randall et al., 2007). Thus, the comprehensive understanding of the mechanisms involved in past abrupt climate change is a key task to improve our ability to accurately project the impacts of future climate change.

1.2 Objectives

This thesis tackles two elements of the climate system whose tipping points are currently considered very critical: the AMOC and South American precipitation. The major goal of this work is to better understand and work out a detailed reconstruction of ocean circulation and climate variability in the western South Atlantic and eastern South America during the last deglaciation, with special emphasis on abrupt climate change.

To accomplish this issue, four central topics were addressed:

- 1) The establishment of the present-day signature of the western South Atlantic upper water column in the isotopic composition of planktic foraminifera from surface sediments;
- 2) The decadal-scale reconstruction of deglacial changes in central and intermediate water masses of the western South Atlantic based on isotopic and trace element composition of planktic and benthic foraminifera;
- 3) The sub-decadal-scale reconstruction of deglacial fluctuations in the climate of eastern South America based on isotopic composition of planktic foraminifera and bulk sediment geochemistry;
- 4) The validation of the physical coherence of the mechanisms suggested herein for paleoceanographic changes with results of an Earth system climate model of intermediate complexity.

1.3 Outline

The main part of this thesis is divided into three manuscripts, which have been published, are under review or will soon be submitted to peer-reviewed international scientific journals.

The first manuscript (Chapter 4) - *Signature of the Brazil-Malvinas Confluence (Argentine Basin) in the isotopic composition of planktonic foraminifera from surface sediments* - aims to determine how different species of planktonic foraminifera record the present-day western South Atlantic upper water column properties in their isotopic composition. For this purpose, a set of 56 surface samples from the continental slope off Brazil, Uruguay and Argentina regularly distributed between 20 and 48°S was selected. The results presented in the first manuscript are of key importance to the rest of the thesis because they allow the accurate identification of the position of the Brazil-Malvinas Confluence (BMC) in the sedimentary record. The BMC is one of the major oceanographic frontal zones in the western South Atlantic. Paleoceanographic reconstructions in areas close to frontal zones, as the one reported in the second manuscript, should unequivocally distinguish between frontal zone migration and water mass properties change. Although these are triggered by completely different mechanisms, both processes could generate a similar signal in the sedimentary record.

In the second manuscript (Chapter 5), *South Atlantic interocean exchange as the trigger for the Bølling warm event*, a high temporal resolution reconstruction of deglacial changes in the upper water column of the western South Atlantic is presented. The reconstruction is based on paired $\delta^{18}\text{O}$ and Mg/Ca data from planktonic and benthic foraminifera from a sediment core raised in the upper slope off southern Brazil. During the last deglaciation, the core site registered high sedimentation rates ($\sim 70 \text{ cm kyr}^{-1}$) that allowed an unprecedented decadal-scale reconstruction of upper water column changes. The cored site is located in a sensitive region of the South Atlantic (three dimensionally in space), where abrupt changes in interocean exchange between the South Atlantic and both neighboring Pacific and Indian Oceans can be recorded. The high temporal resolution and nature of the record enabled a detailed discussion of fundamental processes related to the variability in AMOC strength. Together with changes in insolation, global sea level and greenhouse gases concentration, the variability in AMOC strength is one of the outstanding factors that shaped the last deglaciation. Furthermore, outputs from an Earth system climate model of intermediate complexity were used to verify the adherence of the suggested mechanism for the observed paleoceanographic changes.

The third manuscript (Chapter 6) - *Impact of the Atlantic Multidecadal Oscillation in the South American summer monsoon* - addresses the deglacial fluctuations in climate of eastern South America. Here, the focus was on precipitation changes. Planktic foraminifera $\delta^{18}\text{O}$ and bulk sediment geochemistry from a sediment core raised under the influence of the freshwater plume from the second largest drainage basin in South America are presented. Again, high sedimentation rates which were characteristic of the cored site during the last deglaciation allowed a sub-decadal-scale reconstruction. The results provided insights into high-frequency tropical and subtropical South American precipitation variability under boundary conditions different from the present. Studies of high-frequency precipitation variability are of topical interest as it has been suggested that global warming may significantly interfere on precipitation patterns worldwide.

Additionally to the results presented in the three manuscripts, a significant amount of measurements (e.g. Mg/Ca ratios and stable isotopic compositions of planktic and benthic foraminifera from additional sediment cores) were performed during this thesis. These additional measurements address scientific questions that go beyond the central objectives of this thesis. Therefore, they are not included here. However, considering their topical interest, a brief overview of the potential of these additional measurements is outlined in Chapter 7.

Chapter 2

Environmental setting

2.1 Oceanic circulation

The study area encompasses the western South Atlantic Ocean, and is bathymetrically represented by the western Argentine Basin in the south and the southwestern Brazil Basin in the north. Both basins are separated by the Santos Plateau and the Rio Grande Rise.

The Brazil Current (BC) and the Malvinas Current (MC), together with the Brazil-Malvinas Confluence (BMC), dominate the upper-level circulation in the study area (Fig. 2.1) (Peterson and Stramma, 1991; Stramma and England, 1999). The southward-flowing warm, saline and nutrient-depleted BC originates near 10°S, where the South Equatorial Current (SEC) bifurcates. The BC is characterized as a weak western boundary current carrying subtropical water masses. At 38°S it encounters the MC, which originates as a branch of the Antarctic Circumpolar Current east of the Drake Passage and transports cold, fresh and nutrient-rich subantarctic water masses northward along the Argentinean continental shelf. The MC is assumed to be a strong current with significant bottom flow (Peterson et al., 1996). After having come into contact, the BC and the MC turn southeastward and flow offshore forming the SAC and contributing to the Antarctic Circumpolar Current (ACC), respectively. In a simplified scheme, the BC (and part of the MC) flows into the SAC that contributes to the BGC which delivers its waters to the SEC that eventually gives rise to the BC, closing the subtropical gyre in the South Atlantic.

The gyre is a result of the general atmospheric circulation in low to temperate latitudes, which is dominated by trade-winds and west-winds. Owing to the Coriolis force, air moving from the subtropical high pressure area to the equatorial low pressure zone is diverted to the west, thus the SE-trades emerge. Poleward of the gyre strong west-winds promote eastward flow. These two flows, and the shape of the basin, set up the gyre (Fig. 2.1). During austral winter, the subtropical high pressure area is more strongly developed and situated farther to the northwest. The result is an intensification of SE-trades which tend to shove more heat toward the equator. Simultaneously, and in opposite hemispheres, trade-winds alternate in their strengths, so that in general strong SE-trades co-occur with weak NE-trades, and vice versa (Johns et al., 1998).

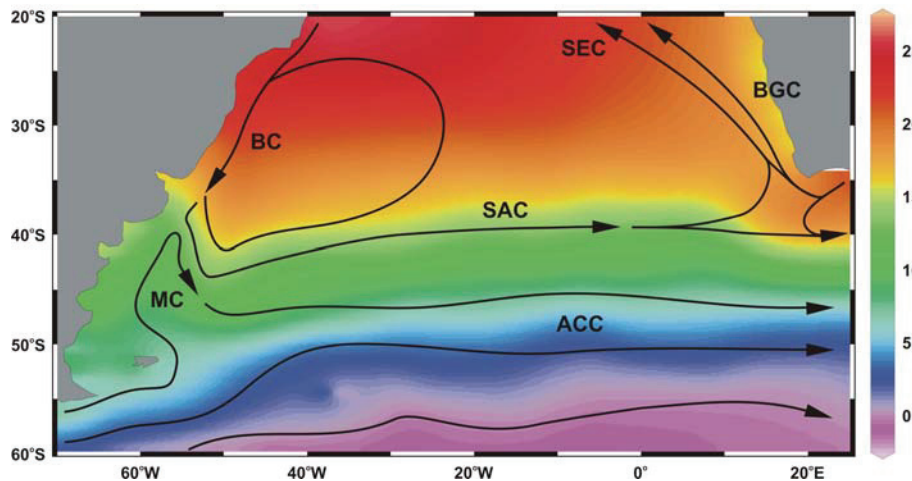


Figure 2.1. Schematic surface circulation in the South Atlantic and Atlantic sector of the Southern Ocean. Mean annual temperature (color shading, in °C) (Conkright et al., 2002) and horizontal circulation (black lines; modified from Stramma and England, 1999) at the surface. The currents are labeled as follows: ACC-Antarctic Circumpolar Current, BC-Brazil Current, BGC-Benguela Current, MS-Malvinas Current, SAC-South Atlantic Current, SEC-South Equatorial Current.

The subtropical gyre associated with the MC and the BMC set up a circulation pattern in the western South Atlantic that has been described as the dominant one for the surface, central and intermediate water masses (Tomczak and Godfrey, 1994; Stramma and England, 1999). Today, the main characteristics of the surface, central and intermediate water masses in the study area are (Fig. 2.2):

- South Atlantic Surface Water (SW) - According to temperature-salinity diagrams (Silveira et al., 1994; Schott et al., 1995), the mixed layer consists of SW with high temperatures ($\sim 20^{\circ}\text{C}$) and salinities (~ 37 psu). This water mass is well characterized down to ~ 100 m water depth, and is present to the north of the BMC.
- Subantarctic Surface Water (SASW) - This water mass shows temperatures varying between 10°C and 5°C , and salinity values around 34.1 psu (Conkright et al., 2002). SASW is present to the south of the BMC.
- South Atlantic Central Water (SACW) - Flowing under the SW and down to ~ 600 m water depth, the SACW shows a nearly linear temperature-salinity relationship which can be well described by a straight line between the temperature-salinity points 6°C , 34.5 psu and 20°C , 36.2 psu (Tsuchiya et al., 1994; Stramma and England 1999).
- Antarctic Intermediate Water (AAIW) - The AAIW irrigates the middle slope between the isobaths of 600 m and 1400 m to the north of the BMC and between 400 m and 1000

m to the south of the BMC and is characterized by a salinity minimum (~ 34.3 psu), temperatures varying between 6°C and 2°C and a high oxygen content at about 700 m (Piola and Gordon, 1989).

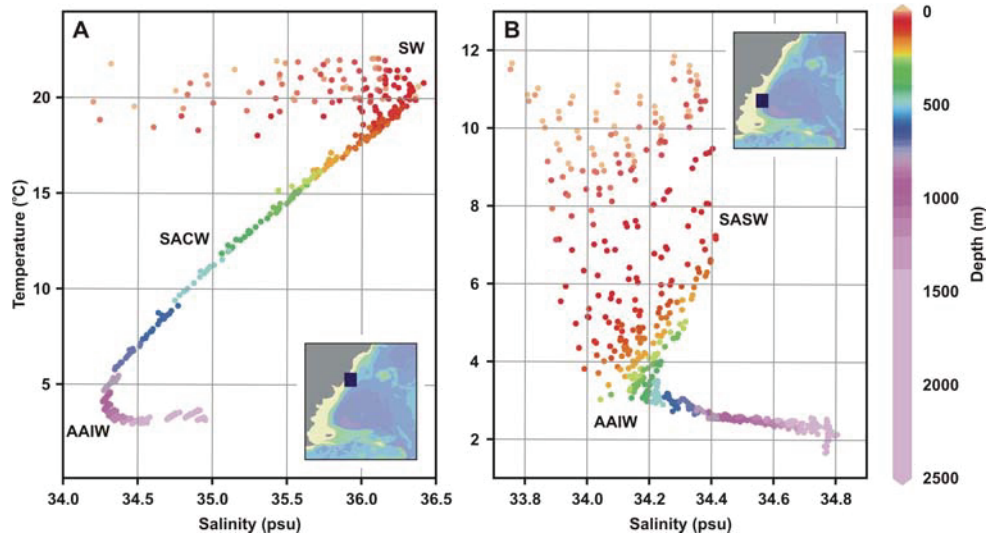


Figure 2.2. Temperature-salinity diagrams for selected stations in the western South Atlantic (Conkright et al., 2002). A: Temperature-salinity diagram for the World Ocean Atlas 2001 stations located between 30.5°S and 34.5°S , and 47.5°W and 51.5°W , i.e. to the north of the Brazil-Malvinas Confluence. B: Temperature-salinity diagram for the World Ocean Atlas 2001 stations located between 41.5°S and 45.5°S , and 55.5°W and 59.5°W , i.e. to the south of the Brazil-Malvinas Confluence. Note the different scales. The water masses are labeled as follows: AAIW-Antarctic Intermediate Water, SACW-South Atlantic Central Water, SASW-Subantarctic Surface Water, SW-South Atlantic Surface Water.

Interocean exchange is a key process controlling the properties of upper water masses in the South Atlantic Ocean (Fig. 2.1) (e.g. Poole and Tomczak, 1999). Gordon et al. (1992) calculated that more than 60% of the Benguela Current central waters are relatively warm and salty waters drawn from the Indian Ocean via Agulhas Leakage (warm water route). For greater depths of the Benguela Current, You et al. (2003) estimated that around 80% of intermediate depth waters are composed by relatively cold and fresh waters from the Pacific Ocean that entered the Atlantic through the Drake Passage (cold water route). These water masses entering the Atlantic from both neighboring oceans help to balance the outflow of North Atlantic Deep Water (NADW) at greater depths and strongly contribute to the northward flowing upper branch of the Atlantic meridional overturning circulation (AMOC) (e.g. Broecker 1991; Gordon et al., 1992). The thermal anomaly related to the inflow of Indian Ocean waters is attenuated along the northward flow but its salinity characteristics persists (Weijer et al., 2002). Consequently, the addition of salty Indian Ocean waters into the South Atlantic may precondition the Atlantic for NADW formation (Gordon et al., 1992; Weijer et al., 2002).

2.2 Atmospheric circulation

Large-scale atmospheric circulation over South America encompasses the main elements of global tropical and subtropical circulation, including the equatorial and mid-latitude low pressure cells, the subtropical high pressure cell, the tropical easterly winds, and the mid-latitude westerly winds (Fig. 2.3). Additionally, particular characteristics of the relief (e.g. the Andes mountain chain) and the nature of the land surface (e.g. the Amazon forest) interact with the main global elements to set up regional-scale atmospheric circulation features and its development through the seasons.

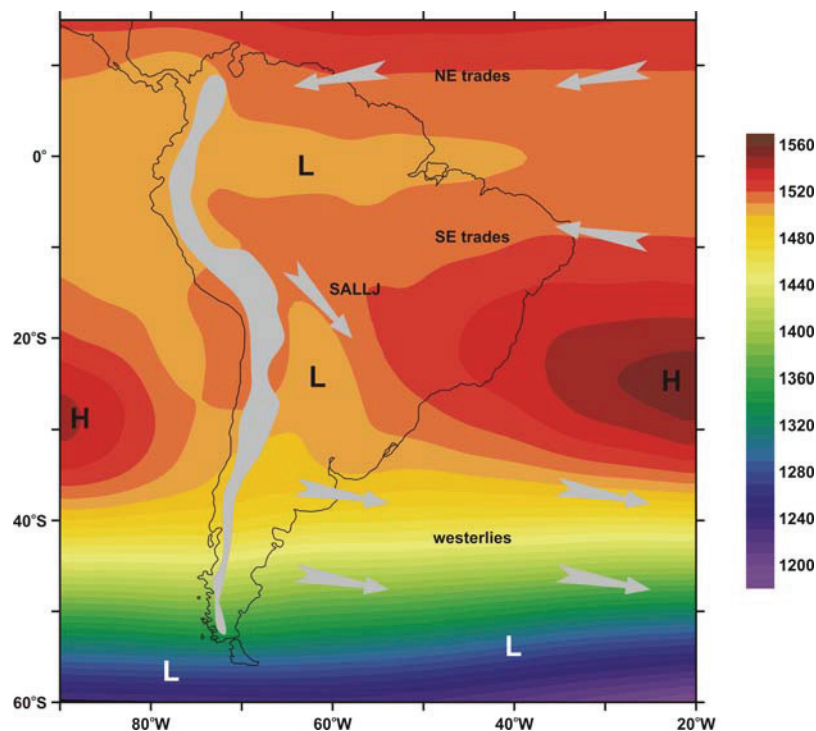


Figure 2.3. Schematic atmospheric circulation over South America (modified from Zhou and Lau, 1998). Color shaded contours indicate long-term annual mean 850 hPa geopotential height in geopotential meters from the NCEP reanalysis climatology (Kalnay et al., 1996). Gray shaded area represents the Andes. The atmospheric features are labeled as follows: H-High pressure cells, L-Low pressure cells, NE trades-Northeasterly trade winds, SALLJ-South American low-level jet, SE trades-Southeasterly trade winds, westerlies-westerly winds.

Precipitation over the PRDB is mainly related to the southward expansion and intensification of the South American summer monsoon (SASM), while austral winter rainfall associated with mid-latitude cyclonic activity over the South Atlantic plays a secondary role (Fig. 2.4) (Zhou and Lau, 1998; Vera et al., 2002). During austral summer, strengthened northeasterly trades enhance the transport of equatorial Atlantic moisture to the Amazon basin, where intense

convection takes place (Fig. 2.3) (Zhou and Lau, 1998). The intensification of the northwesterly South American low-level jet further transports Amazon moisture towards the PRDB, developing the South Atlantic Convergence Zone (SACZ) (Rao et al., 1996). Being one of the main components of the SASM, the SACZ is an elongated NW-SE convective belt that originates in the Amazon Basin, and extends above the northern PRDB and the adjacent subtropical South Atlantic. During austral winter, incursions of mid-latitude air masses into the southern PRDB associated with episodes of enhanced cyclonic activity over the South Atlantic generate winter rainfall that progress northwards along the Atlantic coast (Vera et al., 2002).

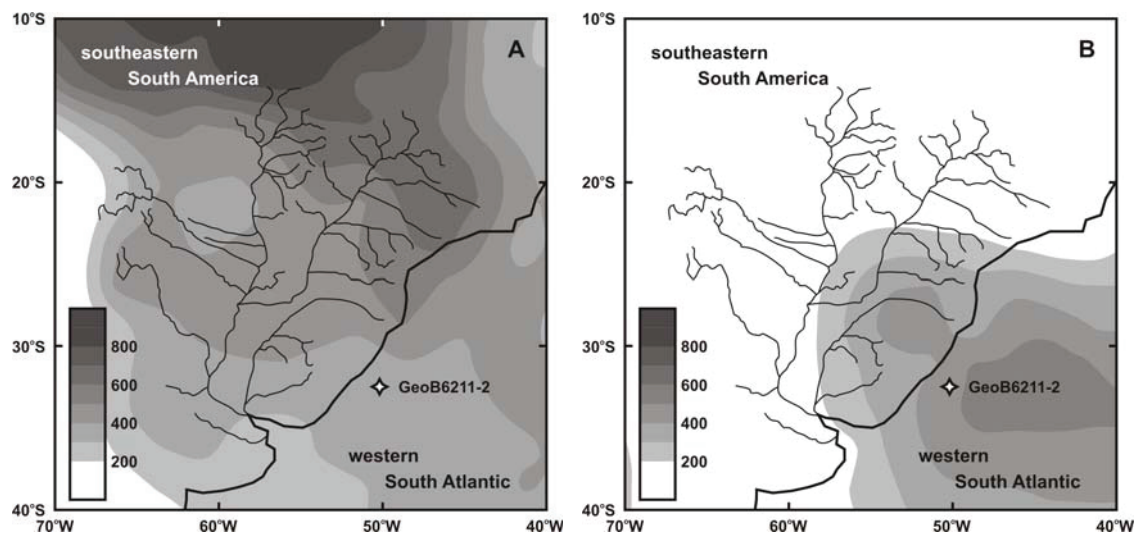


Figure 2.4. Long-term mean seasonal precipitation (in mm) over southeastern South America and the western South Atlantic (Xie and Arkin, 1997). A: December-February. B: June-August. Main tributaries of the La Plata River drainage basin are indicated with thin black lines. Thick black line denotes the coastline. The location of site GeoB6211-2 in the western South Atlantic is also shown.

The annual mean total precipitation in the PRDB is $\sim 1,100$ mm, of which only about 20% ($\sim 21,000 \text{ m}^3 \text{ s}^{-1}$) reaches the western South Atlantic as surface water (e.g. Berbery and Barros, 2002). The other 80 % is evaporated and infiltrated as groundwater. It is clear that any change in evaporation and infiltration may lead to greater relative changes in the basin's surface discharge. Annual mean rainfall over the PRDB decreases from north to south and from east to west (Fig. 2.4). Corresponding amounts range from 1,800 mm in the maritime uplands along the Brazilian coast to 200 mm along the western boundary of the basin (e.g. Garcia and Vargas, 1996). The amplitude of the annual cycle in rainfall also decreases from north to south. The northern part of the basin has a well-defined annual cycle with maximum precipitation during southern hemisphere summer related to the SASM (Zhou and Lau, 1998; Berbery and Barros, 2002). The central and southern parts of the basin have a more uniform seasonal distribution, with maxima during

southern hemisphere spring and autumn, influenced by both the SASM and winter precipitation (Berbery and Barros, 2002; Vera et al., 2002). Since the major rivers in the basin generally run from north to south, this rainfall regime contributes to the attenuation of the seasonal cycle downstream.

Oceanic conditions in the eastern equatorial Pacific and the western South Atlantic play an important role in the adjacent continental climate and affect the PRDB (Doyle and Barros, 2002; Robertson et al., 2003). Interannual variability in precipitation over the PRDB has been related to El Niño-Southern Oscillation whereas interdecadal changes were associated to SST fluctuation in the South Atlantic (Robertson and Mechoso, 2000). On interdecadal time-scales, higher PRDB discharges have been coupled to positive SST anomalies in the western South Atlantic.

2.3 Geology

Four major geological domains are recognized in the South American tectonic plate: (i) the continental interior, a region of a long and complex geological history constituting a vast realm where thick sequences of Paleozoic, Mesozoic and subordinately Cenozoic sediments accumulated; (ii) the western, convergent margin of the plate, along which the continental lithosphere of South America confronts the oceanic floor of the Pacific Ocean, creating a large orogenic belt, the Andes, with several sedimentary basins associated; (iii) the eastern side, a more than 10,000 km-long divergent margin originated by the break-up of the Gondwana paleocontinent and the separation of the South American and African plates since the Mesozoic; and (iv) the northern and southern margins of the plate, marked by a regional transcurrent tectonic regime along major transform faults that define the active contact of the South American plate with the Caribbean and Scotia plates, respectively. Of special interest to this study are the first and second units mentioned above. These geological units constitute the main sources of the terrigenous material delivered by the La Plata River drainage basin (PRDB) during the last deglaciation to the upper continental slope off southeastern South America, where the gravity core studied herein was raised.

Phanerozoic cratonic sequences developed extensively in the continental interior of the South American plate from the Ordovician mainly until the Cretaceous, with some sequences still active during Quaternary times. They configure a series of unconformity-bounded units that resulted from successive phases of subsidence and accumulation of sedimentary rocks, the record of which was interrupted during several periods of widespread erosion. Rocks from the Paraná

Basin, one of the most important Phanerozoic sedimentary basins in South America, outcrop extensively in the PRDB and are briefly described below.

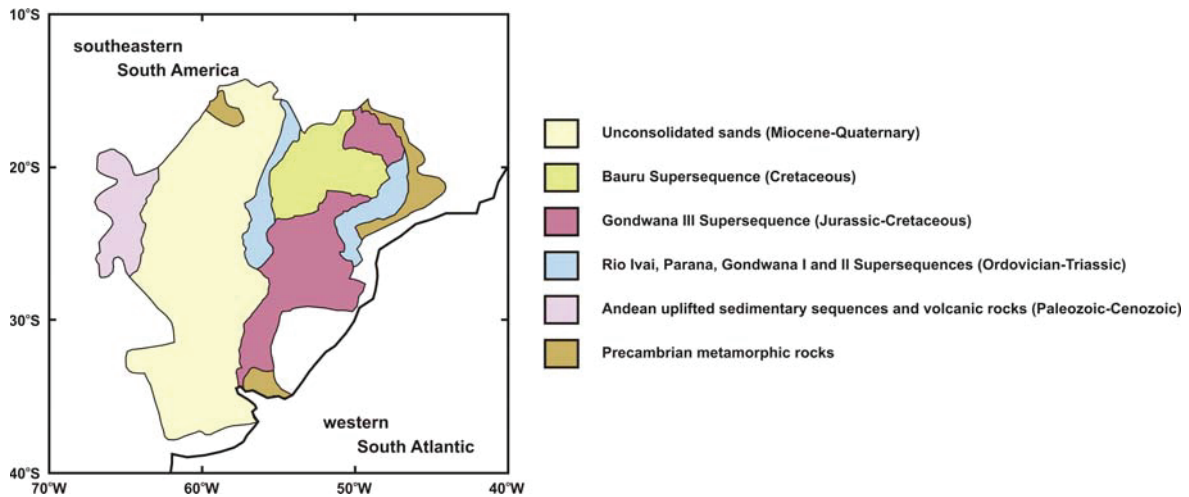


Figure 2.5. Schematic geological map of the La Plata River Drainage Basin in southeastern South America. Thick black line denotes the coastline. Modified from Schenk et al. (1997).

From the bottom to the top, the Paraná Basin is composed by (e.g. Schobbenhaus et al., 1981; Milani and Tomaz Filho, 2000): (i) Rio Ivaí Supersequence (glaciogenic diamictites and lacustrine micaceous shales and fine-grained sandstones); (ii) Paraná Supersequence (lacustrine coarse-grained kaolinite-rich sandstones, siltstones and deltaic sandstones); (iii) Gondwana I Supersequence (glaciogenic diamictites, turbiditic sandstones, conglomerates and varvites; deltaic sandstones; marine siltstones, shales, limestones and sandstones); (iv) Gondwana II Supersequence (lacustrine and fluvial sandstones); (v) Gondwana III Supersequence (eolian sandstones covered by basaltic rocks); and (vi) Bauru Supersequence (alluvial, fluvial and eolian conglomerates and sandstones). From Miocene times onwards, a continental sequence of sands developed on the eastern portion of the Paraná Basin, constituting a wedge of poorly consolidated post-orogenic sediments derived from the Andes.

While in the southeastern part of the PRDB the most commonly outcropping unit is composed of the basaltic rocks (Gondwana III Supersequence), in the northeastern part of the basin the sandstones of the Bauru Supersequence constitute the main source of sediments for the PRDB (Fig. 2.5) (e.g. Schobbenhaus et al., 1981; Milani and Tomaz Filho, 2000). Outcrops in the western half of the PRDB are largely dominated by the poorly consolidated post-orogenic sandy sediments of Late Cenozoic age. In the westernmost part of the PRDB, important sources of sediments are also uplifted sedimentary sequences and intermediate volcanic rocks associated with the Andes

(Depetris et al., 2003). Additionally, Precambrian metamorphic rocks of different grades also crop out in the periphery of the PRDB.

Chapter 3

Methods

3.1 Mg/Ca paleothermometry

Mg/Ca in foraminiferal calcite is an independent paleotemperature proxy that is measured on the same biotic carrier as stable oxygen isotopes ($\delta^{18}\text{O}$), allowing the reconstruction of seawater $\delta^{18}\text{O}$ ($\delta^{18}\text{O}_{\text{sw}}$) and salinity variations without the problems introduced by other paleotemperature proxies like different seasonal signals or different depth habitats of the biotic carriers.

Magnesium is one out of several divalent cations which may substitute for Ca during the formation of biogenic calcite. Its incorporation into foraminiferal calcite is temperature dependent, so that an increase in seawater temperature will be associated with foraminiferal Mg/Ca ratio increase. The temperature sensitivity of foraminiferal Mg/Ca was first reported by Chave (1954) and further refined in the 1960s, 1970s and 1980s (e.g. Duckworth, 1977; Cronblad and Malmgren, 1981). Notwithstanding these early achievements, it was not before the late 1990s that Mg/Ca paleothermometry developed to a widely applied paleoceanographic tool (e.g. Mashiotta et al., 1999; Lea et al., 2000).

The main advantages of Mg/Ca paleothermometry over other paleotemperature proxies are related to: (i) the relatively long residence times of Ca and Mg (10^6 and 10^7 years, respectively) in the oceans that make seawater Mg/Ca ratio to be constant on glacial-interglacial timescales, thus independent of sea level; and (ii) the very fact that Mg/Ca and $\delta^{18}\text{O}$ are measured in the same biotic carrier (i.e. foraminiferal calcite), implies they can be directly combined in order to reconstruct $\delta^{18}\text{O}_{\text{sw}}$, circumventing potential problems introduced by other paleotemperature proxies (e.g. alkenones, TEX_{86}) like different seasonal signals or different depth habitats of the biotic carriers. Despite the obvious utility of Mg/Ca ratios in paleoceanography, problems of (i) dissolution, (ii) gametogenic calcification, (iii) salinity effect on Mg uptake, and (iv) presence of contaminant phases may limit the confidence in Mg/Ca-based paleotemperature reconstructions. Experimentation with artificial seawater indicates that the solubility of calcite is influenced by the degree of supersaturation, surface area exposure, and Mg content (Rushdi et al., 1998). Since high-Mg calcite is more soluble than low-Mg calcite (Rushdi et al., 1998; Davis et al., 2000), partial

dissolution of foraminiferal calcite selectively preserves calcite with lower Mg/Ca, biasing paleotemperature reconstructions towards lower temperatures. Several studies have shown evidence of intratest Mg heterogeneity in foraminifera (e.g. Elderfield et al., 1996; Nürnberg et al., 1996). In addition to environmental variables (i.e. temperature), physiologically controlled biomineralization processes (e.g. gametogenic calcification) may regulate Mg distribution in foraminiferal calcite. Salinity seems to have a significant effect on Mg uptake by foraminiferal calcite (e.g. deMenocal et al., 2007). Earlier studies apparently underestimated salinity effects, and recent results point out that salinity variability in the present-day range may indeed significantly affect Mg/Ca uptake by foraminiferal calcite (e.g. deMenocal et al., 2007). Contamination of foraminiferal calcite may arrive by the presence of unwanted Mg-bearing phases like clays, Mn-carbonates and metal-oxide coatings (e.g. Barker et al., 2003). Meticulous cleaning procedures associated with contamination monitoring are of key importance to avoid contamination.

3.2 Stable isotopes

3.2.1 Stable oxygen isotopes

Stable oxygen isotopes are one of the most important tools for reconstructing past climate, largely because (i) they circulate in the main components of the climate system (i.e. atmosphere, hydrosphere, cryosphere), (ii) they are fractionated whenever a phase transition between or within the reservoirs occurs, (iii) they show a high potential of being recorded in paleoenvironmental archives (e.g. stalagmites, marine carbonates, ice cores), and (iv) the recorded composition can be routinely measured via mass spectrometry.

There are three stable oxygen isotopes, namely ^{16}O (99.76%), ^{17}O (0.04%) and ^{18}O (0.2%). The oxygen isotopic composition of a sample ($\delta^{18}\text{O}$) is generally expressed as a departure of the $^{18}\text{O}/^{16}\text{O}$ ratio from an arbitrary standard as parts per thousand (per mil):

$$\delta^{18}\text{O}(\text{per mil}) = \left[\frac{(^{18}\text{O}/^{16}\text{O})_{\text{sample}} - (^{18}\text{O}/^{16}\text{O})_{\text{standard}}}{(^{18}\text{O}/^{16}\text{O})_{\text{standard}}} \right] \cdot 1000$$

The oxygen isotopic composition of carbonate samples are usually reported relative to the Vienna Peedee Belemnite (VPDB) standard, whereas water samples are reported relative to the Vienna Standard Mean Ocean Water (VSMOW) standard (Coplen, 1996). Due to differences in

preparation techniques, a correction factor of -0.27 ‰ is applied to convert the VSMOW scale into the VPDB scale (Hut, 1987).

Two main types of isotopic fractionation processes occur in natural environments, (i) kinetic and (ii) equilibrium fractionation. Kinetic fractionation separates stable isotopes from each other by their mass and is associated with a unidirectional process (e.g. evaporation, precipitation). Because of kinetic fractionation, water evaporating from the sea surface is depleted in ^{18}O relative to ocean water, while rain precipitating from a cloud is enriched in ^{18}O relative to the cloud's moisture. The tropical oceans are the major source of atmospheric water vapor. Poleward transport of this water results in a gradual rainout and thus in a depletion of ^{18}O in the remaining moisture. Hence, the isotopic composition of precipitation varies strongly with latitude, altitude and continentality. On short time-scales (e.g. seasons), evaporation and precipitation largely control the oxygen isotopic composition of seawater ($\delta^{18}\text{O}_{\text{sw}}$), the source of oxygen for marine carbonate precipitation. On longer time-scales (e.g. glaciations), waxing and waning of isotopically low continental ice masses also has a strong effect on $\delta^{18}\text{O}_{\text{sw}}$. Regarding equilibrium fractionation, temperature-dependent fractionation occurs between two or more substances in chemical equilibrium, e.g. in the system $\text{CO}_2\text{-H}_2\text{O-CaCO}_3$. If CaCO_3 is crystallized slowly in seawater, ^{18}O is slightly concentrated in the calcium carbonate relative to that in seawater. As mentioned, this process is temperature-dependent, with the concentration effect diminishing as temperature increases.

Based on equilibrium fractionation, Urey (1947) first proposed that paleotemperatures could be reconstructed using the composition of oxygen isotopes in carbonate fossils. It turned out that direct paleotemperature estimates exclusively based on $\delta^{18}\text{O}$ of marine carbonates are rather problematic, mainly because the oxygen isotopic composition in marine carbonates varies with temperature and $\delta^{18}\text{O}_{\text{sw}}$. The latter, in turn, depends on local precipitation-evaporation balance and global continental ice volume. Nevertheless, $\delta^{18}\text{O}$ in marine carbonates evolved as one of the main tools in paleoceanography and is presently widely applied in assessing past variability in ocean circulation (e.g. Vidal et al., 1997; Matsumoto and Lynch-Stieglitz, 2003), upper water column structure (e.g. Mulitza et al., 1997; Rühlemann et al., 2001), continental ice volume (e.g. Waelbroeck et al., 2002; Sidall et al., 2003), freshwater input into the oceans (e.g. Duplessy et al., 1991; Maslin et al., 2000), seawater density (e.g. Lynch-Stieglitz et al., 1999), sea surface salinity (e.g. Lea et al., 2000; Schmidt et al., 2004), deep-sea salinity (e.g. Adkins et al., 2002; Schrag et al., 2002) as well as for stratigraphic purposes (e.g. Shackleton and Opdyke, 1973; Martinson et al., 1987).

Foraminifera, unicellular marine organisms, are one of the main components of marine carbonates, and have been extensively used as past $\delta^{18}\text{O}$ signal carriers. When interpreting foraminiferal $\delta^{18}\text{O}$ the following factors have to be taken into account: (i) the pH effect; (ii) the photosynthetic activity of symbiotic algae; (iii) the ontogenetic effect; (iv) seasonality; (v) vertical migration; and (vi) postdepositional effects.

Increased pH and photosynthetic activity both result in a decrease of $\delta^{18}\text{O}$ values in foraminiferal shells (e.g. Spero and Lea, 1993; Spero et al., 1997). Due to an ontogenetic effect, small shells are depleted in ^{18}O compared to larger ones (e.g. Berger et al., 1978; Bemis et al., 1998). Juvenile foraminifers calcify faster and respire at higher rates. During rapid calcification a discrimination of the heavier isotope ^{18}O occurs due to kinetic fractionation. Planktic foraminifera show a temporal (seasonal) distribution pattern, occurring usually in highest abundances during their most preferred conditions of temperature, food and light availability (e.g. Deuser and Ross, 1989; Field, 2004). Such conditions may exist in a specific hydrographic regime for only a short period of the year generating species-specific fluxes to peak during different periods. Since planktic foraminifera live dispersed in the upper water column, their $\delta^{18}\text{O}$ differences are a function of water column stratification and mixed-layer depth (e.g. Fairbanks et al., 1980; Mulitza et al., 1997). Some species migrate vertically up to hundreds of meters within the upper water column to complete their ontogenetic cycle, and precipitate calcite under different temperature and $\delta^{18}\text{O}_{\text{sw}}$ conditions. Thus, the $\delta^{18}\text{O}$ of a whole shell represents an integrated and mass weighted signal. Nevertheless, it has been shown that foraminifera calcify a significant amount of shell calcite in much narrower depth zones than the overall species vertical distribution (e.g. LeGrande et al., 2004). Finally, postdepositional effects like bioturbation and calcite dissolution should also be taken into account while interpreting foraminiferal $\delta^{18}\text{O}$ (e.g. Broecker, 1986; Wu and Berger, 1989).

When the oxygen isotopic composition of foraminiferal calcite and the temperature of calcification (e.g. via Mg/Ca paleothermometry) are known, $\delta^{18}\text{O}_{\text{sw}}$, a proxy for salinity, can be determined based on a paleotemperature equation. In the present study we will refer to the empirical paleotemperature equation of Shackleton (1974):

$$T(^{\circ}\text{C}) = 16.9 - 4.38 \cdot (\delta^{18}\text{O}_{\text{calcite}} - \delta^{18}\text{O}_{\text{sw}}) + 0.1 \cdot (\delta^{18}\text{O}_{\text{calcite}} - \delta^{18}\text{O}_{\text{sw}})^2$$

where T stands for the in-situ temperature during calcite precipitation ($^{\circ}\text{C}$), $\delta^{18}\text{O}_{\text{calcite}}$ represents the oxygen isotopic composition of the calcite (‰, VPDB), and $\delta^{18}\text{O}_{\text{sw}}$ stands for the oxygen isotopic composition (‰, VPDB) of the seawater from which the calcite has been precipitated.

Since foraminifera exhibit species-specific offsets from calcite predicted with empirical relationships (e.g. Bemis et al., 1998; Mulitza et al., 2003), some caution has to be taken while interpreting the absolute $\delta^{18}\text{O}_{\text{sw}}$ values obtained with such equations. However, it has been shown that Shackleton's equation correctly predicts the slope of the $\delta^{18}\text{O}$:temperature relationship over the entire temperature range present in the oceans for the most commonly used species of planktic foraminifera (Mulitza et al., 2003). Since species-specific equations are not available for some species used in this study, we used Shackleton's equation to calculate relative changes in $\delta^{18}\text{O}_{\text{sw}}$.

3.2.2 Stable carbon isotopes

The very fact that the oceans are the largest active carbon reservoir associated to the crucial role of carbon in global climate make the study of stable carbon isotopes a key branch of paleoceanographic research.

There are two stable carbon isotopes in the earth system, ^{12}C and ^{13}C , with natural abundances of 98.89% and 1.11%, respectively. As is the case for $\delta^{18}\text{O}$, the stable carbon isotopic composition of a sample ($\delta^{13}\text{C}$) is generally expressed as a departure of the $^{13}\text{C}/^{12}\text{C}$ ratio from an arbitrary standard (usually VPDB) as per mil:

$$\delta^{13}\text{C}(\text{per mil}) = \left[\frac{(^{13}\text{C}/^{12}\text{C})_{\text{sample}} - (^{13}\text{C}/^{12}\text{C})_{\text{standard}}}{(^{13}\text{C}/^{12}\text{C})_{\text{standard}}} \right] \cdot 1000$$

Foraminifera use marine total dissolved inorganic carbon (ΣCO_2) to precipitate their calcite shells, thereby recording $\delta^{13}\text{C}$ of seawater ΣCO_2 during calcification. The ΣCO_2 comprises the sum of the concentrations of CO_2 (aqueous carbon dioxide), HCO_3^- (bicarbonate), and CO_3^{2-} (carbonate ion), and seawater pH controls the relative proportion of these components. Seawater $\delta^{13}\text{C}_{\Sigma\text{CO}_2}$, in turn, is mainly controlled by (i) the photosynthesis-respiration cycle, (ii) air-sea gas exchange and (iii) ocean circulation. Biological primary production (photosynthesis) in the euphotic zone strongly fractionates stable carbon isotopes concentrating the light isotope ^{12}C in organic matter. Planktic foraminifera dwelling in the euphotic layer thus record the resulting

relative increase in seawater $\delta^{13}\text{C}$. Since nearly all of the organic matter produced by photosynthesis is subsequently remineralized on its way to the bottom of the oceans, deeper water masses usually show lower $\delta^{13}\text{C}_{\Sigma\text{CO}_2}$. Again, foraminifera are able to record this relative decrease in $\delta^{13}\text{C}_{\Sigma\text{CO}_2}$. The photosynthesis-respiration cycle makes $\delta^{13}\text{C}_{\Sigma\text{CO}_2}$ decrease along with increasing nutrient concentration. The isotopic fractionation during air-sea gas exchange in surface ocean is temperature-dependent, with seawater becoming more enriched in ^{13}C relative to the atmosphere by about 1 ‰ per 10°C cooling. As $\delta^{13}\text{C}_{\Sigma\text{CO}_2}$ behaves as a conservative tracer in the deep ocean, changes in $\delta^{13}\text{C}_{\Sigma\text{CO}_2}$ of deep waters may only arise from mixing with water masses of different $\delta^{13}\text{C}$ composition and from remineralisation of organic matter.

The $\delta^{13}\text{C}$ of foraminiferal calcite has been used as a proxy for past oceanic circulation (e.g. Oppo and Fairbanks, 1987; Curry and Oppo 2005), variations of biological productivity (e.g. Ganssen, 1983; Mortlock et al., 1991), changes in nutrient cycling in surface waters (e.g. Ganssen and Sarnthein, 1983; Oppo and Fairbanks, 1989) and variations in the global carbon cycle (e.g. Shackleton, 1977).

The main considerations to be taken into account while interpreting foraminiferal $\delta^{13}\text{C}$ are: (i) the incorporation of isotopically light metabolic CO_2 ; (ii) the carbonate ion concentration ($[\text{CO}_3^{2-}]$) effect; (iii) seasonality; (iv) vertical migration; and (v) postdepositional effects. Larger foraminiferal shells show higher $\delta^{13}\text{C}$ values compared to smaller shells. This size-dependence is due to the incorporation of considerable amounts of respired light carbon for calcite precipitation during the juvenile phase (e.g. Berger et al., 1978; Spero and Lea, 1996). Temperature may affect planktic foraminiferal $\delta^{13}\text{C}$ through its effect on the metabolic rate and on symbiont photosynthesis (e.g. Ravelo and Fairbanks, 1995; Bemis et al., 2000). Carbonate ion concentration shows a significant control on the incorporation of $\delta^{13}\text{C}$ into foraminiferal calcite (Spero et al., 1997). At constant $\delta^{13}\text{C}_{\Sigma\text{CO}_2}$ an increase in the $[\text{CO}_3^{2-}]$ results in lower $\delta^{13}\text{C}$ of foraminiferal calcite, and this effect is species-specific. Seasonality, vertical migration and postdepositional effects have a similar impact on the interpretation of foraminiferal $\delta^{13}\text{C}$ as described for $\delta^{18}\text{O}$.

3.3 X-ray fluorescence core scanner

High-resolution studies on continuous marine sedimentary archives are in demand for the understanding of high-frequency climate change on short times-scales (e.g. seasonal to millennial

time-scales). Recently developed X-ray fluorescence (XRF) core scanners are able to deliver high-resolution down-core bulk sedimentary chemical analyzes tackling part of this issue.

XRF core scanners are computer-controlled core-scanning tools that analyze the chemical composition of sediments directly at the surface of a split sediment core or u-channel. The method is non-destructive, consumable costs are relatively low and sample preparation is minimized compared to conventional chemical analyzes on discrete samples. The high sampling resolution of XRF core scanners can go down to the μm scale. The XRF core scanner used in this study (Avaatech 1 XRF whole-core scanner at the University of Bremen) is equipped with a Molybdenum X-ray source (3-50 kV), a Si(Li) Peltier-cooled PSI energy-dispersive X-ray spectrometer (KevexTM) with a 125 μm Beryllium window and a multi channel analyzer (Röhl and Abrams, 2000). This system configuration allows the analysis of elements from Al (atomic number 13) to Ba (atomic number 56). The detector registers the emission line energies of the X-ray irradiated sample and their frequency over a predefined measure time as element intensities in counts, which are proportional to the element concentrations.

Detailed down-core XRF core scanner measurements have been successfully applied for stratigraphic correlations (e.g. Westerhold et al., 2005), and sedimentary (e.g. Bahr et al., 2005; Hepp et al., 2006) and climatic (e.g. Haug et al., 2001; Kuhlmann et al., 2004) reconstructions on various time scales.

The main disadvantages of the method arise from its dependency on pore space and water content of the analyzed sediment cores (Röhl and Abrams, 2000; Tjallingii et al., 2007). Additionally, it is important to note that XRF scans only analyze the surface of split sediment cores, so that scans of material with a laterally heterogeneous composition may not reflect the real sediment composition.

3.4 Radiocarbon dating

Radiocarbon or ^{14}C dating is by far the most useful dating tool for the study of late Quaternary climatic and oceanographic fluctuations. Because of the widespread distribution of ^{14}C , the technique has been used to date samples of peat, wood, bone, shell, paleosols, marine and lacustrine sediments, corals and atmospheric CO_2 trapped in ice cores. Moreover, the timeframe to which radiocarbon dating can be applied (~50,000 years) spans a period of major global environmental and archeological changes.

After production in the upper atmosphere by neutron bombardment of atmospheric nitrogen atoms, ^{14}C atoms are rapidly oxidized to $^{14}\text{CO}_2$. Isotopically heavy carbon dioxide then diffuses downwards and mixes with the rest of the atmospheric CO_2 , entering into all pathways of the biosphere. An equilibrium has been achieved between the rate of new ^{14}C production in the upper atmosphere and the rate of decay of ^{14}C to nitrogen in the global carbon reservoir. The assumption of an essentially steady concentration of radiocarbon during the period useful for dating is fundamental to the method though, in detail, this assumption is invalid, requiring a correction.

Through constant air-sea gas exchange $^{14}\text{CO}_2$ also enters the oceans. Marine flora and fauna (e.g. foraminifera) assimilate a certain amount of ^{14}C into their tissues and skeletons through photosynthesis and respiration. The ^{14}C content of these materials is in equilibrium with that of ambient seawater because there is a constant exchange of new ^{14}C as old cells die and are replaced. However, as soon as an organism dies the exchange of ^{14}C ceases. From that moment on the ^{14}C content of the organism begins to radioactively decay, being purely a function of time. The age of a fossil sample can then be determined by measuring the sample's ^{14}C content, given that the sample's initial ^{14}C concentration as well as the ^{14}C half-life are known (obviously considering that the sample's age lies within the ^{14}C dating range).

For dating purposes the “Libby half-life” of 5568 ± 30 years (Libby, 1955) is used for ^{14}C to avoid inconsistencies with records generated before 1962, when the value was recalculated to 5730 ± 40 years (Godwin, 1962).

Radiocarbon dated marine samples have to be corrected for the reservoir effect (Bard, 1988). Ocean surface waters are not in isotopic equilibrium with the atmosphere because oceanic circulation brings ^{14}C -depleted waters to the surface to mix with “modern” waters. Consequently, the ^{14}C age of surface waters varies geographically. In the lower latitudes of the world oceans, the mean reservoir age of surface waters is ~ 400 years, whereas in higher latitudes the reservoir effect can be much larger due to widespread upwelling of older waters and the effect of sea-ice, which limits air-sea gas exchange. The extent to which such ^{14}C gradients have been constant over time is of great significance for dating older events in the marine environment and comparing them with terrestrial records (e.g. Butzin et al., 2005).

In contrast to the assumption of constant past atmospheric ^{14}C concentration levels, it is well known that radiocarbon levels had indeed varied through time. Changes in atmospheric ^{14}C concentrations may result from a wide variety of factors, including (i) variations in the rate of

radiocarbon production in the atmosphere, (ii) variations in the rate of exchange of radiocarbon between various geochemical reservoirs and changes in the relative carbon dioxide content of the reservoirs, and (iii) variations in the total amount of carbon dioxide in the atmosphere, biosphere and hydrosphere (Damon et al., 1978). Therefore, ^{14}C ages have to be calibrated in order to calculate absolute (calendar) ages. The scientific community therefore puts much effort to get combined ^{14}C -calendar age measurements from samples of the last 50,000 years (e.g. Hughen et al., 2004). Calendar ages can be obtained directly by dendrochronology and varve chronology as well as by U/Th dating of corals and speleothems.

3.5 The University of Victoria Earth System Climate Model

There is growing consensus that a modern understanding of climate dynamics, i.e. the processes which govern the mean state of the atmosphere, should not circumvent the fact that climate is a result of complex interactions between the abiotic and the biotic worlds. According to this modern concept, the climate system consists of the geosphere (further subdivided into open systems, namely the atmosphere, the hydrosphere, the cryosphere, the pedosphere, and the lithosphere) and the biosphere. Only recently this modern concept of climate has been incorporated into climate models (Claussen et al., 2002). Earth system models of intermediate complexity are designed to describe the natural Earth system, in which the biosphere can play a significant role. Moreover, they include most processes described in comprehensive models albeit in a more reduced form. They explicitly simulate the interactions among several components of the natural Earth system. On the other hand, Earth system climate models of intermediate complexity are simple enough to allow for long-term climate simulations over several thousands of years or even glacial cycles.

We used the University of Victoria (UVic) Earth System Climate Model (ESCM, version 2.8), which is one of the Earth system models of intermediate complexity presently in use (e.g. Weaver et al., 2007a; Weaver et al., 2007b). The UVic ESCM consists of the Modular Ocean Model (MOM, version 2) (Pacanowski, 1996) coupled to a vertically integrated two-dimensional energy-moisture balance model of the atmosphere, a sea ice model (based on the thermodynamic formulation by Semtner (1976) and Hibler (1979) and the dynamic formulation by Hunke and Dukowicz (1997)), a land surface scheme (Cox et al., 1999) and a dynamic global vegetation model (Cox, 2001; Meissner et al., 2003). The UVic ESCM including the atmospheric, ocean and sea ice components is described by Weaver et al. (2001). Monthly wind stress to force the ocean and monthly winds for the advection of heat and moisture in the atmosphere are prescribed from the

NCEP reanalysis climatology (Kalnay et al., 1996). The model is driven by the seasonal variation of solar insolation at the top of the atmosphere.

Chapter 4

Signature of the Brazil-Malvinas Confluence (Argentine Basin) in the isotopic composition of planktonic foraminifera from surface sediments

Cristiano Mazur Chiessi^a, Shannon Ulrich^{b,c}, Stefan Mulitza^c, Jürgen Pätzold^c, Gerold Wefer^c

^aFachbereich Geowissenschaften, Universität Bremen, Postfach 330440, 28334 Bremen, Germany

^bBryn Mawr College, 101 North Merion Avenue, Box C-1082, Bryn Mawr, PA 19010, USA

^cDFG-Research Center Ocean Margins, Universität Bremen, Postfach 330440, 28334 Bremen, Germany

Published in *Marine Micropaleontology* (2007) 64, 52-66

4.1 Abstract

We explored the potential to use the stable isotopic compositions of planktonic foraminifera as a proxy for the position of the Brazil-Malvinas Confluence (BMC) in the Argentine Basin. For this purpose, we measured the oxygen and carbon isotopic compositions of *Globigerinoides ruber* (pink and white varieties measured separately), *Globigerinoides trilobus*, *Globigerina bulloides*, *Globorotalia inflata* and *Globorotalia truncatulinoides* (left- and right-coiling forms measured separately) from a latitudinal transect of 56 surface sediment samples from the continental slope off Brazil, Uruguay and Argentina between 20 and 48°S. Lowest oxygen isotopes values were found in *G. ruber* (pink), followed by *G. ruber* (white) and *G. trilobus* reflecting the highly stratified near surface water conditions north of the BMC. *Globigerina bulloides* was present mainly south of the BMC and records subsurface conditions supporting earlier plankton tow studies. *Globorotalia inflata* and *G. truncatulinoides* (left and right) were both available over the whole transect and calcify in the depth level with the steepest temperature change across the BMC. Accordingly, the $\delta^{18}\text{O}$ of these species depict a sharp gradient of 2‰ at the confluence with remarkably stable values north and south of the BMC. Our data show that the oxygen isotopic composition of *G. inflata* and *G. truncatulinoides* (left and right) are the most reliable indicators for the present position of the BMC and can therefore be used to define the past migration of the front if appropriate cores are available.

4.2 Introduction

The upper-level circulation in the western Argentine Basin is dominated by the Brazil-Malvinas Confluence (BMC) that emerges from the encounter of southward-flowing Brazil Current (BC) and northward-flowing Malvinas (Falkland) Current (MC) (Peterson and Stramma, 1991; Stramma and England, 1999). At the junction, both currents are deflected from the continental margin and flow south-eastward. A dramatically steep gradient in sea-surface temperature is found in the confluence, reaching $1^{\circ}\text{C km}^{-1}$ (Olson et al., 1988). These conditions greatly contribute to make the region not just an important site of water exchange between the Southern Ocean and the subtropical basins but also a major ventilation area for much of the South Atlantic thermocline (Gordon, 1981; Boddem and Schlitzer, 1995). The BMC migrates latitudinally on seasonal, interannual and interdecadal time scales (e.g. Olson et al., 1988; White and Peterson, 1996; Wainer et al., 2000). Still, not much is understood about the dynamics behind the variations in the position of the BMC on longer time scales. In this context, reconstructions of the position of the BMC for climatic conditions different from the present might indicate the forcing factors behind variations of the BMC.

The oxygen isotopic composition ($\delta^{18}\text{O} - \delta$ refers to the comparison of the sample isotopic ratio of $^{18}\text{O}/^{16}\text{O}$ to a standard) of planktonic foraminifera provides one of the most widely used tools for reconstructing past changes in ocean temperature and salinity (e.g. Emiliani, 1954; Duplessy et al., 1991). The $\delta^{18}\text{O}$ of foraminiferal calcite records the temperature and stratification of the upper-water column as well as latitudinal temperature gradients over frontal systems (e.g. Williams and Healy-Williams, 1980; Durazzi, 1981; Mulitza et al., 1997; Matsumoto and Lynch-Stieglitz, 2003; LeGrande et al., 2004; King and Howard, 2005). On the other hand, many factors control the carbon isotopic composition in seawater (photosynthesis-respiration cycle, isotopic fractionation during air-sea exchange and circulation) and its incorporation in planktonic foraminiferal calcite (species specific vital-effects dependent on the carbonate system, photosynthesis, temperature, and incorporation of isotopically light metabolic CO_2), making it a rather complex proxy (e.g. Broecker and Maier-Reimer, 1992; Ravelo and Fairbanks, 1995; Spero et al., 1997). The $\delta^{13}\text{C}$ of foraminiferal calcite has been used as a proxy for past oceanic circulation, variations of biological productivity, and nutrient cycling in surface waters (e.g. Ganssen, 1983; Oppo and Fairbanks, 1987, 1989).

Both oxygen and carbon stable isotopic composition of planktonic foraminifera should also be ideal to monitor the location of the BMC which is associated with strong latitudinal

temperature gradients. This approach, however, is complicated by the fact that the BMC region is associated with drastic meridional changes in the faunal composition of planktonic foraminifera (Boltovskoy et al., 1996). Warm water species (e.g. *Globigerinoides ruber*, *Globigerinoides trilobus*) that dominate the fauna to the north of the confluence practically disappear from the water column southwards, beyond the modal position of the BMC (Boltovskoy et al., 1996, 2000). Hence, the isotopic composition of a single species might not be sufficient and data from several species must be combined to monitor the temperature gradient over the BMC.

In this paper, we explore which species or combination of species provides the best representation of the BMC position in its shell's stable isotopic composition. For this purpose we measured the oxygen and carbon isotopic composition of the planktonic foraminifera species *G. ruber* (pink and white varieties measured separately), *G. trilobus*, *Globigerina bulloides*, *Globorotalia inflata* and *Globorotalia truncatulinoides* (left- and right-coiling forms measured separately) from a latitudinal transect of core tops across the BMC. The data show that a combination of the oxygen isotope composition of *G. inflata* and *G. truncatulinoides* (left and right) gives the most reliable information on the present position of the BMC.

4.3 Regional setting

The study area encompasses the western South Atlantic Ocean from 20 to 48°S and 37 to 60°W, and is bathymetrically represented by the western Argentine Basin in the south and the southern Brazil Basin in the north. Both basins are separated by the Santos Plateau and the Rio Grande Rise (Fig. 4.1).

The BC and the MC, together with the confluence of both currents (BMC), dominate the upper-level circulation in the study area (Peterson and Stramma, 1991; Stramma and England, 1999) (Figs. 4.1 and 4.2). The southward-flowing warm, saline and nutrient-depleted BC originates near 10°S, where the South Equatorial Current bifurcates. It is characterized as a weak western boundary current carrying subtropical water masses. At 38°S it encounters the MC, which originates as a branch of the Antarctic Circumpolar Current east of the Drake Passage and transports cold, fresh and nutrient-rich subantarctic water masses northward along the Argentinean continental shelf. The MC is assumed to be a strong current with significant bottom flow (Peterson et al., 1996). Large-scale warm- and cold-core eddies have been observed on both sides of the confluence (Garzoli and Garraffo, 1989; Garcia et al., 2004) being responsible for the expatriation of planktonic foraminifera across the BMC (Boltovskoy, 1994). After having come into contact, the

BC and the MC turn southeastward and flow offshore forming the South Atlantic Current. In the BMC both the Subtropical and the Subantarctic Fronts get very close to one another and are virtually indistinguishable (Peterson and Stramma, 1991). Different authors (Tomczak and Godfrey, 1994; Stramma and England, 1999) have described this circulation pattern as dominant from the South Atlantic Surface Water (0-100 m), through the South Atlantic Central Water (100-600 m), and down to the Antarctic Intermediate Water (600-1400 m) to the north of the BMC and from the Subantarctic Surface Water (0-400 m) down to the Antarctic Intermediate Water (400-1000 m) to the south of the confluence (Fig. 4.2).

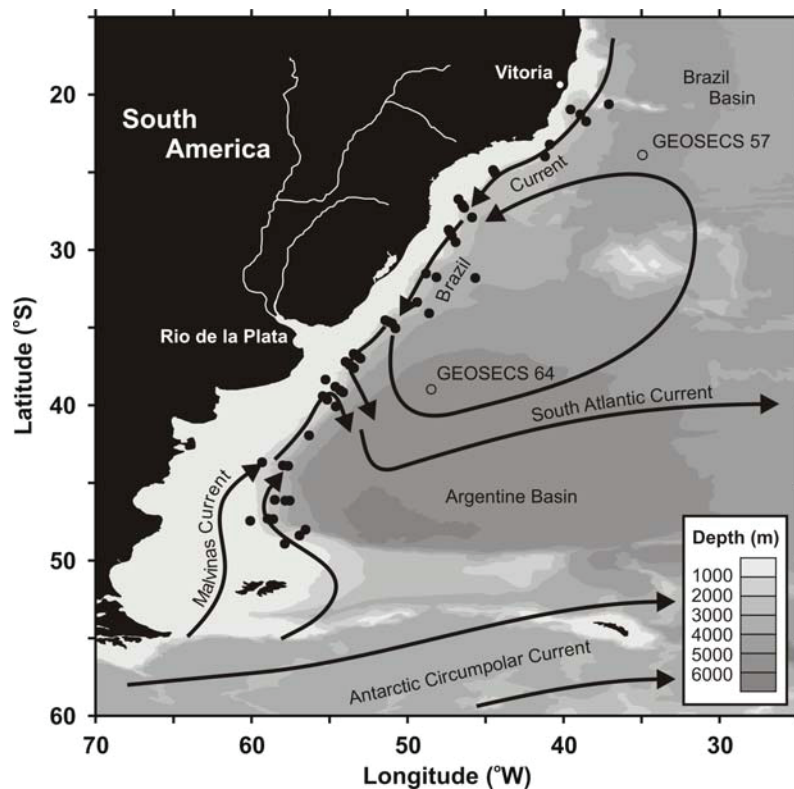


Figure 4.1. Bathymetric map of the western South Atlantic showing the locations of the investigated surface sediment samples (closed circles), selected GEOSECS stations (open circles) and schematic surface currents (arrows) after Peterson and Stramma (1991).

The location at which the currents separate from the coast varies seasonally by up to 930 km, with a northward penetration of the MC during austral winter and early spring and a southward shift of the BC during austral summer and early autumn (Olson et al., 1988). Out-of-phase changes in the mass transport of both the BC and the MC, coupled with a latitudinal displacement of the local wind stress patterns, can explain the large amplitude of the seasonal excursions of the confluence (Provost et al., 1992; Matano et al., 1993; Garzoli and Giulivi, 1994; Wainer et al., 2000).

The global gridded data set of $\delta^{18}\text{O}$ of seawater ($\delta^{18}\text{O}_w$) from LeGrande and Schmidt (2006) shows that the regional $\delta^{18}\text{O}_w/\text{salinity}$ slope is $0.51\text{‰}\ \text{psu}^{-1}$. According to the salinity gradient (Fig. 4.2) an increase in $\delta^{18}\text{O}_w$ from south to north with a major change at the BMC is observed in the study area. Despite sparse measurements, it is possible to observe that the carbon isotopic composition of total dissolved inorganic carbon (DIC) in the upper water column also increases from south to north in the study area showing an abrupt increase at the BMC (Kroopnick, 1980). Two primary components contribute to this trend: (1) the well established inverse correlation between $\delta^{13}\text{C}_{\text{DIC}}$ and nutrient content (Kroopnick, 1985; Broecker and Maier-Reimer, 1992); and (2) the nutrient concentration (Conkright et al., 2002) and primary productivity in the area (Longhurst, 1998; Brandini et al., 2000; Saraceno et al., 2005) that decreases from south to north, in good agreement with the regional oceanographic structure. An exception to the low primary productivity zone to the north of the BMC is found off the Rio de la Plata mouth and the Patos-Mirim lagoon system. Here high continental input of both nutrients and estuarine organic matter associated with shelf break upwelling greatly enhance the chlorophyll a content of local waters (Ciotti et al., 1995). Additionally, upwelling of subantarctic waters at different sites along the southern Brazilian shelf (e.g. Cape Frio at 23°S and Cape Santa Marta at 29°S) as a result of intense offshore Ekman transport increases local primary productivity (Campos et al., 2000). Although upwelled waters show lower $\delta^{13}\text{C}_{\text{DIC}}$, foraminiferal calcite from upwelling areas show higher $\delta^{13}\text{C}$ values as a result of lower carbonate ion concentration ($[\text{CO}_3^{2-}]$) values and/or lower temperature (Peeters et al., 2002). The $[\text{CO}_3^{2-}]$ in the upper water column increases from south to north in the study area (Bainbridge, 1981).

Oceanic conditions in the western Argentine Basin play an important role in the adjacent continental climate and affect the drainage basins of the Rio de la Plata and the Patos-Mirim estuaries (Doyle and Barros, 2002; Robertson et al., 2003). The Rio de la Plata drainage basin is the second largest in South America and its discharge variability was correlated to sea surface temperature (SST) variability in the western South Atlantic mainly on interdecadal time scales (Venegas et al., 1997; Robertson and Mechoso, 2000). Higher discharges have been coupled to positive SST anomalies in the western South Atlantic (Robertson and Mechoso, 2000).

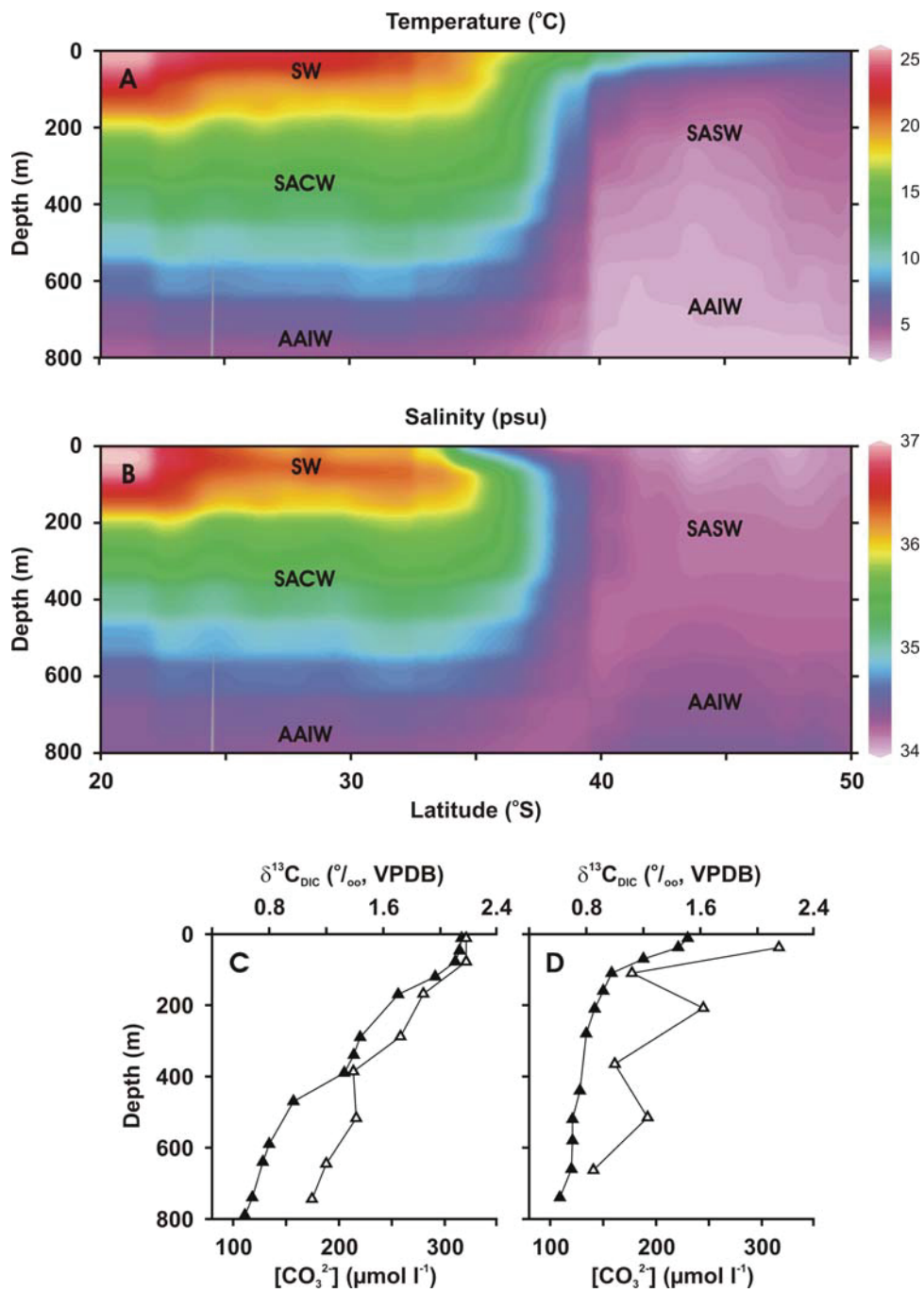


Figure 4.2. Latitudinal transects of annual mean temperature (A) (Conkright et al., 2002), salinity (B) (Conkright et al., 2002), and depth profiles of $\delta^{13}\text{C}_{\text{DIC}}$ (open triangles) (Kroopnick, 1980) and $[\text{CO}_3^{2-}]$ (closed triangles) (Bainbridge, 1981) in the water column for GEOSECS stations 57 (C) and 64 (D). The latitudinal transect closely follows the 1000 m isobath of the continental slope. For the positions of the 1000 m isobath and the GEOSECS stations see Fig. 4.1. The water masses are labeled as follows: AAIW, Antarctic Intermediate Water; SACW, South Atlantic Central Water; SASW, Subantarctic Surface Water; and SW, South Atlantic Surface Water.

4.4 Materials and methods

4.4.1 Laboratory procedures

The surface sediments examined in this study were taken during R/V *Meteor* cruises M23/2 (Bleil et al., 1993), M29/1 (Segl et al., 1994), M29/2 (Bleil et al., 1994), M46/2 (Schulz et al., 2001), M46/3 (Bleil et al., 2001a), M49/3 (Bleil et al., 2001b), and during R/V *Victor Hensen* cruise VHJOPSII/8 (Pätzold et al., 1996). The 56 sediment samples selected were raised from water depths between 200 and 3800 m and cover almost each degree of latitude between 20 and 48°S.

Samples were taken from the uppermost centimeter of 54 multicores and 2 boxcores. All samples were stained and stored in an ethanol Rose Bengal solution until further treatment in the laboratory. Samples were washed over 150 µm sieves and dried in an oven at 60°C. Dry samples were transferred into glass vials. From the > 150 µm residue about 10 well preserved specimens of *G. ruber* (pink and white, 400-550 µm), *G. trilobus* (without sack-like end-chamber, 300-450 µm), *G. bulloides* (400-550 µm), *G. inflata* (300-450 µm) and *G. truncatulinoides* (left and right, 500-650 µm) were picked using a binocular microscope. Size ranges were measured along the longest axis with a measuring reticule.

The stable isotopic composition of the shells was determined using a Finnigan MAT 252 mass spectrometer equipped with an automatic carbonate preparation device. The standard deviation of the laboratory standard was 0.07 and 0.05‰ for $\delta^{18}\text{O}$ and $\delta^{13}\text{C}$, respectively, for the measuring period at the University of Bremen. All values are listed in Table 4.1 and expressed as ‰ deviation from the Vienna Pee Dee belemnite (VPDB) standard, calibrated by NBS 18, 19 and 20 standards. The data presented in this paper are also available at the Pangaea database (<http://www.pangaea.de>).

Different stratigraphic information indicates late Holocene age for all samples (Table 4.1). For some of the samples isotope stratigraphies of gravity cores taken at the same stations have been used (Heil et al., submitted for publication). Three samples of planktonic foraminifera have been ^{14}C AMS dated (Mollenhauer et al., 2006). For samples where both oxygen isotope stratigraphy and ^{14}C AMS measurements were not available, the recent age was confirmed by the presence of stained benthic foraminifera (Harloff and Mackensen, 1997; and this study).

Table 4.1. Sample locations, stratigraphic information and listing of carbon and oxygen isotope data of the measured planktonic foraminifera.

Sample (GeoB)	Latitude (°S)	Longitude (°W)	Depth (m)	Stratigraphy	<i>G. ruber</i> (pink)		<i>G. ruber</i> (white)		<i>G. trilobus</i>		<i>G. bulloides</i>		<i>G. inflata</i>		<i>G. truncatulinoides</i> (right)		<i>G. truncatulinoides</i> (left)	
					$\delta^{13}\text{C}$	$\delta^{18}\text{O}$	$\delta^{13}\text{C}$	$\delta^{18}\text{O}$	$\delta^{13}\text{C}$	$\delta^{18}\text{O}$	$\delta^{13}\text{C}$	$\delta^{18}\text{O}$	$\delta^{13}\text{C}$	$\delta^{18}\text{O}$	$\delta^{13}\text{C}$	$\delta^{18}\text{O}$	$\delta^{13}\text{C}$	$\delta^{18}\text{O}$
2130-1	20.62	37.10	2113	SBF ^a	1.75	-1.21	1.36	-1.44	2.53	-1.00	1.27	1.51	1.68	0.93	1.53	1.42		
2124-1	20.96	39.56	2003	¹⁴ C (290 yr BP) ^b	2.02	-1.30	1.62	-1.37	2.16	-0.91			1.46	0.53	1.85	0.78		
2126-1	21.27	38.93	2537	SBF ^a	1.98	-1.36	1.79	-1.16	2.09	-0.71			1.41	0.70				
2119-2	21.73	38.55	2958	SBF ^a	1.99	-0.82	1.49	-0.68	1.57	-0.15	1.07	1.17	1.52	1.01	1.37	1.45		
3207-2	23.15	40.95	200	SBF ^a	2.19	-1.16	1.71	-0.99	2.15	-0.55			1.07	0.15				
3205-2	23.21	40.89	1140	SBF ^a	1.61	-1.54	1.24	-1.40	0.71	-1.08								
2102-1	23.98	41.20	1805	SBF ^a	1.82	-1.60	1.41	-1.33	2.44	-0.63	1.02	0.73	1.48	0.85	0.93	0.29		
6908-1	24.86	44.52	500	SBF ^a	1.74	-1.27	1.35	-1.18	1.36	-0.39	0.90	1.47	1.33	0.87				
6909-2	24.98	44.44	1032	SBF ^a	1.72	-1.38	1.72	-0.67	1.28	-0.41	1.13	1.24	1.53	0.88	1.48	0.68		
6911-2	25.09	44.37	1604	SBF ^a	1.94	-1.31	1.70	-1.47	1.68	-0.85	0.92	0.63	1.19	0.59	0.92	0.43		
2105-3	26.74	46.74	202	SBF ^a	1.57	-1.24	1.21	-0.60	1.55	-0.30	0.61	0.89	0.99	0.87				
2106-1	27.10	46.50	502	SBF ^a	1.98	-1.49	1.57	-1.05	2.15	-0.61	1.08	1.28	1.46	0.90	1.38	1.52		
2107-5	27.18	46.46	1052	IS ^c	2.10	-1.26	1.76	-1.15	1.78	-0.83	1.17	0.80	1.61	0.70	1.41	0.79		
2104-1	27.29	46.38	1505	SBF ^a	1.96	-1.41	1.41	-1.41	1.38	-1.00	1.10	0.70	1.24	0.76				
2109-3	27.91	45.87	2513	SBF ^a	2.02	-1.48	1.63	-1.20	1.93	-0.77	1.13	0.71	1.63	0.76	1.18	0.82		
6204-2	28.71	47.37	578	SBF ^a	1.60	-1.15	1.65	-1.09	1.34	-0.23	1.03	1.00	1.33	1.09	1.18	0.83		
6203-1	28.83	47.30	1001	SBF ^a	1.78	-1.51	1.54	-1.17	1.37	-0.72	1.05	1.13	1.02	0.92	1.26	0.83		
6202-5	29.09	47.17	1493	SBF ^a	2.04	-1.40	1.86	-1.34	2.27	-0.64	1.26	0.87	1.41	1.00	1.16	0.65		
6205-1	29.50	46.92	2004	SBF ^a	1.80	-1.40	1.73	-1.35	2.21	-0.74	1.04	0.71	1.58	0.92	1.21	0.55		
6210-1	31.52	48.82	2499	SBF ^a	2.03	-1.25	1.81	-0.95	2.35	-0.27	0.94	0.92	1.42	0.89	1.25	0.62		
6209-2	31.76	48.15	3013	SBF ^a	1.67	-1.03	1.48	-0.61	2.70	-0.61	1.15	0.73	1.62	0.86	1.25	0.73		
6208-1	31.81	45.66	3693	SBF ^a							1.05	1.07	1.39	1.11				
6220-1	33.36	49.39	2277	SBF ^a	2.03	-1.06	1.68	-0.80	2.00	-0.72	0.98	0.75	1.45	0.82	1.32	0.74		
6222-2	34.08	48.62	3450	SBF ^a	1.14	-1.04			1.55	-0.20	1.21	1.08	1.55	-0.20	0.77	0.69		
6214-5	34.53	51.44	1567	SBF ^a	1.62	-1.38	0.84	-0.91	1.82	-0.85	0.80	0.94	0.90	0.89				
6216-1	34.62	51.23	2032	SBF ^a	1.65	-1.62	1.11	-1.07	1.56	-0.69	0.82	0.77	1.17	1.06	0.54	0.58		
6217-2	34.72	51.00	2399	SBF ^a	1.51	-1.24	1.38	-1.16	1.62	-0.79	1.50	1.54	1.27	0.93	0.94	0.77		

6218-1	35.05	50.78	2953	SBF ^a	1.64	-1.09	1.17	-1.00	1.62	-0.58	0.98	2.45	1.11	1.10	1.42	1.14	1.05	0.86
6234-1	36.69	53.46	1140	SBF ^a	0.98	-1.16												
6233-1	36.75	53.30	1627	SBF ^a					1.35	0.18	0.88	2.88	1.59	2.57	1.97	1.68	1.46	2.78
6232-1	36.90	53.14	2560	SBF ^a					0.92	-0.67	0.11	1.83	1.06	1.44	1.05	1.04	1.19	2.26
6231-1	36.99	53.02	2955	SBF ^a					1.12	-0.54	0.83	2.26	1.19	1.69	0.98	0.96	1.02	1.62
2802-2	37.20	53.97	1007	SBF ^a							0.31	2.21	1.37	2.61			0.81	1.78
2803-1	37.41	53.71	1162	SBF ^a							0.90	2.70	1.55	2.97			1.41	2.51
2804-2	37.54	53.53	1836	¹⁴ C (0 yr BP) ^b							0.72	2.45	1.27	2.27			1.27	2.79
2805-1	37.61	53.44	2759	¹⁴ C (0 yr BP) ^b							0.52	2.03	1.27	2.13			1.23	2.31
6312-1	38.35	55.26	435	SBF ^a							0.69	2.39	1.33	2.40				
6311-2	38.81	54.63	996	SBF ^a							0.76	2.48	1.44	2.73			1.19	2.76
6310-1	39.04	54.32	1455	SBF ^a							1.00	2.57	1.39	2.65			1.20	2.81
6309-2	39.17	54.14	2869	SBF ^a							1.11	2.71	1.58	2.90			1.39	2.60
6313-2	39.42	55.44	733	SBF ^a							0.67	2.40	1.37	2.67			1.13	2.62
6314-2	39.64	55.15	1187	SBF ^a							0.64	2.61	1.24	2.65			1.15	2.82
6317-2	40.08	54.60	3115	SBF ^a							0.95	2.70	1.36	2.71	1.27	2.41	1.34	2.81
2707-4	41.94	56.32	3167	SBF ^d							0.92	2.37	1.50	2.97			1.35	3.03
2712-1	43.67	59.33	1230	SBF ^d							1.01	2.72	1.21	2.73			1.33	2.67
2714-5	43.87	58.00	2361	SBF ^d							1.10	2.84	1.55	2.87	1.42	2.62	1.42	2.90
2715-1	43.91	57.66	3277	SBF ^d							1.31	2.88	1.70	2.90	1.45	3.11	1.30	3.02
6334-2	46.09	58.52	2597	SBF ^a							0.96	2.71	1.49	2.88	1.60	3.14	1.47	3.08
6330-1	46.14	57.56	3398	SBF ^a							1.30	2.85	1.61	2.94	1.38	2.96	1.47	3.04
6336-2	46.14	57.85	3874	SBF ^a							1.26	2.71	1.54	2.91	1.41	3.21	1.47	3.13
2718-1	47.31	58.97	2991	SBF ^d							1.04	2.63	1.48	2.88			1.33	2.97
2722-2	47.33	58.62	2383	SBF ^d							1.02	2.78	1.46	2.93			1.40	3.12
2719-2	47.44	60.09	684	SBF ^d							0.90	2.53	1.28	2.76			1.29	2.58
2727-1	48.01	56.54	2819	SBF ^d							1.13	2.72	1.54	3.01			1.47	3.15
2726-3	48.39	56.93	1405	SBF ^d							0.95	2.88	1.62	3.03			1.42	3.01
2723-2	48.91	57.88	569	SBF ^d							1.18	2.67	1.65	2.79			1.41	2.67

The abbreviations are defined as follows: IS, isotopic stratigraphy; ¹⁴C, ¹⁴C AMS dating, calibrated calendar age is given in parentheses; and SBF, stained benthic foraminifera. ^a This study; ^b Mollenhauer et al. (2006); ^c Heil et al. (subm.); ^d Harloff and Mackensen (1997).

4.4.2 Comparison to hydrographic data

Temperature, salinity and phosphate concentration have been taken from the 2001 version of the World Ocean Atlas (WOA) (Conkright et al., 2002), and the $\delta^{18}\text{O}_w$ has been extracted from the global gridded data set of LeGrande and Schmidt (2006). The $\delta^{18}\text{O}_w$ has been scaled to VPDB by subtracting 0.27‰ (Hut, 1987). Finally, the predicted $\delta^{18}\text{O}$ of calcite ($\delta^{18}\text{O}_{pc}$) was calculated by solving the paleotemperature equation developed by Shackleton (1974). Planktonic foraminifera exhibit species-specific offsets from calcite predicted with empirical relationships (Bemis et al., 1998; Mulitza et al., 2003), reaching 0.8‰ difference between Shackleton's equation and the one presented by Mulitza et al. (2003) for *G. ruber* (white) at the upper temperature limit. Therefore, $\delta^{18}\text{O}_{pc}$ values obtained with Shackleton's equation should not be used to directly predict $\delta^{18}\text{O}$ of foraminiferal calcite. However, it has been shown that this equation correctly predicts the slope of the $\delta^{18}\text{O}$:temperature relationship over the entire temperature range present in the oceans for the most commonly used species (Mulitza et al., 2003). Since species-specific equations are not available for *G. inflata* and *G. truncatulinoides*, we used Shackleton's equation to calculate changes in $\delta^{18}\text{O}_{pc}$ over the BMC, and compared these changes to the magnitude of measured foraminiferal $\delta^{18}\text{O}$ changes across the confluence. The $\delta^{18}\text{O}_{pc}$ has been calculated for all depth levels of the WOA down to 800 m.

Extensive measurements of the carbon isotopic composition of surface waters over the BMC are not available at present, hampering a direct comparison between $\delta^{13}\text{C}_{\text{DIC}}$ and foraminiferal $\delta^{13}\text{C}$. However, since the $\delta^{13}\text{C}$ of dissolved inorganic carbon decreases along with increasing nutrient concentrations (Kroopnick, 1985; Broecker and Maier-Reimer, 1992) the BMC should be associated with a southward decrease of $\delta^{13}\text{C}_{\text{DIC}}$. We compared $\delta^{13}\text{C}$ of foraminiferal calcite to phosphate concentration from the WOA in order to try to identify the position of the front. Additionally, $\delta^{13}\text{C}_{\text{DIC}}$ (Kroopnick, 1980) and $[\text{CO}_3^{2-}]$ (Bainbridge, 1981) from the Geochemical Ocean Sections Study (GEOSECS) were used for further evaluation of *G. inflata* carbon isotopic composition.

Considering the lack of published foraminiferal seasonal flux measurements for the study area, and that the $\delta^{18}\text{O}_w$ data set from LeGrande and Schmidt (2006) reflect annual mean conditions, we used annual mean WOA values for comparison to the stable isotopic measurements. The occurrence of seasonality in foraminiferal flux could impose some bias in our comparison to annual mean WOA values, as suggested by King and Howard (2001, 2003) for the Southern Ocean

and Southwest Pacific. The $\delta^{18}\text{O}_{\text{pc}}$ and phosphate concentration were plotted along a latitudinal transect for the most relevant depths in Figs. 4.3 and 4.4, respectively. To delineate the hydrographic transect plotted in Figs. 4.2, 4.3 and 4.4 we first calculated the mean position of each group of surface samples within an interval of 1° of latitude and then connected these points. The resulting transect closely follows the 1000 m isobath of the continental slope.

4.5 Results

4.5.1 Oxygen isotopes

Globigerinoides ruber (pink) generally shows the lowest $\delta^{18}\text{O}$ values of all examined species, followed by *G. ruber* (white) and *G. trilobus* (Fig. 4.3). Most of the oxygen isotope values of *G. ruber* (pink and white) are lower than the $\delta^{18}\text{O}_{\text{pc}}$ for the shallowest depths calculated with the annual mean WOA data. The $\delta^{18}\text{O}$ values of these three species show a slight increase along with increasing latitude and decreasing surface water temperatures. The lowest $\delta^{18}\text{O}$ value for *G. ruber* (pink) is an exception that appears around the southernmost limit of its occurrence and which is consistent with the low surface water $\delta^{18}\text{O}$ anomaly at the outflow of the Rio de la Plata. By contrast, the oxygen isotope composition of *G. ruber* (white) and *G. trilobus* do not show low $\delta^{18}\text{O}$ values at the latitude of the Rio de la Plata outflow. If we use the species-specific $\delta^{18}\text{O}$:temperature relationships available for *G. ruber* (white) and *G. trilobus* from Mulitza et al. (2003), we get calculated calcification depth ranges of 0-100 m and 30-150 m for each species, respectively. Where parallel measurements are available, *G. ruber* (white) and *G. trilobus* show on average 0.21 and 0.66‰ higher $\delta^{18}\text{O}$ values, respectively, than *G. ruber* (pink). The mean difference between *G. ruber* (white) and *G. trilobus* accounts for 0.44‰. According to the species' biological preferences (Bijma et al., 1990), *G. ruber* (pink and white) and *G. trilobus* were just available in our samples raised to the north of the front.

The oxygen isotopic values of *G. bulloides*, *G. inflata* and *G. truncatulinoides* (left and right) are very similar to each other (Fig. 4.3), with *G. bulloides* depicting slightly lower ratios than *G. inflata* and *G. truncatulinoides* (left and right). *Globorotalia inflata* and *G. truncatulinoides* (left and right) were available over the whole transect and show a strong decrease of 2‰ associated with the BMC. However, some of the $\delta^{18}\text{O}$ values measured remain high even about 2° to the north of the main temperature increase at 250 m water depth. Remarkably stable $\delta^{18}\text{O}$ values were generally found for both species over the whole transect, especially south of the BMC.

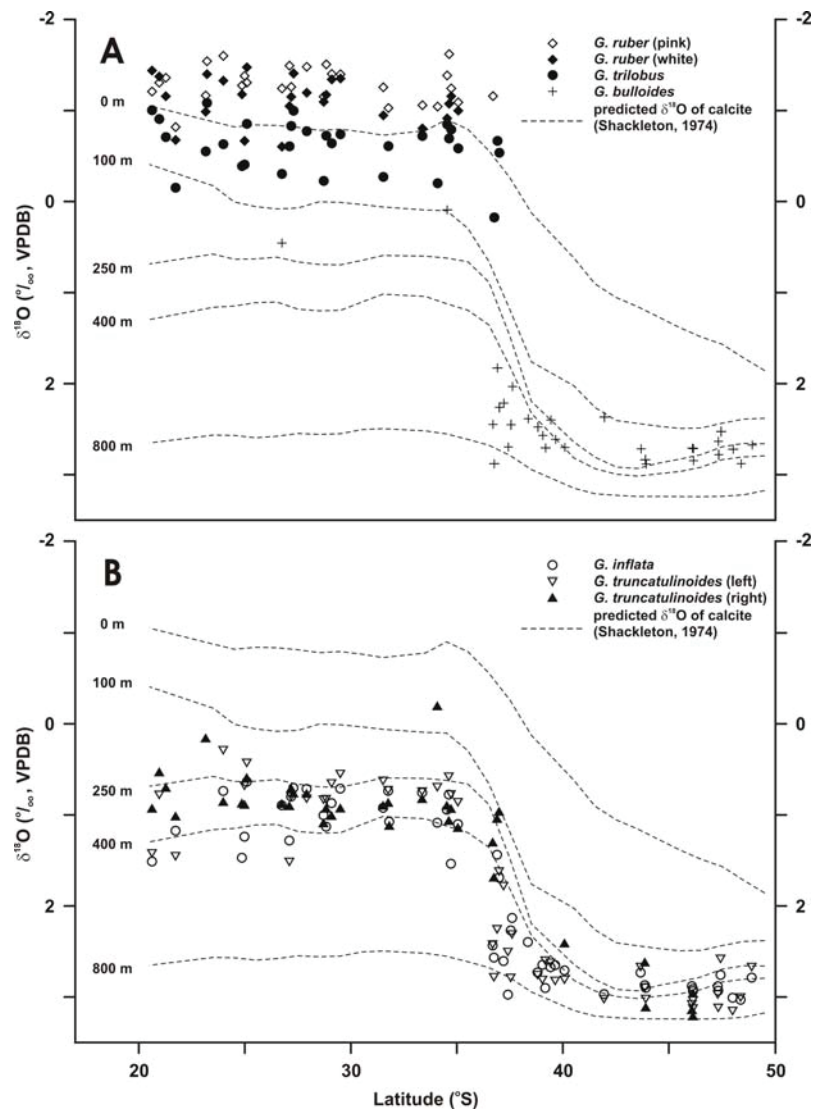


Figure 4.3. A comparison of latitudinal variations in predicted $\delta^{18}\text{O}$ of calcite at selected depth levels (dashed lines) and observed $\delta^{18}\text{O}$ values from the species measured in this work (see legend inside each panel). The predicted $\delta^{18}\text{O}$ values were calculated by extracting the $\delta^{18}\text{O}$ of seawater from the global data set of LeGrande and Schmidt (2006), scaling these values to VPDB using the Hut (1987) suggestion, and finally using the Shackleton (1974) paleotemperature equation. The latitudinal transect closely follows the 1000 m isobath of the continental slope. For the position of the 1000 m isobath see Fig. 4.1.

4.5.2 Carbon isotopes

Among all measured species *G. trilobus* and *G. ruber* (pink) show the highest $\delta^{13}\text{C}$ values (Fig. 4.4). A decrease in $\delta^{13}\text{C}$ along with a latitudinal increase in upper water column nutrient concentrations was found for *G. ruber* (pink and white) and *G. trilobus*, according to the inverse correlation between nutrient and $\delta^{13}\text{C}_{\text{DIC}}$ (Kroopnick, 1985; Broecker and Maier-Reimer,

1992). In contrast, the $\delta^{13}\text{C}$ values of *G. bulloides* and *G. inflata* increase with increasing latitude. The gradient is much stronger for *G. bulloides* than for *G. inflata*. The $\delta^{13}\text{C}$ values of these species are positively correlated with phosphate concentrations and negatively correlated with temperature from the WOA for the expected calcification depth ranges. The $\delta^{13}\text{C}$ values of *G. truncatulinoides* (left and right) do not show a distinct trend with latitude, depicting remarkably stable values south of the BMC and more scattered values north of the front.

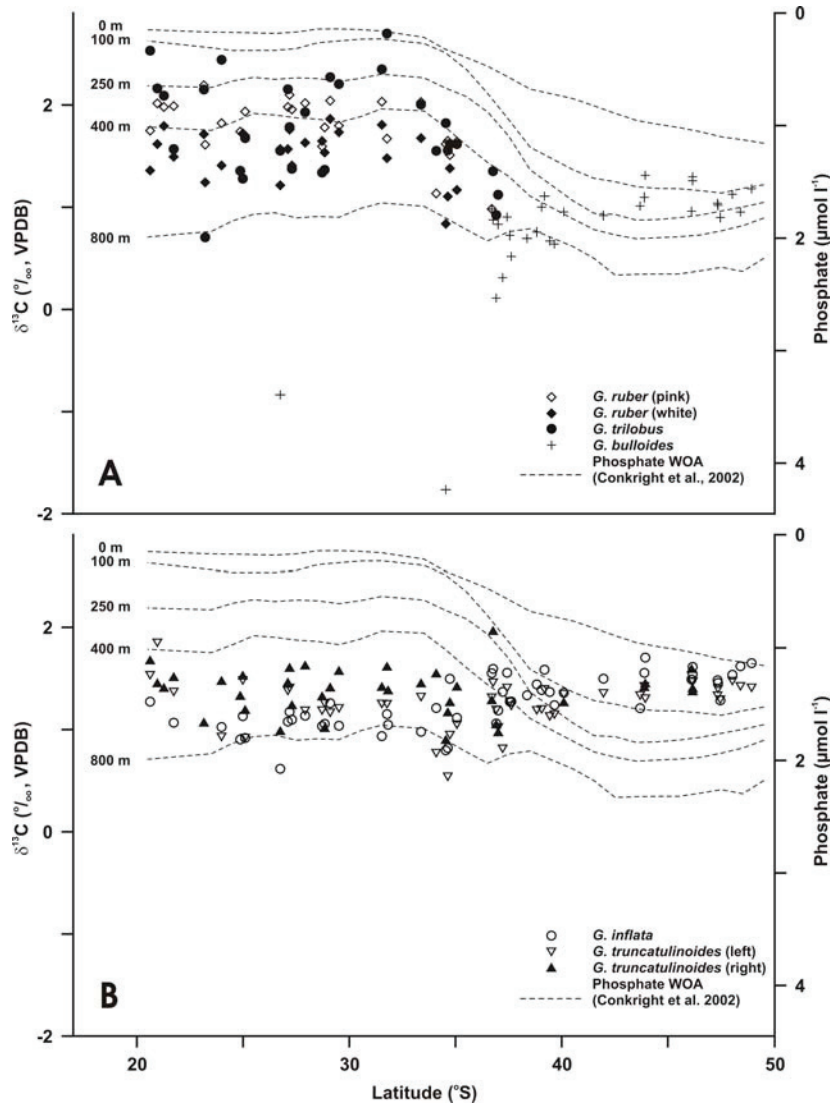


Figure 4.4. A comparison of latitudinal variations in phosphate concentration at selected depth levels (dashed lines) and observed $\delta^{13}\text{C}$ values from the species measured in this work (see legend inside each panel). Phosphate values are from the 2001 version of the World Ocean Atlas (Conkright et al., 2002). Note that the scales of $\delta^{13}\text{C}$ and phosphate have been adjusted for the Redfield slope of $1.1\text{‰} (\mu\text{mol l}^{-1})^{-1}$ phosphate (Broecker and Maier-Reimer, 1992). The latitudinal transect closely follows the 1000 m isobath of the continental slope. For the position of the 1000 m isobath see Fig. 4.1.

4.6 Discussion

4.6.1 Recording of BMC properties in oxygen isotope ratios of planktonic foraminifera

Globigerinoides ruber (pink and white) and *G. trilobus* are generally assumed to reflect near surface water conditions due to their shallow habitat (Fairbanks et al., 1980, 1982). Where parallel measurements of both species from the same sample were possible, increasingly heavier values of $\delta^{18}\text{O}$ were found for *G. ruber* (pink), *G. ruber* (white) and *G. trilobus*, respectively. Since the oxygen isotope values for living specimens of both species are undistinguishable (Mulitza et al., 2003) and considering that there is no significant difference in the seasonal flux for both species (Deuser, 1987; Deuser and Ross, 1989), it is likely that this pattern reflects slightly different calcification depths. We propose that *G. ruber* (pink) calcifies in the uppermost water column, *G. ruber* (white) registers slightly deeper conditions and *G. trilobus* records even deeper water column properties. A similar trend on calcification depths has also been observed by Duplessy et al. (1981) in the Indian Ocean. Although registered by just one sample, the shallow water low $\delta^{18}\text{O}$ anomaly characteristic of the Rio de la Plata outflow is recorded only by *G. ruber* (pink), indicating that *G. ruber* (white) and *G. trilobus* indeed have deeper calcification depths and are not affected by isotopically light fresh waters (Fig. 4.3). The Rio de la Plata plume is mainly restricted to the continental shelf, hardly reaching the shelf break, but extreme precipitation anomalies (e.g. during El Niño) over the Plata drainage basin may cause an offshore spread of the plume (Piola et al., 2005). During these events the outermost limit of the isotopically light waters may locally affect our samples, since they were collected at the shelf break or even farther offshore. The calculated calcification depth ranges with species-specific equations for *G. ruber* (white) and *G. trilobus* also indicate the species' stratified calcification depths. Therefore, *G. ruber* (pink and white) and *G. trilobus* record the upper water column conditions north of the BMC.

Globigerina bulloides can tolerate a wide range of temperatures. It is commonly found in transitional to polar water masses, but is also typical of upwelling environments regardless of their geographic position (Hemleben et al., 1989; Zaric et al., 2005). *Globigerina bulloides* is considered a surface dweller, and reflects the spring bloom in the North Atlantic (Ganssen and Kroon, 2000). In our samples, *G. bulloides* was available from surface samples to the south of the BMC, directly below the front and from two samples raised to the north of the confluence. *Globigerina bulloides* shows the highest oxygen isotope values of all measured presumably shallow dwelling species (Fig. 4.3). These values were generally very close to the $\delta^{18}\text{O}$ values of deep dwelling *G. inflata* and *G. truncatulinoides* (left and right). The latitudinal change across the BMC in $\delta^{18}\text{O}$ for *G.*

bulloides amounts to about 2.4‰ which is consistent with the predicted $\delta^{18}\text{O}_{\text{pc}}$ change for the depth range between 200 and 300 m and is significantly higher than the change predicted for surface waters (Fig. 4.3). This depth range is much deeper than the habitat observed in plankton tows in the North Atlantic (Fairbanks et al., 1980, 1982), but consistent with observations of Mortyn and Charles (2003) from plankton tows performed in the Atlantic sector of the Southern Ocean. These authors concluded that *G. bulloides* is not strictly a surface dweller in the region, having even measured maximum abundance of this species around 200 m water depth in a plankton tow operated at 41°S. It must also be taken into account that we measured large specimens of *G. bulloides* (400-550 μm) which may be partially responsible for the heavy $\delta^{18}\text{O}$ values. Niebler et al. (1999) have shown that indeed large (> 400 μm) specimens of *G. bulloides* from surface sediments show $\delta^{18}\text{O}$ values up to 0.8‰ heavier than the values depicted by smaller size fractions (200-250 μm). In accordance with previous studies, we suggest that a deeper calcification or at least a significantly deeper encrustation of big specimens (400-550 μm) of *G. bulloides* may take place in the South Atlantic.

Globorotalia inflata and *G. truncatulinoides* (left and right) are known to move deeper in the water column as they age where they continue to accumulate mass by the addition of a secondary calcite crust (Lohmann, 1995; Mulitza et al., 1997; Wilke et al., 2006). As much as 50% of the total mass of *G. truncatulinoides* shells may be made up of secondary crust (Lohmann and Schweitzer, 1990; Lohmann, 1995). Our data support those findings, since the magnitude of $\delta^{18}\text{O}$ change recorded at the BMC by *G. inflata* and *G. truncatulinoides* (left and right) are consistent with a calcification of much of the shell in water depths between 200 and 400 m (Fig. 4.3). Generally, the $\delta^{18}\text{O}$ values of both deep dwelling species are remarkably stable south of the confluence and show a sharp decrease of 2‰ at the BMC within just 2° of latitude. This latitudinal range can be easily accommodated within the seasonal variability of the BMC location (Olson et al., 1988). It is significant that the extent of $\delta^{18}\text{O}$ change across the BMC for *G. inflata* and *G. truncatulinoides* (left and right) are very similar. This suggests that calcification temperatures are comparable for these species. North of the front an increase in $\delta^{18}\text{O}$ variability is related to the high stratification of the upper water column. Taking into account the $\delta^{18}\text{O}$ values and the occurrence of both species all over the transect, the oxygen isotope composition of deep dwelling foraminifera, i.e. *G. inflata* and *G. truncatulinoides*, might be the best indicator for reconstructions of the past positions of the BMC. It is noteworthy, however, that reconstructions based on *G. truncatulinoides* south of BMC are limited to the last ~300 kyr BP (Kennett, 1970; de Vargas et al., 2001).

The decrease of the $\delta^{18}\text{O}$ values observed for *G. bulloides*, *G. inflata* and *G. truncatulinoides* (left and right) associated with the BMC seems to be slightly shifted to the north with respect to the position of the BMC (Fig. 4.3). This might be explained by three factors. First, the annual mean values in the WOA might not reflect the true annual mean position of the BMC, since winter observations are still sparse in the area. Second, it might be possible that oceanic currents and large-scale eddies carry planktonic foraminifera away from their natural habitats to regions where they continue to live but do not reproduce. This phenomenon is known as expatriation (Berger, 1970; Bijma et al., 1990; Boltovskoy, 1994), and may play a role at the BMC, because this is a region of central water formation that is subducted at the BMC and continues to flow in north-eastward direction (Stramma and England, 1999). Third, the main flux of these 3 species may be concentrated during the months in which the BMC is located to the north of its mean position (austral winter and early spring) (Olson et al., 1988). Indeed, King and Howard (2001, 2003) observed higher fluxes of *G. bulloides* and *G. inflata* during spring for the Southern Ocean and Southwest Pacific.

4.6.2 Recording of BMC properties in carbon isotope ratios of planktonic foraminifera

The occurrence of *G. ruber* (pink and white) and *G. trilobus* is limited to the region north of the BMC, which is characterized by a low phosphate content (0.12-0.57 $\mu\text{mol l}^{-1}$ at 0 m). Thus, the insignificant correlation coefficients observed between nutrient content and the $\delta^{13}\text{C}$ values of *G. ruber* (pink and white) and *G. trilobus* (0.46, 0.33 and 0.16, respectively) are not surprising (Fig. 4.5).

Globigerina bulloides is available over a broader range of phosphate contents (0.22-1.12 and 0.75-1.8 $\mu\text{mol l}^{-1}$ at 0 and 250 m, respectively) but shows a positive correlation with nutrient concentrations and hence a negative correlation with temperature and with $\delta^{13}\text{C}_{\text{DIC}}$ of surface waters (Fig. 4.5). Culturing experiments have shown that temperature has a large influence on the carbon isotopic composition of *G. bulloides* (Bemis et al., 2000). The respiration rate and therefore the amount of incorporated light metabolic CO_2 increases with increasing temperature. The slope of $-0.2\text{‰ }^{\circ}\text{C}^{-1}$ temperature increase is not far from the slope observed in culture experiments by Bemis et al. (2000), which suggests that temperature is the main factor influencing relative changes in the carbon isotopic composition of *G. bulloides*. This relationship may be used to give additional evidence for the position of the BMC, when measured on a time slice.

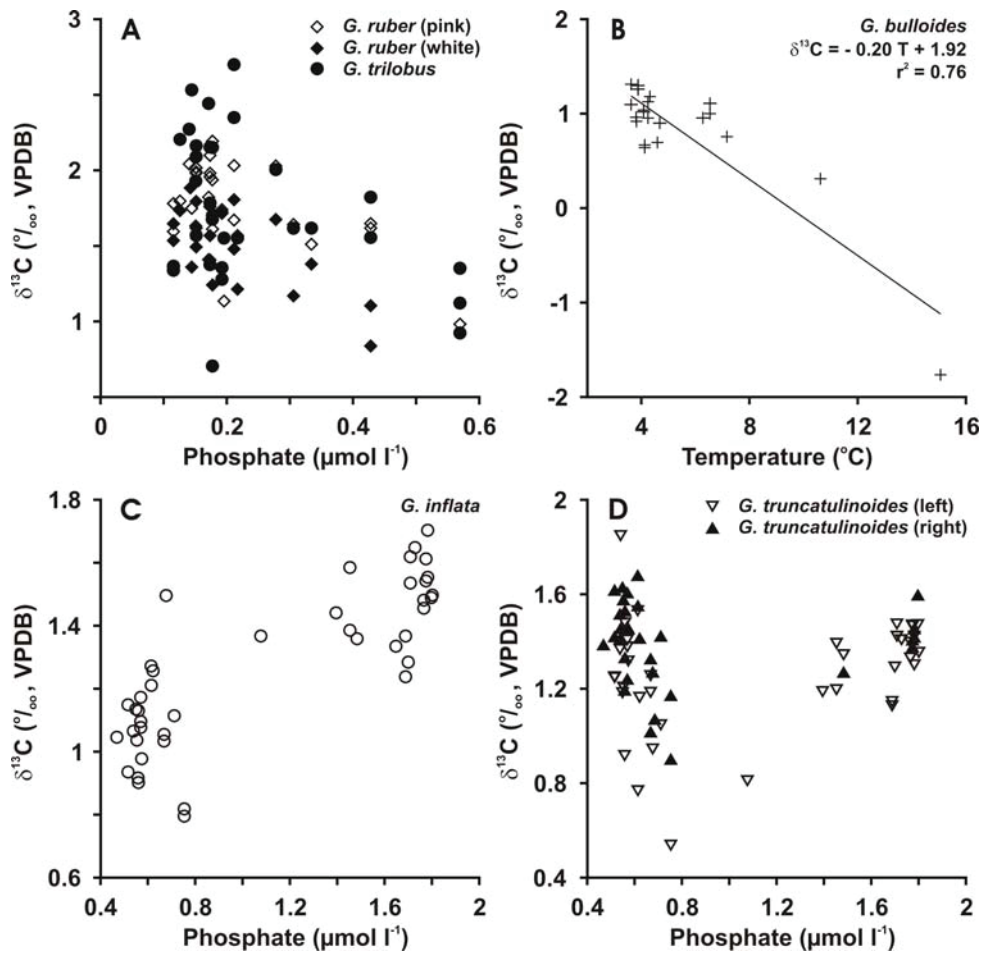


Figure 4.5. A: $\delta^{13}\text{C}$ of *G. ruber* (pink and white) and *G. trilobus* versus phosphate concentration in surface waters (0m). B: $\delta^{13}\text{C}$ of *G. bulloides* versus temperature at 250 m. Line indicates linear regression. C: $\delta^{13}\text{C}$ of *G. inflata* versus phosphate concentration at 250 m. D: $\delta^{13}\text{C}$ of *G. truncatulinoides* (left and right) versus phosphate concentration at 250 m. See legend inside each panel. Phosphate and temperature values are from the 2001 version of the World Ocean Atlas (Conkright et al., 2002). Note different scales.

Measurements of $\delta^{13}\text{C}$ over the whole transect were possible for *G. inflata* and *G. truncatulinoides* (left and right). Just as found for *G. bulloides*, the $\delta^{13}\text{C}$ values of *G. inflata* show a positive correlation with nutrient concentrations (Fig. 4.5). The $\delta^{13}\text{C}$ values of *G. truncatulinoides* (left and right), on the other hand, depict no trend with nutrient concentrations (Fig. 4.5). Wilke et al. (2006) have recently shown that the $\delta^{13}\text{C}$ of *G. inflata* is mainly controlled by the $\delta^{13}\text{C}_{\text{DIC}}$ of the seawater and its $[\text{CO}_3^{2-}]$, and the influence of other effects, such as temperature, are negligibly small. These two main influencing parameters act in opposite directions, and Wilke et al. (2006) have calculated $\delta^{13}\text{C}/[\text{CO}_3^{2-}]$ slopes for *G. inflata* of -0.013‰ to -0.015‰ ($\mu\text{mol kg}^{-1}$) $^{-1}$. In order to assess the effect of both factors on the $\delta^{13}\text{C}$ of *G. inflata* we used $\delta^{13}\text{C}_{\text{DIC}}$ (Kroopnick, 1980) and

[CO₃²⁻] (Bainbridge, 1981) values for the only two GEOSECS stations available in the study area where both parameters have been measured (Fig. 4.1). Since this species adds a significant amount of its shell below the thermocline (Wilke et al., 2006), we used interpolated values for 250m water depth. The net effect of both parameters would result in *G. inflata* shells with a 0.91 to 1.1‰ heavier carbon isotopic composition for the individuals calcified around GEOSECS station 64 (southern station) in relation to the shells calcified near station 57 (northern station). Indeed, our observed data show a comparable trend. However, the observed difference is lower, accounting for 0.37‰ if we consider samples collected approximately at the same latitudes as the GEOSECS stations. Some factors that could be responsible for the remaining difference include: (1) the $\delta^{13}\text{C}/[\text{CO}_3^{2-}]$ slopes from Wilke et al. (2006) have been calculated for specimens smaller (250-355 μm) than the ones we have selected (300-450 μm); (2) GEOSECS $\delta^{13}\text{C}_{\text{DIC}}$ and [CO₃²⁻] values reflect the conditions during the sampling period which is not necessarily coincident with *G. inflata* peak flux for the study area; and (3) the location of our samples and the GEOSECS stations do not agree, since our samples were collected some longitudinal degrees to the west of the GEOSECS stations and the main calcification depth of *G. inflata* may change according to slightly different upper water column stratification conditions between our sampling locations and GEOSECS stations.

The greater scattering shown by the $\delta^{13}\text{C}$ values of *G. truncatulinoidea* (left and right) to the north of the BMC (Fig. 4.4) could be a result of the even deeper encrustation depths characteristic of this species (e.g. Lohmann and Schweitzer, 1990; Mulitza et al., 1997) associated with the highly stratified nature of the upper water column on the northern side of the confluence.

4.7 Paleocceanographic implications and conclusions

We have measured the oxygen and carbon isotopic composition of *G. ruber* (pink and white), *G. trilobus*, *G. bulloidea*, *G. inflata* and *G. truncatulinoidea* (left and right) on a latitudinal transect across the BMC. Our results show that the oxygen isotope composition of deep dwelling *G. inflata* and *G. truncatulinoidea* (left and right) record the steep subsurface temperature gradient across the front and are the most reliable indicators of the latitudinal position of the BMC. These species are ideal for this purpose because they occur over the whole transect and grow in water masses with low seasonal variability. The oxygen and carbon isotopic composition of *G. bulloidea* also records subsurface temperature gradients, but *G. bulloidea* was mainly present south of the modern position of the BMC. The $\delta^{13}\text{C}$ of *G. ruber* (pink and white), *G. trilobus*, *G. inflata* and *G.*

truncatulinoides (left and right) shows no significant trend across the front and is hence of limited use for determining the past location of the BMC.

Acknowledgments: This work was supported by the Deutsche Forschungsgemeinschaft as part of the DFG-Research Center Ocean Margins of the University of Bremen, the CNPq-Brazil Fellowship granted to C. M. C. and the RCOM Summer Student Fellowship completed by S. U. Thanks to Kai-Uwe Hinrichs and Birgit Schminke for their support and Monika Segl for help with the isotope analyses. Logistic and technical assistance was provided by the Captain and Crew of the R/V *Meteor* and R/V *Victor Hensen*. We also thank two anonymous reviewers for their thorough and constructive comments. This is RCOM publication No. 0469.

Chapter 5

South Atlantic interocean exchange as the trigger for the Bølling warm event

Cristiano Mazur Chiessi, Stefan Mulitza, André Paul, Jürgen Pätzold, Jeroen Groeneveld, Gerold Wefer

MARUM-Center for Marine Environmental Sciences, University of Bremen, Leobener Strasse, 28359 Bremen, Germany

Accepted for publication in *Geology*

5.1 Abstract

North Atlantic high latitudes experienced an abrupt temperature increase of 9°C within a couple of decades during the transition from Heinrich event 1 (H1) to the Bølling warm event, but the mechanism responsible for this warming remains uncertain. Here we address this issue presenting high-resolution last deglaciation planktic and benthic foraminiferal records of temperature and oxygen isotopic composition of seawater ($\delta^{18}\text{O}_{\text{sw}}$) for the subtropical South Atlantic permanent thermocline and intermediate depths. During the transition, we identify a warming of $\sim 6.5^\circ\text{C}$ and an increase in $\delta^{18}\text{O}_{\text{sw}}$ of 1.2 ‰ at the permanent thermocline, and a simultaneous warming of $\sim 3.5^\circ\text{C}$ with no significant change in $\delta^{18}\text{O}_{\text{sw}}$ at intermediate depths. Most of the warming can be explained by tilting the South Atlantic east-west isopycnals from a flattened towards a steepened position associated with a collapsed (H1) and strong (Bølling) Atlantic meridional overturning circulation (AMOC), respectively. However, this zonal seesaw explains an increase of just 0.3 ‰ in permanent thermocline $\delta^{18}\text{O}_{\text{sw}}$. Considering that $\delta^{18}\text{O}_{\text{sw}}$ at the South Atlantic permanent thermocline is strongly influenced by the inflow of salty Indian Ocean upper waters, we suggest that a strengthening in the Agulhas Leakage has taken place at the transition from H1 to the Bølling being responsible for the change in $\delta^{18}\text{O}_{\text{sw}}$ recorded in our site. Our records highlight the important role played by Indian-Atlantic interocean exchange as the trigger for the resumption of the AMOC and the Bølling warm event.

5.2 Introduction

The increase in sea-surface temperature in the Southern Ocean, initial sea-ice retreat around Antarctica and atmospheric CO₂ rise began as early as 19 cal kyr BP. In contrast, deglacial changes in the high latitudes of the North Atlantic did not commence until ~14.7 cal kyr BP. This delay and the abrupt nature of the northern high latitudes deglacial response are usually linked to the variability of the Atlantic meridional overturning circulation (AMOC). After the last glacial maximum (LGM), a first short-lived meltwater pulse around 19 cal kyr BP delivered to the Nordic Seas (Clark et al., 1996) and subsequent melting of icebergs from the Laurentide ice sheet (Heinrich event 1 (H1)) (Bond et al., 1992) generated a dramatic quasi-cessation of the AMOC (McManus et al., 2004). The slowdown of the AMOC lasted until ~14.7 cal kyr BP and cooled the North Atlantic. Concurrent to the resumption of the AMOC the higher latitudes of the North Atlantic experienced an abrupt warming of up to 9°C within a couple of decades, known as the Bølling warm event (Severinghaus and Brook, 1999). The transition from the H1 to the Bølling is probably the most striking climatic feature of the Northern Hemisphere high latitudes during the last deglaciation. Yet, it is still not clear which mechanism was responsible for this transition (e.g. Knorr and Lohmann, 2003; Weaver et al., 2003; Weber and Drijfhout, 2007). A strong candidate is the strengthening of the inflow of Indian Ocean waters into the South Atlantic via Agulhas Leakage, as modeled by Weijer et al. (2002) and Knorr and Lohmann (2003). According to the modeled scenario, an amplified Agulhas Leakage would increase the salinity of the upper Atlantic Ocean and precondition the Atlantic for NADW formation. The lack of proxy data with sufficient temporal resolution from sensitive sites has so far hindered the appropriate evaluation of the modeled hypothesis. Here we address this issue with a high temporal resolution record (~15 yr spacing between adjacent measurements) from the subtropical South Atlantic.

5.3 Material and methods

We investigated the last deglaciation section (from ~90 to 550 cm core depth) of marine sediment core GeoB6211-2 recovered from the upper continental slope off southeastern South America (32.50°S, 50.24°W, 657 m water depth) (Fig. 5.1A). Our age model for GeoB6211-2 is based on seven accelerator mass spectrometry (AMS) radiocarbon measurements (Leibniz-Laboratory for Radiometric Dating and Stable Isotope Research, Kiel, Germany). Raw radiocarbon dates were calibrated with the CALIB 5.0.2 software (Stuiver and Reimer, 1993) and the Marine04 calibration curve (Hughen et al., 2004) (Supplementary material Table 5.1 and Fig. 5.4).

We measured Mg/Ca ratios and oxygen isotopic composition ($\delta^{18}\text{O}$) in the tests (shells) of deep-dweller planktic foraminifera *Globorotalia inflata* and benthic foraminifera *Uvigerina bifurcata* to estimate past temperature and $\delta^{18}\text{O}$ of seawater ($\delta^{18}\text{O}_{\text{sw}}$) variation at the permanent thermocline and at the bottom of the water column, respectively. We converted Mg/Ca ratios to temperatures ($T_{\text{Mg/Ca}}$) using empirical equations for *G. inflata* (see Supplementary material) and *U. bifurcata* (Lear et al., 2002). $\delta^{18}\text{O}$ in foraminiferal calcite ($\delta^{18}\text{O}_{\text{c}}$) is controlled by the calcification temperature and the $\delta^{18}\text{O}_{\text{sw}}$, which depends on local $\delta^{18}\text{O}_{\text{sw}}$ and mean oceanic $\delta^{18}\text{O}_{\text{sw}}$ related to continental ice volume. To infer changes in local $\delta^{18}\text{O}_{\text{sw}}$, a proxy for salinity, we combined $T_{\text{Mg/Ca}}$ and $\delta^{18}\text{O}_{\text{c}}$ in the paleotemperature equation from Shackleton (1974). Finally, we corrected the $\delta^{18}\text{O}_{\text{sw}}$ values for continental ice volume changes using an updated version of the sea level curve of Lambeck and Chappell (2001) multiplied by a constant coefficient of 1.0 ‰/130 m (Schrag et al., 2002), to get ice volume corrected $\delta^{18}\text{O}_{\text{sw}}$ ($\delta^{18}\text{O}_{\text{ivc-sw}}$).

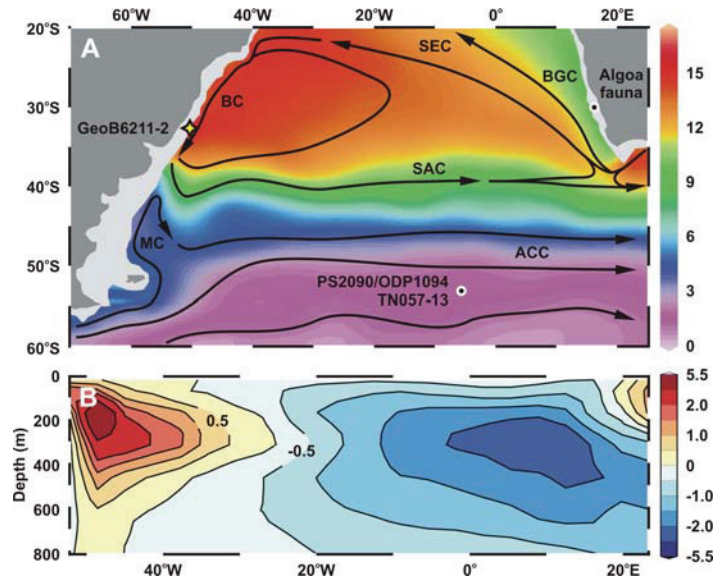


Figure 5.1. Location of paleoclimatic archives discussed in the text and temperature anomalies in the South Atlantic between the “Bølling-like” and “Heinrich-like” modeled climate states. A: Mean annual temperature (color shading, in °C) (Conkright et al., 2002) and horizontal circulation (black lines) (modified from Stramma and England, 1999) at ~300 m water depth in the South Atlantic and the Southern Ocean. Yellow star indicates location of GeoB6211-2 and black dots represent other paleoclimatic archives (Alga fauna, Pether, 1994; TN057-13, Shemesh et al., 2002; PS2090/ODP1094, Bianchi and Gersonde, 2004). The currents are labeled as follows: ACC-Antarctic Circumpolar Current, BC-Brazil Current, BGC-Benguela Current, MS-Malvinas Current, SAC-South Atlantic Current, SEC-South Equatorial Current. B: Simulated temperature anomalies (“Bølling-like” - “Heinrich-like”) for an east-west transect at 35.1°S across the South Atlantic (color shading, in °C).

We used the University of Victoria (UVic) Earth System Climate Model (ESCM, version 2.8) (Weaver et al., 2001) to simulate a “Bølling-like” (BL, active AMOC) and a “Heinrich-like” (HL, collapsed AMOC) climate state. We compared both states focusing on the difference in ocean temperature due to the AMOC collapse. For further information on methods see Supplementary material.

5.4 Results and discussion

The benthic $\delta^{18}\text{O}$ record shows an abrupt change of 1.1 ‰ towards lower values around 15 cal kyr BP and an excursion of ~ 0.6 ‰ towards higher values from 13.5 to 12 cal kyr BP (Fig. 5.2A). $T_{\text{Mg/Ca}}$ reveal an increase of $\sim 3.5^\circ\text{C}$ for the bottom of the water column at around 15 cal kyr BP (Fig. 5.2B). Not as clearly defined as the $T_{\text{Mg/Ca}}$ change around 15 cal kyr BP, bottom water $\delta^{18}\text{O}_{\text{ivc-sw}}$ ($\delta^{18}\text{O}_{\text{ivc-bsw}}$) decrease 0.5 ‰ across the major step in benthic $\delta^{18}\text{O}$ (Fig. 5.2C). Whereas the $T_{\text{Mg/Ca}}$ change is highly significant (Lear et al., 2002), that is not the case for the decrease in $\delta^{18}\text{O}_{\text{ivc-bsw}}$, which is smaller than the typical 2σ for $\delta^{18}\text{O}_{\text{ivc-sw}}$ reconstructions (~ 0.8 ‰) (Schmidt, 1999). At the permanent thermocline, our planktic $\delta^{18}\text{O}$ record shows centennial-scale oscillations superimposed on a long-term trend of decreasing values (0.6 ‰) for the whole period with relatively little change at 15 cal kyr BP (0.2 ‰ decrease) and no clear trend during the interval from 13.5 to 12 cal kyr BP (Fig. 5.2D). On the other hand, similarly to the benthic $\delta^{18}\text{O}$ record, $T_{\text{Mg/Ca}}$ at the permanent thermocline show an abrupt increase of $\sim 6.5^\circ\text{C}$ at around 15 cal kyr BP followed by gradual cooling and an excursion of $\sim 2.0^\circ\text{C}$ towards lower temperatures from 13.5 to 12 cal kyr BP (Fig. 5.2E). Calculated $\delta^{18}\text{O}_{\text{ivc-sw}}$ for the permanent thermocline ($\delta^{18}\text{O}_{\text{ivc-ptsw}}$) follows the trend of the $T_{\text{Mg/Ca}}$ record and shows an abrupt increase (~ 1.2 ‰) at around 15 cal kyr BP followed by gradual decrease and an excursion of ~ 0.6 ‰ towards lower values from 13.5 to 12 cal kyr BP (Fig. 5.2F). For the permanent thermocline, changes in $T_{\text{Mg/Ca}}$ and $\delta^{18}\text{O}_{\text{ivc-ptsw}}$ are highly significant at least for the major steps around 15 cal kyr BP (Schmidt, 1999).

The tilt of the contours of equal seawater density (isopycnals) in a latitudinal transect across the subtropical South Atlantic is arguably a clear evidence for the present-day relatively strong AMOC (e.g. Hall and Bryden, 1982). The tilt is particularly steep in the upper ocean (say first 1000 m) and reflects the northward flowing upper branch of the AMOC, since the wind-driven component of the geostrophic flow is closed in the subsurface ocean. During periods of a slowdown (strengthening) in the AMOC like during H1 (Bølling-Allerød) one would expect a flattening (steepening) of these contours, affecting the distribution of temperature and salinity.

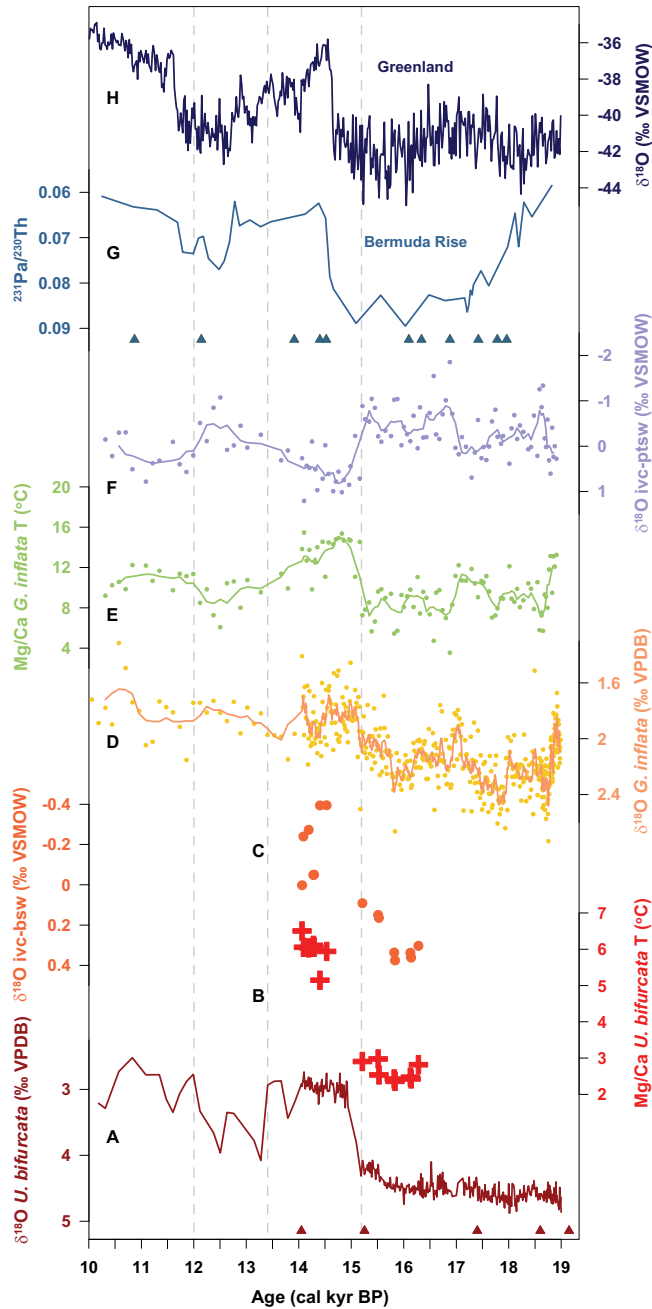


Figure 5.2. Last deglaciation records from GeoB6211-2, Atlantic meridional overturning circulation and Greenland climate. A: GeoB6211-2 *U. bifurcata* $\delta^{18}\text{O}$. B: GeoB6211-2 *U. bifurcata* Mg/Ca temperatures. C: GeoB6211-2 continental ice volume corrected seawater $\delta^{18}\text{O}$ for the bottom of the water column, calculated using *U. bifurcata* Mg/Ca temperatures and $\delta^{18}\text{O}$, the paleotemperature equation of Shackleton (1974) and an updated version of the sea level curve of Lambeck and Chappell (2001) multiplied by a constant coefficient of 1.0 ‰/130 m (Schrag et al., 2002). D: GeoB6211-2 *G. inflata* $\delta^{18}\text{O}$. E: GeoB6211-2 *G. inflata* Mg/Ca temperatures. F: GeoB6211-2 continental ice volume corrected seawater $\delta^{18}\text{O}$ for the permanent thermocline calculated as in (C) but using *G. inflata* Mg/Ca temperatures and $\delta^{18}\text{O}$. G: GGC5 $^{231}\text{Pa}/^{230}\text{Th}$ (McManus et al., 2004). H: North Greenland Ice Core Project (NGRIP) $\delta^{18}\text{O}$ (NGRIP members, 2004) plotted versus the Greenland Ice Core Chronology 2005 (GICC05) (Rasmussen et al., 2006). Individual measurements (dots) and five-point running average (curve) are shown for (C), (D), and (E). Age control points (triangles) are shown below each respective curve. Vertical dashed lines indicate major changes in our records. VPDB-Vienna Peedee belemnite. VSMOW-Vienna standard mean ocean water.

Given the present-day temperature field in the South Atlantic (Fig. 5.1A), a flattening (steepening) in the isopycnals would generate a relative cooling (warming) at any given depth in the upper western South Atlantic and a warming (cooling) at the same depth in the opposite side of the basin (Fig. 5.5). Similar changes are also expected for salinity and $\delta^{18}\text{O}_{\text{sw}}$.

An abrupt strengthening in AMOC took place at the transition from the H1 to the Bølling, where it shifted from an almost shutdown to near present-day values (e.g. McManus et al., 2004). Accordingly, a shift in the slope of the isopycnals at 32.5°S in the South Atlantic going from a horizontal position (collapsed AMOC) towards the present-day situation (relatively strong AMOC) would alone cause a temperature increase at our core site of around 5°C and 3°C for the permanent thermocline and the bottom of the water column, respectively (Fig. 5.5). These values are very close to the abrupt changes we measured at ~15 cal kyr BP.

An abrupt strengthening in AMOC took place at the transition from the H1 to the Bølling, where it shifted from an almost shutdown to near present-day values (e.g. McManus et al., 2004). Accordingly, a shift in the slope of the isopycnals at 32.5°S in the South Atlantic going from a horizontal position (collapsed AMOC) towards the present-day situation (relatively strong AMOC) would alone cause a temperature increase at our core site of around 5°C and 3°C for the permanent thermocline and the bottom of the water column, respectively (Fig. 5.5). These values are very close to the abrupt changes we measured at ~15 cal kyr BP.

The temperature anomalies in an east-west transect at 35.1°S across the South Atlantic between our HL and BL climate states ran with the UVic ESCM support this interpretation (Figs. 5.1B and 5.6). The east-west dipole-pattern in temperature anomalies (zonal seesaw) shows positive (negative) values in the western (eastern) side of the basin and is most pronounced in the permanent thermocline. The vertical structure and the magnitude of the simulated temperature anomalies compare favorably with the present-day difference between two stations located at both extremes of the subtropical South Atlantic (Fig. 5.5) and seem to be generated by a shift in the slope of the isopycnals.

A similar tilt in the isopycnals explains an increase of ~0.3 ‰ and 0.05 ‰ in $\delta^{18}\text{O}_{\text{sw}}$ for the permanent thermocline and the bottom of the water column (Fig. 5.5). Around 15 cal kyr BP we estimated an increase as big as 1.2 ‰ in $\delta^{18}\text{O}_{\text{ivc-ptsw}}$ and a decrease of 0.5 ‰ in $\delta^{18}\text{O}_{\text{ivc-bsw}}$, although the latter value should be interpreted with caution since it is smaller than the associated error. The discrepancy of the observed and estimated changes in $\delta^{18}\text{O}_{\text{sw}}$, especially for the permanent

thermocline, clearly requires an additional process to have happened synchronous to the steepening in the isopycnals at around 15 cal kyr BP.

Interocean exchange is a key process controlling the properties of upper water masses in the South Atlantic Ocean (e.g. Poole and Tomczak, 1999). Gordon et al. (1992) calculated that more than 60% of the Benguela Current central waters are relatively warm and salty waters drawn from the Indian Ocean via Agulhas Leakage. For greater depths of the Benguela Current, You et al. (2003) estimated that around 80% of intermediate depth waters is composed by relatively cold and fresh waters from the Pacific Ocean that entered the Atlantic through the Drake Passage. These water masses entering the Atlantic from both neighboring oceans help to balance the outflow of NADW at greater depths and strongly contribute to the northward flowing upper branch of the AMOC (e.g. Broecker 1991; Gordon et al., 1992). The thermal anomaly related to the inflow of Indian Ocean waters is attenuated along the northward flow but its salinity characteristics persists (Weijer et al., 2002). Consequently, the addition of salty Indian Ocean waters into the South Atlantic may precondition the Atlantic for NADW formation (Gordon et al., 1992; Weijer et al., 2002). Past changes in magnitude and intensity of the Agulhas Leakage indeed impacted the properties of upper water masses in the South Atlantic with possible consequences for the strength of the AMOC, as already described for glacial-interglacial time-scales (e.g. Peeters et al., 2004). Increased Agulhas Leakage is generally assigned to interglacials, whereas the opposite situation has been described for the glacials. Somewhere during the deglaciation we expect to have a shift from the weak glacial Agulhas Leakage into its interglacial mode of operation.

Since the waters of the Brazil Current bathing our site are drawn from the South Equatorial Current that in turn is fed by the Benguela Current (Fig. 5.1A), strong changes in Agulhas Leakage should be readily detectable at central water depths at our site, by changes in $\delta^{18}\text{O}_{\text{ivc-ptsw}}$. After the LGM where we expect to have a weak Agulhas Leakage (e.g. Paul and Schäfer-Neth, 2003; Peeters et al., 2004), the first outstanding peak in $\delta^{18}\text{O}_{\text{ivc-ptsw}}$ (and consequently in salinity) recorded in our site occurs around 15 cal kyr BP. We calculated that up to 0.3 ‰ of increase in $\delta^{18}\text{O}_{\text{ivc-ptsw}}$ could be explained by a steepening in the South Atlantic east-west isopycnals associated to the strengthening of the AMOC. The still unexplained difference between observed and estimated changes (0.9 ‰) could be driven by an abrupt strengthening of the Agulhas Leakage at ~15 cal kyr BP, concurrent (within age model uncertainties) to the resumption of the AMOC and the onset of the Bølling warm event in the higher latitudes of the North Atlantic.

Two high resolution records of surface seawater $\delta^{18}\text{O}_{\text{ivc-sw}}$ ($\delta^{18}\text{O}_{\text{ivc-ssw}}$) show higher salinities along the route of warm and salty water transport from the Indian to the Atlantic Ocean between 18 and 14.5 cal kyr BP and during the Younger Dryas (Levi et al., 2007) (Fig. 5.3B). These periods of increased salinity in the Indian Ocean coincide with the low salinity periods recorded at the permanent thermocline in our site. The strengthening of the Agulhas Leakage at around 15 cal kyr BP released the accumulated salty waters to the South Atlantic Ocean controlling the changes in $\delta^{18}\text{O}_{\text{sw}}$ of both sites.

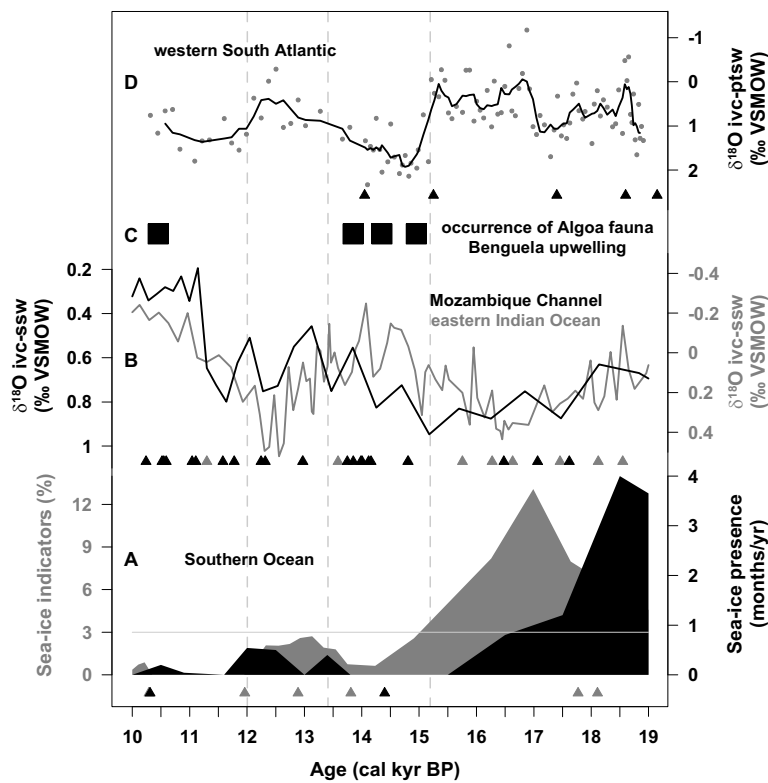


Figure 5.3. Comparison of deglacial changes in GeoB6211-2 permanent thermocline seawater $\delta^{18}\text{O}$ with paleoclimatic records from the Indian and Southern Oceans. A: Sea-ice duration in the Atlantic sector of the Southern Ocean; black shaded area (TN057-13), sea-ice presence estimated by transfer function (Shemesh et al., 2002); gray shaded area (PS2090/ODP1094), sea-ice extent assessed by relative abundance of *Fragilariopsis curta* and *F. cylindrus*, where a relative abundance greater than 3% denotes a recurrent presence of winter sea-ice (Bianchi and Gersonde, 2004). B: Continental ice volume corrected sea surface $\delta^{18}\text{O}$ from the eastern tropical Indian Ocean MD98-2165 (gray trace) and from the Mozambique Channel MD79-257 (black trace) (Levi et al., 2007). C: Occurrence of Alga fauna in the Benguela upwelling area (Pether, 1994). D: GeoB6211-2 continental ice volume corrected seawater $\delta^{18}\text{O}$ for the permanent thermocline (see caption of Fig. 5.2). Individual measurements (dots) and five-point running average (curve) are shown. Age control points (black/gray coded triangles) are shown below each respective curve. Vertical dashed lines indicate major changes in our records. VSMOW-Vienna standard mean ocean water.

At 14.9 cal kyr BP, the first appearance of Alga fauna (warm-temperate endemic bivalves from the Agulhas Bank and the SW Indian Ocean) in the Benguela upwelling area (cool-temperate) reflects the first strong inflow of Indian Ocean waters into the South Atlantic after the LGM (Fig. 5.3C) (Pether, 1994). This observation fits remarkably well into our explanation to the abrupt increase in $\delta^{18}\text{O}_{\text{ivc-ptsw}}$ recorded in our site.

The two better resolved records (regarding temporal resolution and age model) of sea-ice extent in the Atlantic sector of the Southern Ocean agree that at ~15 cal kyr BP maximum extension of winter sea-ice retreated to the south of 53°S for the first time during the deglaciation (Shemesh et al., 2002; Bianchi and Gersonde, 2004) (Fig. 5.3A). This marked retreat was most probably associated to a southward shift in the meridional density gradient across the frontal zones around Antarctica (Borowski et al., 2002). As the frontal zones shifted southwards, the northern boundary of the Antarctic Circumpolar Current also retreated southwards (Borowski et al., 2002; Paul and Schäfer-Neth, 2003). Simultaneously, more Agulhas Current waters were able to reach the South Atlantic and the Agulhas Leakage recovered its interglacial strength. The high salinity waters formerly accumulated in the upper water column of the Indian Ocean (Levi et al., 2007) flooded the central depths of the South Atlantic and were clearly detected as a 0.9 ‰ anomaly in our $\delta^{18}\text{O}_{\text{ivc-ptsw}}$ record.

5.5 Conclusions

At ~15 cal kyr BP our high-resolution records from the permanent thermocline of the western subtropical South Atlantic show a warming of ~6.5°C and an increase in $\delta^{18}\text{O}_{\text{ivc-ptsw}}$ of 1.2 ‰ while at intermediate depths we identify a warming of ~3.5°C and no significant change in $\delta^{18}\text{O}_{\text{ivc-bsw}}$. Most of the warming (5°C and 3°C, respectively) can be explained by tilting the South Atlantic east-west isopycnals from a horizontal position (collapsed AMOC, as during the H1) towards its present-day situation (relatively strong AMOC, as during the Bølling). On the other hand, the same tilt explains just 0.3 ‰ change in $\delta^{18}\text{O}_{\text{ivc-ptsw}}$ requiring an additional process to be responsible for the remaining 0.9 ‰. Salinity in the central water masses of the South Atlantic is strongly influenced by the inflow of salty Indian Ocean upper waters into the South Atlantic. We suggest that a strengthening in Agulhas Leakage has taken place at ~15 cal kyr BP being responsible for the strong change in $\delta^{18}\text{O}_{\text{ivc-ptsw}}$ at the western subtropical South Atlantic. Our records are consistent with modeling results and together highlight the important role played by

Indian-Atlantic interocean exchange as the trigger for the resumption of the AMOC and the Bølling warm event.

Acknowledgments: We thank M. Segl for help with the isotope analyses and J. Lynch-Stieglitz and J.R.E. Lutjeharms for discussion. Logistic and technical assistance was provided by the Captain and crew of R/V *Meteor*. Work was funded by the DFG-Research Center / Excellence Cluster “The Ocean in the Earth System”, and the Brazilian National Council for Scientific and Technological Development Fellowship granted to C.M. Chiessi. This is MARUM publication No. XXXX.

5.6 Supplementary material

5.6.1 Age model

The age model for core GeoB6211-2 is based on seven accelerator mass spectrometry (AMS) radiocarbon measurements (Leibniz-Laboratory for Radiometric Dating and Stable Isotope Research, Kiel, Germany) (Table 5.1, Fig. 5.4). Raw radiocarbon dates were calibrated with the CALIB 5.0.2 software (Stuiver and Reimer, 1993) and the Marine04 calibration curve (Hughen et al., 2004).

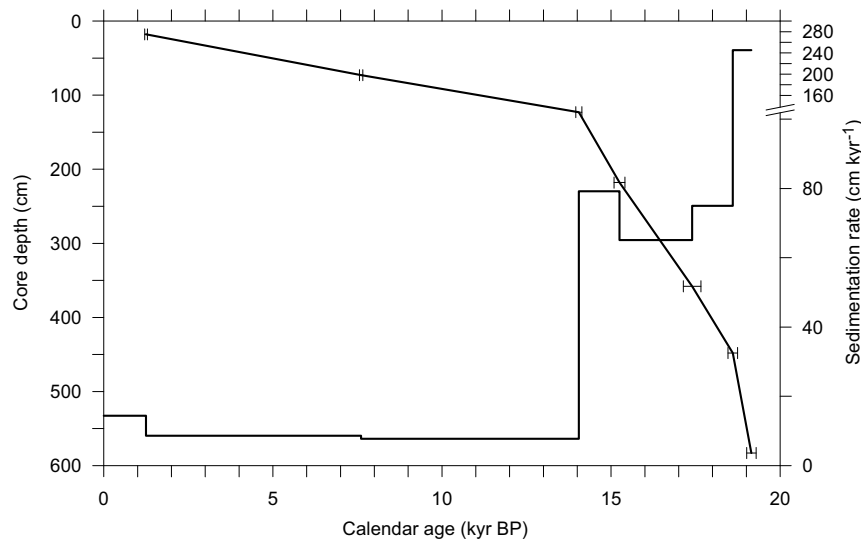


Figure 5.4. Age model and sedimentation rates for core GeoB6211-2.

The good agreement between measured $\delta^{18}\text{O}$ values for *Globorotalia inflata* and *U. peregrina* averaged for the uppermost 5 cm of GeoB6211-2 (0.94 ‰ and 2.91 ‰, respectively) and the predicted $\delta^{18}\text{O}$ of calcite ($\delta^{18}\text{O}_{\text{pc}}$) (1.02 ‰ and 2.97 ‰, respectively) allowed us to assign modern age to the uppermost cm of GeoB6211-2. We calculated $\delta^{18}\text{O}_{\text{pc}}$ using seawater $\delta^{18}\text{O}$ ($\delta^{18}\text{O}_{\text{sw}}$) from LeGrande and Schmidt (2006), temperature from our in situ CTD deployments and the paleotemperature equation from Shackleton (1974). The depth recorded in the $\delta^{18}\text{O}$ of *G. inflata* was assumed to be between 250 m and 300 m. Note that *Uvigerina bifurcata* was not available in the uppermost section of the core so we measured *U. peregrina*. Ages between ^{14}C AMS values were linearly interpolated.

Table 5.1. AMS radiocarbon dates and calibrated ages used to construct the age model for core GeoB6211-2.

Lab ID	Core depth (cm)	Species	Radiocarbon age $\pm 1\sigma$ error (yr BP)	Calibrated age (cal kyr BP)	2σ calibrated age range (cal kyr BP)
KIA30528	18	<i>G. ruber</i> (pink and white) and <i>G. sacculifer</i>	1685 \pm 30	1.25	1.30 – 1.16
KIA30527	73	<i>G. ruber</i> (pink and white)	7145 \pm 55	7.61	7.73 – 7.50
KIA30526	123	<i>G. ruber</i> (pink and white) and <i>G. sacculifer</i>	12600 \pm 70	14.05	14.24 – 13.84
KIA30525	218	<i>G. ruber</i> (pink and white) and <i>G. sacculifer</i>	13340 \pm 80	15.25	15.63 – 14.98
KIA30524	358	Mixed planktic foraminifera*	14860 \pm 90	17.40	17.86 – 16.88
KIA30531	448	<i>Yoldia riograndensis</i>	15590 \pm 100	18.60	18.79 – 18.43
KIA30530	583	<i>Yoldia riograndensis</i>	16400 \pm 120	19.15	19.43 – 18.96

*Mixed planktic foraminifera contained *G. ruber* (pink and white), *G. sacculifer*, *G. bulloides*, *G. siphonifera*, *T. quinqueloba*, *G. glutinata*, *G. uvula*, *G. conglobatus*, and *G. falconensis*.

We decided not to apply an additional reservoir age to the two oldest ^{14}C AMS values of our core measured on epibenthic bivalve shells based on two main reasons: (i) $\delta^{14}\text{C}$ measurement from 693 m water depth for GEOSECS station 60 (32.97°S, 42.50°W) (Stuiver and Östlund, 1980), the closest GEOSECS station to our site, when converted to calibrated age using the conventional radiocarbon age equation from Stuiver and Polach (1977), the calibration software CALIB 5.0.2 (Stuiver and Reimer, 1993) and the IntCal04 calibration curve (Reimer et al., 2004) with no reservoir correction results in a value of 470 ± 35 cal yr BP; this value is close to the 400 yr assigned to the mixed layer at latitudes between 40°N and 40°S (Bard, 1988); at the time of the GEOSECS cruise, bomb-radiocarbon penetration was not deeper than ~450 m for station 60 (Broecker et al., 1995), showing that no bomb-radiocarbon could have lowered the $\Delta^{14}\text{C}$ measured value at 693 m water depth at GEOSECS station 60; and (ii) the relatively high velocity (20 m yr^{-1}) of bomb-radiocarbon penetration at around 30°S for central water masses of the South Atlantic as estimated by Broecker et al. (1995) with data from two different cruises (GEOSECS and SAVE) performed 15 years from each other reflects the relatively quick ventilation of the upper water column at around 30°S in the South Atlantic.

Moreover, the use of questionable corrections in reservoir age for the oldest two bivalve-based calibrated ^{14}C AMS values from our core (18.6 and 19.15 cal kyr BP) would not change our

conclusions, which are grounded on the younger planktic foraminifera-based calibrated ^{14}C AMS values.

We assume no regional deviation from the global reservoir age because the core position lies far from upwelling zones and significantly to the north of the southern polar front. Additionally, the marine reservoir correction database compiled by Reimer and Reimer (2001) shows no data for our site.

5.6.2 Sedimentation rates

Sedimentation rates for GeoB6211-2 show a two-step decrease from the Last Glacial Maximum (LGM) to the Early Holocene (Fig. 5.4). Mean values decrease from ~ 250 to 70 cm kyr^{-1} at around 19 cal kyr BP and from ~ 70 to 10 cm kyr^{-1} at around 14 cal kyr BP. Both changes in sedimentation rates are remarkably synchronous (within age model uncertainties) to outstanding events of sea level rise related to meltwater pulses (Fairbanks, 1989; Bard et al., 1990, Yokoyama et al., 2000). During the LGM, a ~ 130 m lower sea level shifted the coastline very close to our site, especially considering the depth of the shelf break (140 m) in this portion of the Argentine Basin. Submarine channels indicate that the La Plata River extended northwards over the LGM exposed continental shelf (Ewing and Lonardi, 1971; Lonardi and Ewing, 1971). During the LGM, the huge sedimentary load of the La Plata River was directly delivered to the Rio Grande Cone, a major sedimentary feature in the western Argentine Basin where our core was raised. The stepwise rise in sea level following the LGM caused abrupt displacements of the coastline towards the continent (i.e. away from our site) and trapped a major part of the sedimentary load of the La Plata River in the inner shelf controlling the stepwise decrease in sedimentation rate at our site.

5.6.3 Foraminiferal $\delta^{18}\text{O}$ and Mg/Ca

The last deglaciation section (from ~ 90 to 550 cm core depth) of core GeoB6211-2 was sampled at 1 cm intervals for stable oxygen isotope analysis on *G. inflata* (350-500 μm) and *U. bifurcata* (500-650 μm). Taxonomy for identification of benthic foraminifera followed Boltovskoy et al. (1980) and Lutze (1986). For each sample, about 10 and 5 well preserved specimens of *G. inflata* and *U. bifurcata*, respectively, were analyzed on a Finnigan MAT 252 mass spectrometer equipped with an automatic carbonate preparation device. Isotope results were calibrated relative to

the Vienna Pee Dee belemnite (VPDB) using NBS18, 19 and 20 standards. The standard deviation of the laboratory standard was lower than 0.07 ‰ for the measuring period.

Mg/Ca analyses on *G. inflata* (350-500 μm) were run on a subset of samples with 1-7 cm spacing depending on the sedimentation rate. Fifteen samples distributed around 15 cal kyr BP were also selected for Mg/Ca analyses on *U. bifurcata* (500-650 μm). For each sample we selected about 20 and 30 well preserved specimens of *G. inflata* and *U. bifurcata*, respectively. Specimens were gently crushed and cleaned following the cleaning protocol of Barker et al. (2003). Dissolved samples were analyzed by ICP-OES (Perkin Elmer Optima 3300 R). Standards ($n = 43$) and replicate analyses on the same samples ($n = 15$), which were cleaned and analyzed during different sessions, show mean reproducibility of ± 0.02 and ± 0.09 Mg/Ca mmol/mol, respectively. Each point of Mg/Ca estimate represents an average of three replicate Mg/Ca analyses measured on the same session. Additionally, Fe/Ca, Mn/Ca and Al/Ca ratios were monitored to identify contaminant clay particles and manganese-rich carbonate coatings, which might affect foraminiferal Mg/Ca ratios (Barker et al., 2003). The absence of co-variation between Mg/Ca and Fe/Ca, Mn/Ca and Al/Ca ($r^2 < 0.02$, for all ratios) attests our Mg/Ca analyses are not biased by contaminants. We converted *G. inflata* Mg/Ca ratios to temperatures using the empirical equation $\text{Mg/Ca} = 0.831 \exp(0.066 T)$ ($r^2 = 0.78$), based on 25 surface samples from the South Atlantic ranging from 3°C to 16°C. Details on the Mg/Ca-temperature calibration equation for *G. inflata* will be published elsewhere.

5.6.4 Tilting the isopycnals of the subtropical South Atlantic

In order to quantify the potential effect that a tilt in the isopycnals of the upper subtropical South Atlantic would have on the water column properties above our core site we calculated the differences in temperature and $\delta^{18}\text{O}_{\text{sw}}$ between stations 32.5°S/49.5°W and 32.5°S/15.5°E for every depth of the World Ocean Atlas 2001 (Conkright et al., 2002) and the gridded data set of $\delta^{18}\text{O}_{\text{sw}}$ from LeGrande and Schmidt (2006) from the surface down to 1500 m water depth (Fig. 5.5).

5.6.5 Freshening of Antarctic Intermediate Water (AAIW) at ~15 cal kyr BP

Because of the unfavorable signal to noise relation associated to our ice volume corrected bottom seawater $\delta^{18}\text{O}$ ($\delta^{18}\text{O}_{\text{ivc-bsw}}$) reconstruction, the following interpretation of the observed trend in $\delta^{18}\text{O}_{\text{ivc-bsw}}$ should be treated with caution.

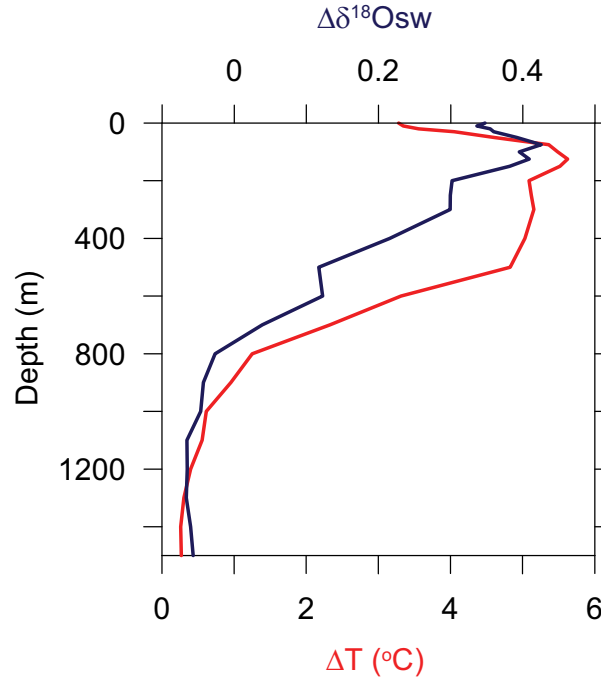


Figure 5.5. Depth profiles of the difference in temperature and $\delta^{18}\text{O}$ of seawater between two stations located at both extremes (49.5°W and 15.5°E) of a latitudinal transect across the South Atlantic at 32.5°S (Conkright et al., 2002, LeGrande and Schmidt, 2006). The higher differences in the upper water column reflect the northward flowing relatively strong upper branch of the present-day Atlantic meridional overturning circulation.

The bottom of the water column at our site shows a decrease in $\delta^{18}\text{O}_{\text{ivc-bsw}}$ of 0.5‰ around 15 cal kyr BP, clearly opposed to the increase in ice volume corrected permanent thermocline $\delta^{18}\text{O}$ ($\delta^{18}\text{O}_{\text{ivc-ptsw}}$) of $\sim 1.2\text{‰}$ observed for the same period. The apparently contradictory decrease in $\delta^{18}\text{O}_{\text{ivc-bsw}}$ is actually expected if we consider that: (i) today the conditions recorded by the benthic foraminifera at our site correspond to the boundary between South Atlantic Central Water (SACW) and AAIW where the influence of relatively warm and salty Indian Ocean waters is rather small; (ii) during the LGM the boundary between SACW and AAIW was even shallower than today (Paul and Schäfer-Neth, 2004) so that the bottom conditions at our site were largely controlled by AAIW and the input of cold and fresh waters from the southeastern Pacific Ocean; (iii) the strengthening of the Agulhas Leakage was probably related to a synchronous increase of mass transport from the Pacific Ocean into the South Atlantic (Knorr and Lohmann,

2003); and (iv) the abrupt input of isotopically light waters from the melting Patagonian Ice Sheet (PIS) directly to the formation region of AAIW could have decreased its salinity. Modeling results supported by field evidence indeed suggest that the PIS lost ~85% of its volume between 14.5 and 13.7 cal kyr BP (Hubbard et al., 2005; Turner et al., 2005). Freshening of AAIW would as well intensify North Atlantic Deep Water formation and the Atlantic meridional overturning circulation (AMOC) (Weaver et al., 2003).

5.6.6 *Brief model description, experimental design, results and discussion*

We used the University of Victoria (UVic) Earth System Climate Model (ESCM, version 2.8), which consists of the Modular Ocean Model (MOM, version 2; Pacanowski, 1996) coupled to a vertically integrated two-dimensional energy-moisture balance model of the atmosphere, a sea ice model (based on the thermodynamic formulation by Semtner (1976) and Hibler (1979) and the dynamic formulation by Hunke and Dukowicz (1997)), a land surface scheme (Cox et al., 1999) and a dynamic global vegetation model (Cox, 2001; Meissner et al., 2003). The UVic ESCM including the atmospheric, ocean and sea ice components is described by Weaver et al. (2001). Monthly wind stress to force the ocean and monthly winds for the advection of heat and moisture in the atmosphere are prescribed from the NCEP reanalysis climatology (Kalnay et al., 1996). The model is driven by the seasonal variation of solar insolation at the top of the atmosphere.

We generated two different climate states, one (BL, for “Bølling-like”) with an active, the other (HL, for “Heinrich-like”) with a collapsed AMOC. Experiment BL was initialized from a near-equilibrium LGM state with an AMOC reduced by 25%, in terms of the maximum of the meridional overturning streamfunction as compared to a present-day control simulation (~15 vs. ~20 Sv, respectively, $1 \text{ Sv} = 1 \times 10^6 \text{ m}^3 \text{ s}^{-1}$). Experiment HL was initialized from experiment BL at 17.8 cal kyr BP and subject to additional freshwater discharge to the North Atlantic Ocean through the St. Lawrence River, at a rate of 0.1 Sv for a period of 100 years. While the LGM experiment was forced by insolation, atmospheric CO₂ concentration and ice sheets fixed at their 21.0 cal kyr BP values, experiments BL and HL were both forced by changing insolation, atmospheric CO₂ concentration and ice sheets. The wind stress and wind fields in the atmospheric component were allowed to adjust to changes in sea-surface temperature according to a geostrophic wind feedback parameterization (Weaver et al. 2001). In experiment HL, the AMOC totally collapsed. In contrast, experiment BL reached a maximum overturning of ~18 Sv in the year 16.45 cal kyr BP. In our discussion we compared experiment BL at this stage with experiment HL and thus focused on the difference in ocean temperature due to AMOC collapse.

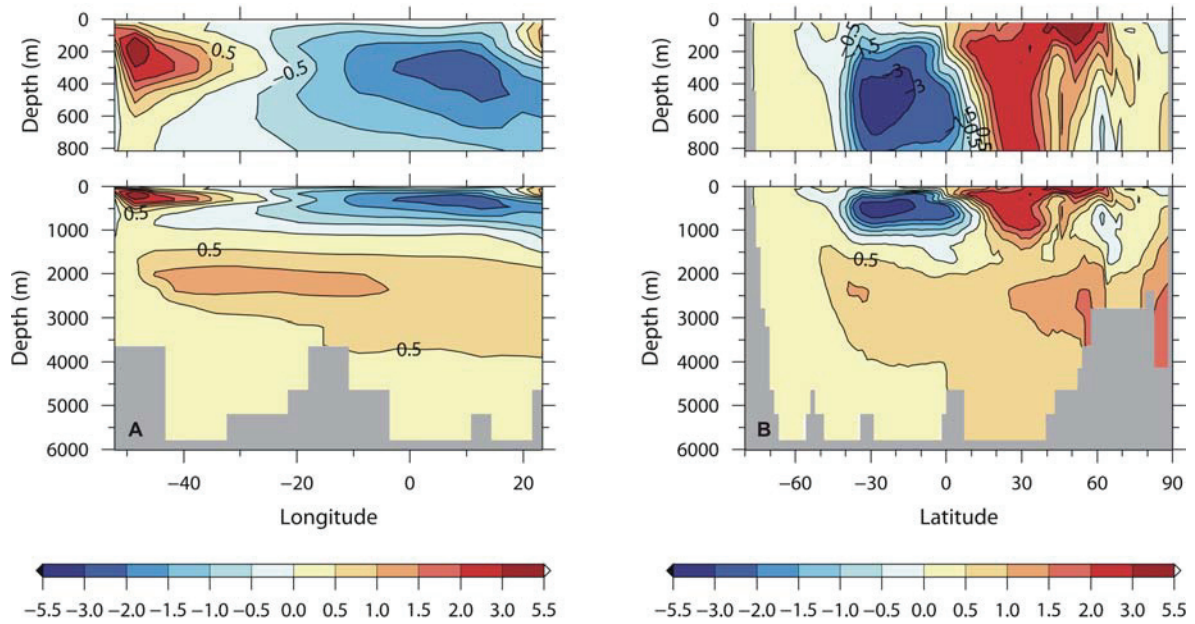


Figure 5.6. Temperature anomalies in the Atlantic Ocean between the modeled climate states “Bølling-like” and “Heinrich-like”. A: East-west transect of temperature anomalies (“Bølling-like” – “Heinrich-like”) at 35.1°S across the South Atlantic. B: Zonally averaged temperature anomalies (“Bølling-like” – “Heinrich-like”) for a north-south transect across the entire Atlantic basin. For model setup and experimental design see the “Model results” section in the supplementary material.

The strengthening of the AMOC, expressed as the comparison between the BL and the HL climate states, is related to a widespread redistribution of heat in the Atlantic basin (Fig. 5.6). Figure 5.6A depicts the temperature anomalies (BL – HL) for an east-west transect at 35.1°S, and Fig. 5.6B displays the zonally averaged temperature anomalies (again BL – HL) for a north-south transect across the entire Atlantic. Both transects show a dipole-pattern in temperature anomalies that are stronger in the upper ocean (say first 1000 m). Whereas the north-south dipole-pattern in temperature (Fig. 5.6B) has been widely discussed (e.g. Crowley, 1992; Manabe and Stouffer, 1997; Rühlemann et al., 2004) we report for the first time an east-west dipole in temperature anomalies at subtropical latitudes in the South Atlantic (Fig. 5.6A). This zonal seesaw seems to be related to a shift in the slope of the isopycnals, that tilt from a flattened position during HL (collapsed AMOC) towards a steepened position during the BL (relatively strong AMOC), generating the warm (cold) anomaly in the western (eastern) South Atlantic. The core of the warming is found between 50 and 500 m water depth, similar to the depth profile of expected temperature change displayed in Fig. 5.5. Indeed, the abrupt warming we observed at ~15 cal kyr BP is higher at the permanent thermocline (6.5°C) compared to the temperature change in the base of the water column (3.5°C).

Chapter 6

Impact of the Atlantic Multidecadal Oscillation in the South American summer monsoon

Cristiano Mazur Chiessi, Stefan Mulitza, Jürgen Pätzold, Gerold Wefer

MARUM-Center for Marine Environmental Sciences, University of Bremen, Leobener Strasse,
28359 Bremen, Germany

To be submitted to *Geophysical Research Letters*

6.1 Abstract

The impact of the Atlantic Multidecadal Oscillation (AMO) on the South American Summer Monsoon (SASM) is investigated using ~4.500 years long records of the La Plata River drainage basin (PRDB) discharge variability. We measured the stable oxygen isotopic composition of shallow-dweller planktic foraminifera (controlled by the PRDB plume), and Ti intensity in bulk sediment (controlled by the source of the terrigenous sediments) from the last deglaciation section of a marine sediment core. Spectral and wavelet analyses of our records indicate a periodic oscillation of about 60 years in both the extension of the PRDB plume and the source of the terrigenous sediments. We conclude that the observed oscillation reflects variability in the SASM activity associated to the AMO. Sea surface temperature and atmospheric circulation anomalies triggered by the AMO would control the variability in SASM activity. Our results point out to a clear impact of the AMO on the SASM.

6.2 Introduction

The Atlantic Multidecadal Oscillation (AMO) is a large-scale pattern of fluctuation in sea surface temperature (SST) in the Atlantic with period of ~65 years, possibly associated with variability in the Atlantic thermohaline circulation (THC) (Delworth and Mann, 2000; Kerr, 2000). The AMO positive phase is characterized by coherent widespread warm (cold) SST anomalies in the North Atlantic (South Atlantic) when the THC is supposed to be at a maximum (Delworth and Mann, 2000; Knight et al., 2005). During the transition towards its negative phase, this pattern first diminishes then eventually re-establishes in the opposite sense, when much of the North Atlantic (South Atlantic) SST is anomalously cool (warm). For AMO's negative phase it is believed that the THC reaches minimum intensity. The impact of AMO in the climate system has been described mainly around the North Atlantic, controlling Sahel drought (Folland et al., 1986), the frequency of Atlantic hurricane (Goldenberg et al., 2001), and the strength of North American and European summer climate (Sutton and Hodson, 2005). Recent evidences point out to an AMO imprint reaching as far as the Asian summer monsoon (Lu et al., 2006).

Instrumental and proxy records from southeastern South America show significant changes in rainfall and river flow in the La Plata River drainage basin (PRDB) for the last 250 years with period of ~50 years (Collischonn et al., 2001; Soubiès et al., 2005). Persistent phases of dry (e.g. 1940s-1950s) and wet (e.g. 1970s-1980s) climate have been observed, and are remarkably synchronous to opposite changes in Sahel precipitation (Folland et al., 1986; Collischonn et al., 2001; Soubiès et al., 2005). Yet, it is not possible to determine whether these fluctuations are genuinely oscillatory from the relatively short records alone. Here we address this issue presenting two proxy records of the PRDB discharge variability with decadal resolution covering a period of approximately 4500 years.

6.3 Environmental setting and methods

Our decadal-scale discharge records of the PRDB are based on marine sediment core GeoB6211-2 recovered from the upper continental slope off southeastern South America (32.50°S, 50.24°W, 657 m water depth) (Fig. 6.1). We focus on the period between 18.6 and 14.05 cal kyr BP where we found high (~70 cm kyr⁻¹) and constant sedimentation rates, allowing high-resolution sampling rates. Details of GeoB6211-2 ¹⁴C-based age model are provided in the Supplementary material.

Covering a catchment area of $\sim 3,200,000$ km² in southeastern South America and discharging annually ~ 670 km³ of fresh water into the western South Atlantic (Fig. 6.1) the PRDB is the second largest drainage basin in the continent. Under present-day conditions, the hydrology above site GeoB6211-2 is strongly influenced by the PRDB discharge. Accordingly, the upper 20 m of the water column at our site show annual mean sea surface salinity (SSS) and oxygen isotopic composition ($\delta^{18}\text{O}$) as low as 33 practical salinity units (psu) and 0.01 ‰, respectively (Conkright et al., 2002; LeGrande and Schmidt, 2006). A site not affected by the PRDB fresh water plume some 400 km to the east shows annual mean SSS of 36 psu and $\delta^{18}\text{O}$ of 0.77 ‰ for the same depth range. During the last deglaciation the fresh water plume of the PRDB probably had an even stronger influence above our core site because of the lower sea level, which displaced the coastline and the plume's core very close to our site. Submarine channels indicate that the deglacial PRDB extended northwards over the exposed continental shelf, delivering its huge sedimentary load directly to our core site (Lonardi and Ewing, 1971).

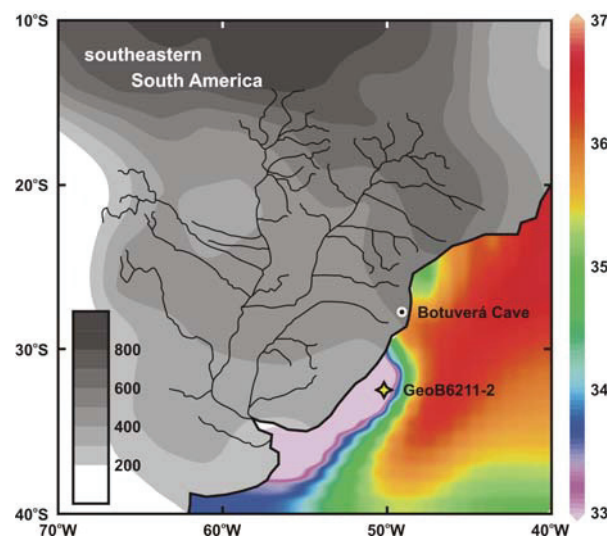


Figure 6.1. Map showing the location of site GeoB6211-2 in the western South Atlantic, Botuverá Cave in southeastern South America (Cruz et al., 2005), long-term mean annual sea surface salinity (in psu) (Conkright et al., 2002), long-term mean December-February precipitation (in mm) (Xie and Arkin, 1997), and La Plata River drainage basin main tributaries.

Because the PRDB discharge profoundly affected the hydrology and the composition of the terrigenous sediments at our site during the deglaciation, we hypothesize that significant changes in precipitation over the PRDB would be manifested in the $\delta^{18}\text{O}$ of shallow-dwelling planktic foraminifera and the chemical composition of the terrigenous fraction of GeoB6211-2.

We measured $\delta^{18}\text{O}$ in tests of planktic foraminifera *Globigerinoides ruber* (250-350 μm) white variety that dwells in the uppermost water column and reflect mixed layer conditions (Chiessi et al., 2007). Titanium (Ti) intensities in bulk sediment were determined using an X-ray fluorescence core scanner (XRF-CS). The sampling step for $\delta^{18}\text{O}$ was 10 mm and the measuring step for Ti was 5 mm resulting in a temporal resolution of ~ 14 and 7 years, respectively (see Supplementary material).

Considering that the eolian input to our site is relatively small (Mahowald et al., 2006), we use Ti intensities in GeoB6211-2 as a simple chemical proxy for fluvial terrigenous sediment input. Indeed, Ti has been widely used as an indicator of fluvial terrigenous input to marine sediments (Arz et al., 1998; Peterson et al., 2000) due to its insensitive behavior to environmental redox fluctuations and to its common presence in the suspended sediment load of continental-sized drainage basins. In the PRDB, the widespread occurrence of basalts in the southern half of the basin is responsible for the relatively high Ti content in the suspended sediment load of the basin's southern tributaries if compared to the northern tributaries (Depetris et al., 2003).

Two different methods of time-series analyses were performed to verify whether or not the fluctuations recorded in our $\delta^{18}\text{O}$ and Ti records were periodic. We used the software REDFIT (Schulz and Mudelsee, 2002) to explore our records in the frequency domain. To evaluate possible changes through time in the statistical properties of the oscillations from our $\delta^{18}\text{O}$ and Ti records, we carried out wavelet analyses. For this purpose, our records were investigated using the online facility of the Program in Atmospheric and Oceanographic Science at the University of Colorado at Boulder (<http://paos.colorado.edu/research/wavelets/>) (Torrence and Compo, 1998).

6.4 Results

Our planktic $\delta^{18}\text{O}$ record shows multidecadal-scale fluctuations superimposed on a long-term trend of increasing values (0.3 ‰) from 18.6 until ~ 17.7 cal kyr BP, decreasing values (0.6‰) until ~ 15.5 cal kyr BP and stable values for the rest of the period (Fig. 6.2). The amplitude of the multidecadal fluctuations is as big as 0.4 ‰. Our Ti record also shows multidecadal-scale fluctuations but no clear long-term trend rather than a discrete transition towards lower values between ~ 16.0 and 15.5 cal kyr BP.

Spectral analyses performed with the software REDFIT (Schulz and Mudelsee, 2002) confirmed the presence of statistically significant high-frequency oscillations in our records. The spectra of both $\delta^{18}\text{O}$ and Ti records depict peaks at periods of ~ 60 and 300 years above the 95% confidence level (Fig. 6.3). For the $\delta^{18}\text{O}$ spectrum, the peak at ~ 60 years is significant even at the 99% confidence level. The wavelet analyses also estimated periods of ~ 60 and 300 years above the 95% confidence level (see Supplementary material). The ~ 60 years period is stronger in the $\delta^{18}\text{O}$ record between 18.6 and 17.0 cal kyr BP and again between 15.0 and 14.05 cal kyr BP. The ~ 300 years period of the $\delta^{18}\text{O}$ record is focused between 18.6 and 16.5 cal kyr BP. For the Ti record, the ~ 60 years period is focused between 16.0 and 15.0 cal kyr BP whereas the ~ 300 years period is stronger between 17.5 and 15.0 cal kyr BP.

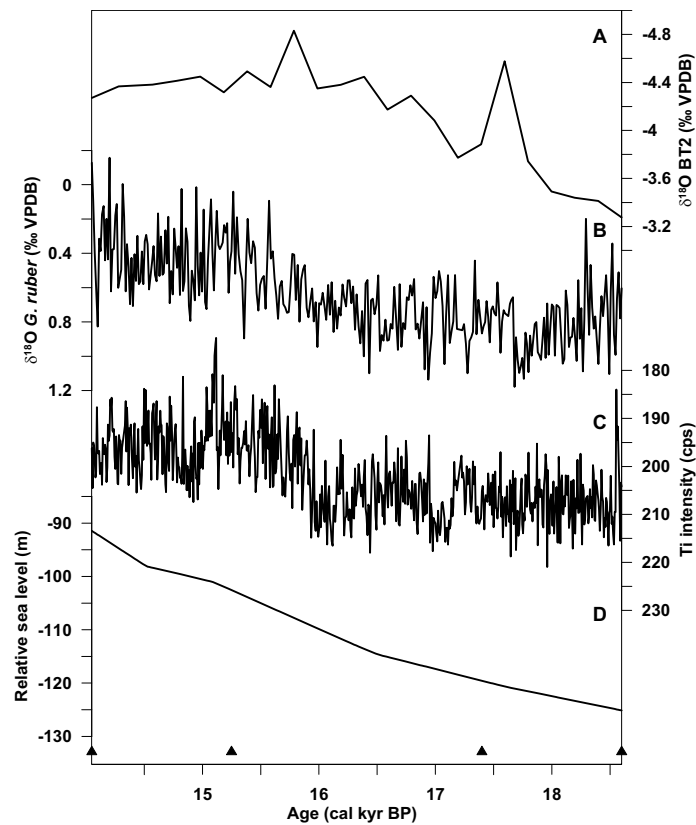


Figure 6.2. Proxy records of the La Plata River Drainage Basin discharge variability compared to a southeastern South America record of rainfall variability (Cruz et al., 2005) and relative sea level (Lambeck and Chappell, 2001). A: Botuverá Cave BT2 stalagmite $\delta^{18}\text{O}$ (Cruz et al., 2005). B: GeoB6211-2 *G. ruber* $\delta^{18}\text{O}$. C: GeoB6211-2 Ti intensity in counts per second. D: Relative sea level (Lambeck and Chappell, 2001). Triangles along the lower x-axis indicate AMS radiocarbon-based age control points for core GeoB6211-2.

6.5 Discussion

The multidecadal oscillation observed in our $\delta^{18}\text{O}$ record could be generated by fluctuations with a similar period in either SST or seawater $\delta^{18}\text{O}$, or still by a combination of both. Due to the relatively high amplitude (0.4 ‰) of the oscillation, we consider rather unlikely that the whole signal could be generated by SST variability alone, which would require a $\sim 2^\circ\text{C}$ oscillation in SST. Instrumental and proxy SST data show maximum amplitude of $\sim 0.5^\circ\text{C}$ for multidecadal variability during the last three centuries in the Atlantic (Delworth and Mann, 2000). Additionally, local seawater $\delta^{18}\text{O}$ is strongly influenced by the PRDB fresh water plume that could have shown multidecadal oscillation in size due to variations in PRDB discharge, reflecting rainfall variability over the continent. In this case, the upper water column above our site would be successively occupied by different mixtures between the continental and the marine end-members. Today the study area shows a strong zonal gradient in seawater $\delta^{18}\text{O}$. A conservative estimation for the present-day gradient is $\sim 0.002 \text{ ‰ km}^{-1}$ according to LeGrande and Schmidt (2006). This gradient was probably steeper during the last deglaciation. Thus, relatively small fluctuations in the PRDB plume could generate our signal.

Two processes could control the Ti multidecadal oscillation in GeoB6211-2: (i) fluctuations in the relative amount of terrigenous sediments in relation to the biogenic fraction (i.e. biogenic calcite, aragonite, opal and organic matter); or (ii) fluctuations in the composition of the terrigenous fraction, due to changes in the source area of the sediment. We favor the latter since there is no evidence of major changes in the biogenic fraction for the studied period (Müller, 2004).

Precipitation over the PRDB is mainly related to the southward expansion and intensification of the South American summer monsoon (SASM), while austral winter rainfall associated with mid-latitude cyclonic activity over the South Atlantic plays a secondary role (Zhou and Lau, 1998; Vera et al., 2002). During austral summer, strengthened northeasterly trades enhance the transport of equatorial Atlantic moisture to the Amazon basin, where intense convection takes place (Zhou and Lau, 1998). The intensification of the northwesterly South American low-level jet further transports Amazon moisture towards the PRDB, developing the South Atlantic Convergence Zone (SACZ) (Rao et al., 1996). Being one of the main components of the SASM, the SACZ is an elongated NW-SE convective belt that originates in the Amazon Basin, and extends above the northern PRDB and the adjacent subtropical South Atlantic (Fig. 6.1). During austral winter, incursions of mid-latitude air masses into the southern PRDB associated with episodes of enhanced cyclonic activity over the South Atlantic generate winter rainfall that

progress northwards along the Atlantic coast (Vera et al., 2002). Thus, annual mean rainfall over the PRDB decreases from north to south and from east to west. Interannual variability in precipitation over the PRDB has been related to El Niño-Southern Oscillation whereas interdecadal changes were associated to SST fluctuation in the South Atlantic (Robertson and Mechoso, 2000).

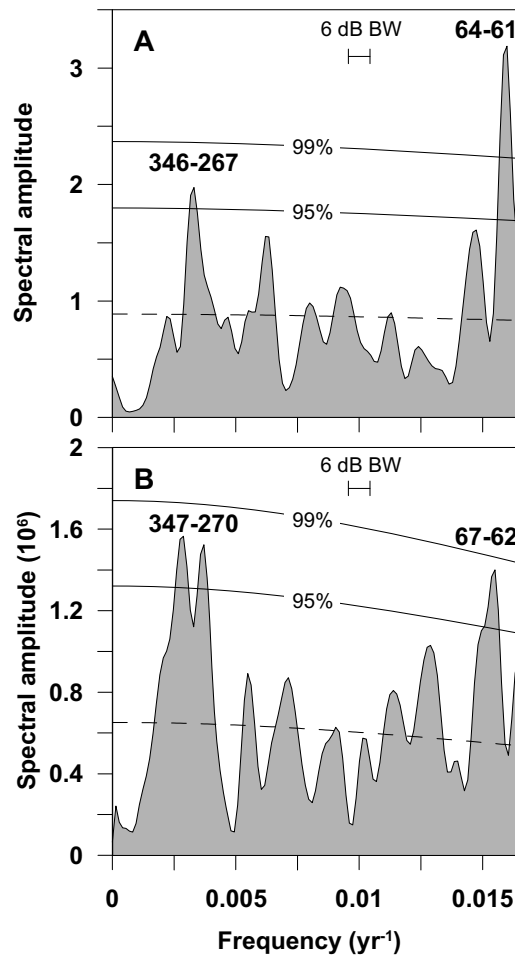


Figure 6.3. Spectral analyses of Geob6211-2 (A) *G. ruber* $\delta^{18}\text{O}$ and (B) Ti records. Peaks that exceed the 95% confidence level are labeled with their periods (in years). Analyses were performed with the software REDFIT (Schulz and Mudelsee, 2002), which uses the Lomb-Scargle periodogram for unevenly spaced data. The number of overlapping segments chosen was 4, and a Welch type spectral window was used. The 6 dB bandwidth (BW) determines the frequency resolution. Stippled line depicts the red-noise spectrum. Smooth lines depict 95% and 99% confidence levels.

We propose that the ~60 years period present in our records is related to a fluctuation with similar period in SASM/SACZ activity associated to the AMO. Ocean-atmosphere interactions in the South Atlantic might be one of the mechanisms linking the AMO to the SASM/SACZ. During the negative AMO phase, a weak THC would be associated with a weakening of the North Brazil Current and a strengthening of the Brazil Current, decreasing cross-equatorial heat transport and accumulating heat in the South Atlantic. Warming of the western

South Atlantic would enhance SACZ activity and rainfall over southeastern South America, increasing the PRDB discharge. On interdecadal time scales, instrumentally measured positive rainfall anomalies in the PRDB were indeed linked to enhanced SACZ activity caused by warmer SST in the western South Atlantic (Robertson and Mechoso, 2000).

Another mechanism that might link AMO and SAMS/SACZ involves the position of the Intertropical Convergence Zone (ITCZ) in the equatorial Atlantic. Modeling results show that during periods of weak THC (e.g. negative AMO phase) the ITCZ is shifted to the south causing a positive anomaly in moisture transport into the Amazon basin (Zhang and Delworth, 2005). The anomalous cross-equatorial moisture flow would enhance convection in the Amazon, ultimately reinforcing the South American low-level jet and precipitation in the PRDB during austral summer (i.e. SASM/SACZ) (Díaz and Aceituno, 2003). Additionally, the southward migration of the ITCZ would generate a southward displacement of the SASM/SACZ system as a necessary response of the Hadley circulation, as proposed by Cruz et al. (2005). The southward displacement and intensification of the SASM/SACZ would significantly increase summer precipitation in the southern Ti-rich half of the PRDB. This would increase erosion and the total suspended sediment load in the southern tributaries of the PRDB, eventually increasing Ti content of the terrigenous fraction of the sediments delivered to our core site. Moreover, warming of the western South Atlantic and the synchronous increase in PRDB discharge would both act lowering $\delta^{18}\text{O}$ values in our *G. ruber* record, enhancing the amplitude of the recorded multidecadal signal.

During periods of positive AMO, cooling of the western South Atlantic and northward migration of the ITCZ would lead to decreased SASM/SACZ activity and a northward displacement of the main summer rainfall belt. In this case, a significant portion of the SASM precipitation would fall outside the PRDB, decreasing the basin's mean discharge, the size of the offshore plume, and the Ti content of the terrigenous fraction of the sediments delivered to our site.

The long-term changes in *G. ruber* $\delta^{18}\text{O}$ could be related to orbital-scale changes in SASM/SACZ activity as recorded in $\delta^{18}\text{O}$ from a stalagmite recovered in Botuverá Cave, southern Brazil (Cruz et al., 2005) (Fig. 6.2). A decrease in stalagmite $\delta^{18}\text{O}$ until ~15.5 cal kyr BP followed by stable values for the rest of the period is closely mirrored by our record. Lower stalagmite $\delta^{18}\text{O}$ values were interpreted to be related to a stronger SASM/SACZ (Cruz et al., 2005). Yet, the increase in *G. ruber* $\delta^{18}\text{O}$ between 18.6 and ~17.7 cal kyr BP finds no counterpart in the stalagmite record. Variations in global sea level due to melting of continental ice could also have some impact on the long-term changes of our $\delta^{18}\text{O}$ record. For the period from 18.6 to 14.05 cal kyr

BP Lambeck and Chappell (2001) estimated a nearly linear increase of ~30 m in global sea level (Fig. 6.2). Thus, melting of continental ice would produce a linear decrease of ~0.25 ‰ in seawater $\delta^{18}\text{O}$ (Schrag et al., 2002), leaving the increase in our *G. ruber* $\delta^{18}\text{O}$ record between 18.6 and ~17.7 cal kyr BP unresolved.

In the absence of abrupt sea level changes, the decrease in Ti intensity observed in our record between ~16.0 and 15.5 cal kyr BP points out to a decrease in the relative contribution of the southern Ti-rich half of the PRDB to the terrigenous fraction that reached our core site. We suggest that between ~16 and 15.5 cal kyr BP the SACZ have migrated from the southern to the northern half of the PRDB, decreasing erosion and runoff in the southern half of the basin. Since the displacement took place within the PRDB, the basin's mean discharge remained unaltered, as suggested by our planktic $\delta^{18}\text{O}$ record. This shift in the SACZ position is synchronous (within age model uncertainties) with the transition from Heinrich event 1 to the Bølling-Allerød, where a major increase in Atlantic THC would have shifted the ITCZ to the north (Peterson et al., 2000; McManus et al., 2004).

We hypothesize that the ~300 years period present in our records could be a harmonic of the statistically stronger ~60 years period, what is supported by the lack of evidence in the climate system of an oscillation with a similar multicentennial period.

6.6 Conclusions

Our ~4500 years long records of PRDB discharge, as reconstructed from planktic foraminiferal oxygen isotopic composition and bulk sediment Ti intensities in a marine sediment core from the western South Atlantic, show statistically significant oscillation with period of ~60 years. We conclude that the observed oscillation reflects variability in the SASM/SACZ activity associated to the AMO. During negative (positive) AMO phase, the anomalously warm (cold) South Atlantic would increase (decrease) SACZ activity and displace the main belt of SASM precipitation to the south (north). Amplified (reduced) SACZ activity would increase (decrease) rainfall over the PRDB and the basin's isotopically low discharge into the western South Atlantic, affecting the composition of the upper water column above our site. The southward (northward) displacement of the SACZ would increase (decrease) rainfall and erosion on the southern Ti-rich half of the PRDB, eventually increasing (decreasing) the Ti content of the terrigenous fraction of the sediments delivered to our core site. Our results are consistent with instrumental and late

Holocene proxy records from the PRDB and together point out to a clear impact of the AMO on the SASM/SACZ.

Acknowledgments: We thank M. Segl and U. Röhl for help with the isotopes and XRF analyses, respectively, and H. Behling, F.W. Cruz Jr. and C. González for discussion. This study was funded by the DFG-Research Center/Excellence Cluster “The Oceans in the Earth System”, and the CNPq-Brazil Fellowship granted to C. M. Chiessi. Data presented in this study are available at the Pangaea database (<http://www.pangaea.de>). This is MARUM publication No. XXXX.

6.7 Supplementary material

6.7.1 Age model

The age model for core GeoB6211-2 is based on seven accelerator mass spectrometry (AMS) radiocarbon measurements (Leibniz-Laboratory for Radiometric Dating and Stable Isotope Research, Kiel, Germany) (Table 5.1, Fig. 5.4). Raw radiocarbon dates were calibrated with the CALIB 5.0.2 software (Stuiver and Reimer, 1993) and the Marine04 calibration curve (Hughen et al., 2004). Ages between ^{14}C AMS values were linearly interpolated.

We decided not to apply an additional reservoir age to the two oldest ^{14}C AMS values of our core measured on epibenthic bivalve shells based on two main reasons: (i) $\Delta^{14}\text{C}$ measurement from 693 m water depth for GEOSECS station 60 (32.97°S, 42.50°W) (Stuiver and Östlund, 1980), the closest GEOSECS station to our site, when converted to calibrated age using the conventional radiocarbon age equation from Stuiver and Polach (1977), the calibration software CALIB 5.0.2 [Stuiver and Reimer, 1993] and the IntCal04 calibration curve (Reimer et al., 2004) with no reservoir correction results in a value of 470 ± 35 cal yr BP; this value is close to the 400 years assigned to the mixed layer at latitudes between 40°N and 40°S (Bard, 1988); at the time of the GEOSECS cruise, bomb-radiocarbon penetration was not deeper than ~450 m for station 60 (Broecker et al., 1995), showing that no bomb-radiocarbon could have lowered the $\Delta^{14}\text{C}$ measured value at 693 m water depth at GEOSECS station 60; and (ii) the relatively high velocity (20 m yr^{-1}) of bomb-radiocarbon penetration at around 30°S for central water masses of the South Atlantic as estimated by Broecker et al. (1995) with data from two different cruises (GEOSECS and SAVE) performed 15 years from each other reflects the relatively quick ventilation of the upper water column at around 30°S in the South Atlantic.

We assume no regional deviation from the global reservoir age because the core position lies far from upwelling zones and significantly to the north of the southern polar front. Additionally, the marine reservoir correction database compiled by Reimer and Reimer (2001) shows no data for our site.

Sedimentation rates for GeoB6211-2 show a two-step decrease from the Last Glacial Maximum (LGM) to the Early Holocene (Fig. 5.4). Mean values decrease from ~250 to 70 cm kyr^{-1} at around 19 cal kyr BP and from ~70 to 10 cm kyr^{-1} at around 14 cal kyr BP. Both changes in

sedimentation rates are remarkably synchronous (within age model uncertainties) to outstanding events of sea level rise related to meltwater pulses (Fairbanks, 1989; Bard et al., 1990; Yokoyama et al., 2000). During the LGM, a ~130 m lower sea level shifted the coastline very close to our site, especially considering the depth of the shelf break (140 m) in this portion of the Argentine Basin. Submarine channels indicate that the La Plata River extended northwards over the LGM exposed continental shelf (Lonardi and Ewing, 1971). During the LGM, the huge sedimentary load of the La Plata River was directly delivered to the Rio Grande Cone, a major sedimentary feature in the western Argentine Basin where our core was raised. The stepwise rise in sea level following the LGM caused abrupt displacements of the coastline towards the continent (i.e. away from our site) and trapped a major part of the sedimentary load of the La Plata River in the inner shelf controlling the stepwise decrease in sedimentation rate at our site.

6.7.2 Foraminiferal $\delta^{18}O$

The section from 123 to 448 cm core depth of core GeoB6211-2 was sampled at 10 mm intervals for stable oxygen isotope analysis on *Globigerinoides ruber* (white) (250-350 μm). For each sample, about 10 well preserved specimens of *G. ruber* were analyzed on a Finnigan MAT 252 mass spectrometer equipped with an automatic carbonate preparation device. Isotope results were calibrated relative to the Vienna Peedee belemnite (VPDB) using NBS18, 19 and 20 standards. The standard deviation of the laboratory standard was lower than 0.07 ‰ for the measuring period.

6.7.3 X-ray fluorescence core scanner

The section from 123 to 448 cm core depth of core GeoB6211-2 was scanned at 5 mm intervals with an X-ray fluorescence core scanner (XRF-CS) (Röhl and Abrams, 2000) for Ti intensities in bulk sediment. Prior and after daily analysis, the instrument was calibrated against a set of pressed powder standards (Jansen et al., 1998). The sediment surface was covered with Ultralene® X-ray transmission foil to avoid desiccation of the sediment and contamination of the measurement unit. Each measurement covers an area of 0.4 cm^2 (0.4 cm long \times 1 cm wide). To obtain statistically significant data we used 30 s count time, 10 kV X-ray voltage and a current of 0.7 mA. Acquired XRF spectra were processed with the WinAxil and WinBatch software packages. The resulting data are expressed as element intensities in counts per second (cps).

6.7.4 Time-series analyses

Prior to time-series analyses, long-term trends in each record were removed by expressing the values as residuals from a 25 and 51 point moving average for the $\delta^{18}\text{O}$ and Ti records, respectively.

The software REDFIT 3.8 (Schulz and Mudelsee, 2002) was used to perform spectral analyses of the $\delta^{18}\text{O}$ and Ti time-series. The two main advantages of this method are: (i) it can be directly applied to temporally unevenly spaced records which avoid tapering of high frequencies; and (ii) it estimates the red-noise spectrum which allows the identification of significant frequencies. The appropriateness of the first-order autoregressive process used by the method was positively checked for both time-series. Spectral analyses were performed with 1000 Monte-Carlo simulations, an oversampling factor of 4 for the Fourier transform, four segments with 50 % overlapping, and a Welch window-type.

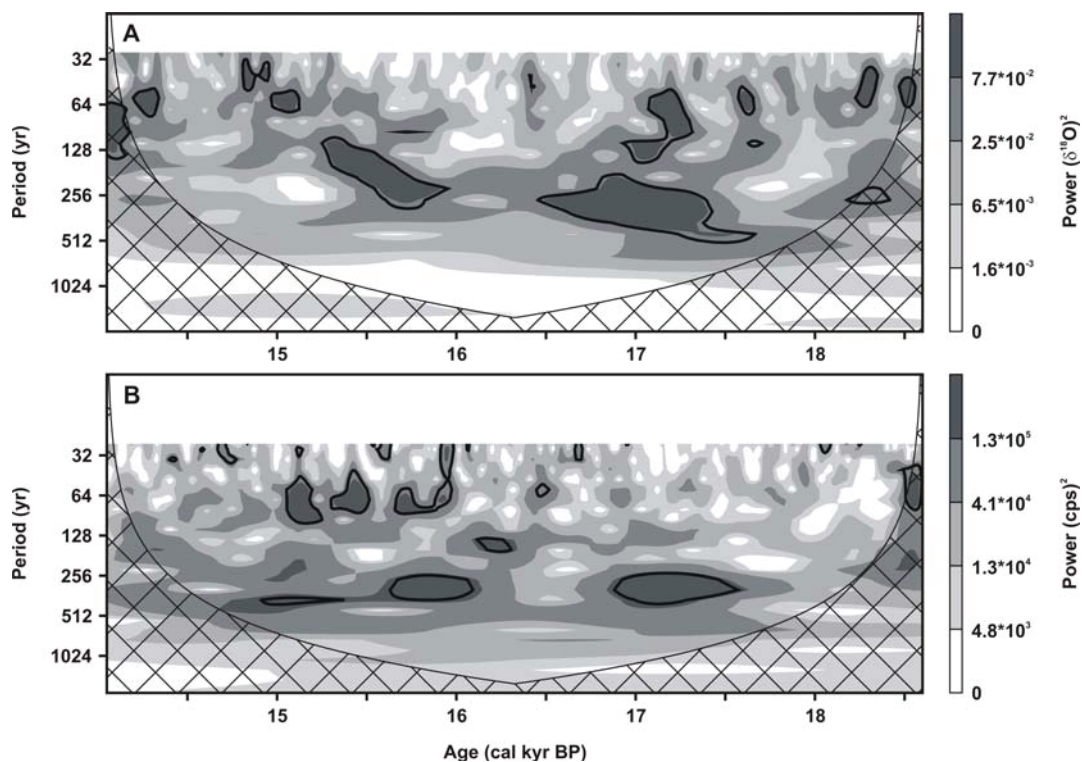


Figure 6.4. Wavelet analyses of the (A) $\delta^{18}\text{O}$ and (B) Ti records of site GeoB6211-2. The analyses were performed using the online facility of the Program in Atmospheric and Oceanographic Science at the University of Colorado at Boulder (<http://paos.colorado.edu/research/wavelets/>) (Torrence and Compo, 1998). The wavelet analyses of both records were performed using a Morlet wavelet, a frequency parameter of 6, a starting scale of 2, a scale width of 0.25 and a 5 % significance level (black contour) with a red-noise background spectrum.

Wavelet analyses of the $\delta^{18}\text{O}$ and Ti records of site GeoB6211-2 were performed using the online facility of the Program in Atmospheric and Oceanographic Science at the University of Colorado at Boulder (<http://paos.colorado.edu/research/wavelets/>) (Torrence and Compo, 1998). Since the algorithm is not able to analyze unevenly spaced time-series, the detrended records were evenly re-sampled. For the re-sampling we used simple interpolation at 14 and 7 years steps for $\delta^{18}\text{O}$ and Ti, respectively. The time-steps chosen correspond to the temporal resolution of the original time-series. The wavelet analyses of both records were performed using a Morlet wavelet, a frequency parameter of 6, a starting scale of 2, a scale width of 0.25 and a 5 % significance level with a red-noise background spectrum. The results are depicted in Fig. 6.4.

Chapter 7

Final remarks

7.1 Summary and conclusions

In this thesis, the paleoceanographic and paleoclimatic evolution of the western South Atlantic and eastern South America during the last deglaciation with special emphasis on abrupt climate change were investigated. The conclusions presented are based on inorganic geochemistry results (e.g. planktic and benthic foraminiferal stable oxygen isotopes and Mg/Ca ratios, bulk sediment Ti intensities) and outputs from an Earth system climate model of intermediate complexity.

This investigation established the present-day signature of the western South Atlantic upper water column (focused on the Brazil-Malvinas Confluence (BMC)) in the stable isotopic compositions of planktic foraminifera. Therefore, the oxygen and carbon isotopic compositions of seven planktic foraminifera species from 56 surface sediment samples raised from the continental slope off Brazil, Uruguay and Argentina between 20 and 48°S were measured. Based on the data the following conclusions were drawn:

- The lowest oxygen isotopes values were found in *Globigerinoides ruber* (pink), followed by *G. ruber* (white) and *Globigerinoides trilobus* reflecting the highly stratified near surface water conditions north of the BMC, where these species occur.
- *Globigerina bulloides* was present mainly south of the BMC and the species' oxygen and carbon isotopic composition record subsurface conditions supporting earlier plankton tow studies.
- *Globorotalia inflata* and *Globorotalia truncatulinoides* (left and right) were both available over the whole transect and calcify at a depth level with the steepest temperature change across the BMC. Accordingly, the oxygen isotopic composition of these species depict a sharp gradient of 2 ‰ at the confluence, with remarkably stable values north and south of the BMC. The oxygen isotopic composition of both species are the most reliable indicators for the present position of the BMC and can therefore be used to define the past migration of the front.

- The carbon isotopic composition of *G. ruber* (pink and white), *G. trilobus*, *G. inflata* and *G. truncatulinoides* (left and right) shows no significant trend across the front and is of limited use in determining the past location of the BMC.

Based on isotopic and trace element compositions of planktic and benthic foraminifera the last deglaciation changes in central and intermediate water mass in the western subtropical South Atlantic were reconstructed with decadal-scale resolution. The data come from a ^{14}C dated marine sediment core raised off southern Brazil (GeoB6211-2, 32.50°S/50.24°W/657 m water depth), and allow the following conclusions:

- Around 15 cal kyr BP the records from the permanent thermocline showed a warming of $\sim 6.5^\circ\text{C}$ and an increase in ice-volume corrected oxygen isotopic composition of seawater ($\delta^{18}\text{O}_{\text{ivc-sw}}$) of 1.2 ‰ while at intermediate depths a warming of $\sim 3.5^\circ\text{C}$ and no significant change in $\delta^{18}\text{O}_{\text{ivc-sw}}$ were identified.
- Most of the warming (5°C for the permanent thermocline and 3°C for intermediate depths) can be explained by tilting the South Atlantic east-west isopycnals from a horizontal position (collapsed Atlantic meridional overturning circulation (AMOC), as during Heinrich event 1) towards its present-day situation (relatively strong AMOC, as during the Bølling warm event).
- The same tilt explains just 0.3 ‰ change in the permanent thermocline $\delta^{18}\text{O}_{\text{ivc-sw}}$ and requires an additional process to be responsible for the remaining 0.9 ‰. Salinity in the central water masses of the South Atlantic is strongly influenced by the inflow of salty Indian Ocean upper waters. A strengthening in inflow of India Ocean waters (i.e. in the Agulhas Leakage) around 15 cal kyr BP is suggested, being responsible for the strong change in the permanent thermocline $\delta^{18}\text{O}_{\text{ivc-sw}}$ at the western South Atlantic.
- The temperature anomalies between the “Heinrich-like” and the “Bølling-like” climate states simulated with the University of Victoria Earth System Climate Model were consistent with the proxy-based reconstructions. Two dipole patterns in temperature anomalies were recognized in the Atlantic Ocean, namely in the north-south and east-west directions. While the north-south dipole was extensively described before, an east-west dipole pattern in temperature anomalies in the subtropical South Atlantic is showed for the first time. The east-west dipole (zonal seesaw) seems to be generated by a shift in the slope of the isopycnals.

-
- Taken together, these results highlight the important role played by the Indian-Atlantic interocean exchange as the trigger for the resumption of the AMOC and the Bølling warm event.

The fluctuations in precipitation over eastern South America for a period of approximately 4500 years during the last deglaciation were reconstructed in sub-decadal-scale resolution based on the oxygen isotopic composition of planktic foraminifera and bulk sediment Ti intensities. The conclusions were based on marine sediment core GeoB6211-2 (32.50°S/50.24°W/657 m water depth) raised under the influence of the La Plata River drainage basin (PRDB) discharge, as follows:

- The PRDB discharge records show statistically significant oscillation with period of approximately 60 years.
- The observed oscillation most probably reflects variability in the South American summer monsoon (SASM) / South Atlantic Convergence Zone (SACZ) activity associated with the Atlantic Multidecadal Oscillation (AMO).
- During negative (positive) AMO phase, the anomalously warm (cold) South Atlantic would increase (decrease) SACZ activity and displace the main belt of SASM precipitation to the south (north). Amplified (reduced) SACZ activity would increase (decrease) rainfall over the PRDB and the basin's isotopically low discharge into the western South Atlantic, affecting the composition of the upper water column above the cored site.
- The southward (northward) displacement of the SACZ would increase (decrease) rainfall and erosion on the southern Ti-rich half of the PRDB, eventually increasing (decreasing) the Ti content of the terrigenous fraction of the sediments delivered to the cored site.
- These results are consistent with the instrumental and late Holocene proxy records from the PRDB and together point to a clear impact of the AMO on the SASM/SACZ.

7.2 Future studies

The results presented in this thesis demonstrate the extraordinary potential of marine sediment samples from the tropical and subtropical western South Atlantic to calibrate proxies and reconstruct paleoceanographic and paleoclimatic changes with high temporal resolution. The manuscripts presented as part of this thesis used up just a fraction of this potential in order to answer some specific scientific questions for which this project was undertaken. While those

questions were to a great extent answered, other issues of topical interest emerged. Mainly as a consequence of the findings reported here, but also related to the natural development of the science of climate change during recent years. In this context, some future perspectives and ongoing projects that may further assimilate the remarkable potential of western South Atlantic marine sediment samples and on the other hand address the newly emerged questions are summarized below.

On the second manuscript (Chapter 5) part of the conclusions was based on relative changes in Mg/Ca paleotemperatures from deep-dweller planktic foraminifera *G. inflata*. In order to accurately convert Mg/Ca ratios into paleotemperatures, a species-specific calibration curve is needed. Ideally, such a calibration curve should: (i) cover the full range of Mg/Ca ratios present in the downcore record; (ii) be elaborated with shells belonging to the same size fraction as the one used for the downcore record; (iii) be established with surface samples of attested recent age; and (iv) be based on surface samples from the same biogeographic area as the downcore record. The set of surface samples used in the first manuscript (Chapter 4) (Chiessi et al., 2007) fulfils all mentioned conditions and is well suited for the elaboration of a Mg/Ca:temperature calibration curve for *G. inflata*. Deep-dweller planktic foraminifera show a high potential on recording changes in properties of the upper ~500 m of the water column (e.g. Mulitza et al., 1997; LeGrande et al., 2004; Chiessi et al., 2007; Cléroux et al., 2007), where most of the energy storage and oceanic heat transport actually occurs (Liu and Philander, 2001). In this context, a Mg/Ca:temperature calibration curve for *G. inflata* as well as detailed information of the species ecological preferences in the western South Atlantic would greatly contribute to paleoceanographic studies in the South Atlantic. Although the calibration curve has already been mentioned in the second manuscript (Chapter 5), a significant amount of information related to *G. inflata* ecological preferences together with details on the calibration curve will be published on a separate manuscript (ongoing work in collaboration with J. Groeneveld, MARUM-Center for Marine Environmental Sciences, University of Bremen, Germany).

Preliminary observations indicated that the benthic foraminiferal assemblages from sediment core GeoB6211-2 show significant downcore changes. Benthic foraminiferal assemblages are an important proxy for reconstructing changes in primary productivity and the flux of organic matter to the sea floor (e.g. Altenbach and Sarnthein, 1989; Loubere, 1991; Jorissen et al., 1995; De Rijk et al., 2000). Considering that the La Plata River discharge greatly controlled primary productivity above site GeoB6211-2 through the input of nutrients and organic matter, downcore variability in the benthic foraminiferal assemblages could disclose environmental changes in the

PRDB. As highlighted in the third manuscript (Chapter 6), the PRDB is the second largest drainage basin in South America, covering a significant portion of the South American tropical and subtropical latitudes where different biomes and climate regimes interact (e.g. Zhou and Lau, 1998; Eva et al., 2002). Especially for the last deglaciation, sediment core GeoB6211-2 shows high sedimentation rates ($\sim 70 \text{ cm kyr}^{-1}$) which would allow a high temporal resolution reconstruction of the environmental changes in the PRDB. Moreover, terrestrial environmental reconstructions based on marine archives have some advantages over existing continental records (e.g. Behling, 2002; Iriarte, 2006), which include (i) a better constrained chronology and (ii) the fact that marine archives record a basin-integrated signal (ongoing work in collaboration with W. Duleba, IGC-Institute of Geosciences, University of São Paulo, Brazil; and H. Filipsson, CGB-GeoBiosphere Science Centre, Lund University, Sweden).

During the last deglaciation, the stratification of the upper water column in the western South Atlantic experienced abrupt changes, as showed in the second manuscript (Chapter 5). Lynch-Stieglitz et al. (2006) also raised the possibility of profound changes taking place in the South Atlantic water column stratification during the last glacial maximum (LGM) if compared to the Holocene. While this study addresses the evolution of the physical properties in the upper water column (e.g. temperature and salinity) during the entire last deglaciation at two different depths in the western South Atlantic, Lynch-Stieglitz et al. (2006) compare benthic foraminiferal $\delta^{18}\text{O}$ from 18 different depths (from ~ 500 to 2000 m water depth), but only for two time-slices, namely the LGM and the Holocene. The results presented in the second manuscript (Chapter 5) and by Lynch-Stieglitz et al. (2006) suggest that significant changes happened in the structure of the South Atlantic water column, with major consequences for AMOC strength and paleocirculation. A comprehensive reconstruction of the physical properties in the water column including LGM, Heinrich event 1, Bølling-Allerød, Younger Dryas, Preboreal, mid Holocene, late Holocene, and pre-industrial time-slices for a collection of sediment cores similar to the one presented by Lynch-Stieglitz et al. (2006) could shed additional light on the evolution of the water column stratification in the western South Atlantic and allow for the verification of the behavior of each water mass during periods of significantly different boundary conditions. Therefore, high temporal resolution sediment cores from the western South Atlantic covering deep, intermediate and central water masses with accurate age control are needed. Sediment core GeoB6211-2 raised in the Rio Grande Cone as well as other sediment cores belonging to the same downslope transect, fulfill these conditions (Schulz et al., 2001; Wefer et al., 2001). Additionally, sediment cores raised at the Santos Plateau (Bleil et al., 1993; Heil et al., submitted for publication) some latitudinal degrees to the north of the Rio Grande Cone could be used to complement the downslope transect (ongoing

work in collaboration with S. Mulitza, MARUM-Center for Marine Environmental Sciences, Bremen, Germany; L. Cotton, School of Earth and Ocean Sciences, Cardiff University, United Kingdom; and L. Vidal, CEREGE-Centre Européen de Recherche et d'Enseignement des Géosciences de l'Environnement, Paul Cézanne University, France).

Understanding the internal, unforced variability of the climate system on multidecadal time-scales is of substantial importance to society. Not only does an appropriate understanding of such variability have significant implications for long-term climate projections, but it is precisely this time-scale on which anthropogenic impacts on climate are likely to be expressed more noticeably (Meehl et al., 2007). A clear understanding of the internal variability of the climate system that might be expected in the absence of exogenous climate forcings is critical for the problem of anthropogenic signal detection. Instrumental and proxy records from southeastern South America show significant changes in rainfall and river flow for the last two centuries with period of about 50 years (Collischonn et al., 2001; Soubiès et al., 2005), but the records are not long enough to allow for a clear identification of an oscillatory signal. The results presented in the third manuscript (Chapter 6) suggested that last deglaciation precipitation over southeastern South America was strongly impacted by the AMO. Thus, high temporal resolution reconstructions of PRDB discharge for the late Holocene could clarify this issue. So far, there is no marine sediment core suitable for one such high temporal resolution late Holocene reconstruction. However, the forthcoming R/V *Meteor* cruise M78/3 (scheduled for May/June/July 2009) will most probably deliver the needed sedimentary archives, since high sedimentation rate shelf areas close to the PRDB mouth will be cored. In this context, questions of topical interest as multidecadal natural precipitation variability over southeastern South America during the last two millennia could be addressed.

Acknowledgments

*Everything we encounter leaves traces behind.
Everything contributes imperceptibly to our education.*

Johann W. von Goethe

I owe a particular debt of gratitude to Prof. Dr. Gerold Wefer who gave me the greatly appreciated opportunity to undertake this project and, with accurate suggestions, advised me throughout. The second expert evaluation report about this thesis was kindly provided by Prof. Dr. Dierk Hebbeln, to whom I am grateful.

During my three years stay at Bremen, I got excellent supervision from Dr. Stefan Mulitza. I am much obliged for the very opportunity to work with him, and immensely grateful that he shared his knowledge and encouraged those around him to do the same. Special thanks also go to Dr. Jürgen Pätzold that with his great enthusiasm helped me in different ways from the very beginning of this endeavor.

I would like to thank Dr. André Paul for his important insights into ocean circulation. His generosity is an inspiration to me. I was introduced to the Mg/Ca world by Dr. Jeroen Groeneveld, to whom I am grateful.

I very much enjoyed the chance of being part of the “Bremen Complex”, i.e. the MARUM-Center for Marine Environmental Sciences and the Department of Geosciences of the University of Bremen. The dwelling with the people working on both institutions resulted in a substantial improvement to this work and, in a long-term perspective, to my career. I am grateful to all the researchers at the MARUM and the Department of Geosciences that somehow contributed to this work. Particularly, I would like to mention Dr. Babette Böckel, Dr. Helena Filipsson, Dr. Mahyar Mohtadi, Prof. Dr. Gesine Mollenhauer, Dr. Oscar Romero, Dr. Stephan Steinke, Dr. Jan-

Berend Stuut and Dr. Mark Trevethan. Proficient lab assistance was provided by Dr. Martin Kölling, Dr. Ursula Röhl, Dr. Monika Segl and their respective teams. The following undergraduate students helped me with lab work: Niklas Allroggen, Victoria Fübner and Henrike Schlösser. Thank you for that!

A significant part of a graduate student's education involves scientific and non-scientific discussions with other graduate students. In Bremen, it was not different. I thank all my colleagues, but especially Igaratza Fraile-Ugalde, Phillip Franke, Gerrit M. N. Heil (now Dr.), Heather Johnstone, Markus Raitzsch, Daniel Rincon-Martinez, Rik Tjallingii (now Dr.) and Iris Wilke (now Dr.). The constant exchange of thoughts with Catalina González was very educative, and I am grateful to her.

Many people outside Bremen contributed with scientific discussions that improved different parts of this thesis. This group of people includes Dr. Helge W. Arz, Christine Barras, Prof. Dr. Hermann Behling, Dr. Caroline Cléroux, Laura Cotton, Dr. Xavier Crosta, Dr. Francisco W. Cruz Jr., Dr. Trond M. Dokken, Dr. Wania Duleba, Dr. Christophe Fontanier, Dr. Paulo C. F. Giannini, Dr. Frank Lamy, Dr. Johann R. E. Lutjeharms, Dr. Jean Lynch-Stieglitz, Prof. Dr. Sonia M. B. Oliveira, Dr. Frank J. C. Peeters, Dr. André O. Sawakuchi, Dr. Jun Tian, Shannon Ulrich, Dr. Laurence Vidal and Dr. Ilana Wainer. I am sincerely thankful to all of you!

My parents, Angela M. Chiessi and Luiz S. Chiessi, are deeply acknowledged for their assistance, whenever necessary. Sofia Chiessi, my daughter, showed me the essentials, thereby greatly contributing to the route this project followed. Finally, incalculable support was provided by Maïté Proutière, my wife. To her go my warmest thanks!

This work was funded by the German Research Foundation (DFG) through the Research Center/Excellence Cluster "The Oceans in the Earth System", and by the CNPq-National Council for Scientific and Technological Development, Brazil.

References

- Adkins, J.F., McIntyre, K., Schrag, D.P., 2002. The salinity, temperature, and $\delta^{18}\text{O}$ of the glacial deep ocean. *Science* 298, 1769-1773.
- Alley, R.B., Marotzke, J., Nordhaus, W.D., Overpeck, J.T., Peteet, D.M., Pielke Jr., R.A., Pierrehumbert, R.T., Rhines, R.T., Stocker, T.F., Talley, L.D., Wallace, J.M., 2003. Abrupt climate change. *Science* 299, 2005-2010.
- Altenbach, A.V., Sarnthein, M., 1989. Productivity record in benthic foraminifera. In: Berger, W.H., Smetacek, V.S., Wefer, G., (Eds.), *Productivity of the Ocean: Present and Past*. Wiley, Chichester. pp. 255-269.
- Arz, H.W., Pätzold, J., Wefer, G., 1998. Correlated millennial-scale changes in surface hydrography and terrigenous sediment yield inferred from last-glacial marine deposits off northeastern Brazil. *Quaternary Research* 50, 157-166.
- Bahr, A., Lamy, F., Arz, H., Kuhlmann, H., Wefer, G., 2005. Late glacial to Holocene climate and sedimentation history in the NW Black Sea. *Marine Geology* 214, 309-322.
- Bainbridge, A.E., 1981. *GEOSECS Atlantic expedition, Hydrographic data, 1972-1973*. US Government Printing Office, Washington 1, 121 pp.
- Bard, E., 1988. Correction of accelerator mass spectrometry ^{14}C ages measured in planktonic foraminifera: Paleoceanographic implications. *Paleoceanography* 3, 635-645.
- Bard, E., Hamelin, B., Fairbanks, R.G., Zindler, A., 1990. Calibration of the ^{14}C timescale over the past 30,000 years using mass spectrometric U–Th ages from Barbados corals. *Nature* 345, 405-410.
- Barker, S., Greaves, M., Elderfield, H., 2003. A study of cleaning procedures used for foraminiferal Mg/Ca paleothermometry. *Geochemistry, Geophysics, Geosystems* 4, 8407, doi:10.1029/2003GC000559.
- Behling, H., 2002. South and southeast Brazilian grasslands during Late Quaternary times: a synthesis. *Palaeogeography, Palaeoclimatology, Palaeoecology* 177, 19-27.
- Behling, H., Arz, H.W., Pätzold, J., Wefer, G., 2000. Late Quaternary vegetational and climate dynamics in northeastern Brazil, inferences from marine core GeoB 3104-1. *Quaternary Science Reviews* 19, 981-994.
- Bemis, B.E., Spero, H.J., Bijma, J., Lea, D.W., 1998. Reevaluation of the oxygen isotopic composition of planktonic foraminifera: Experimental results and revised paleotemperature equations. *Paleoceanography* 13, 150-160.
- Bemis, B.E., Spero, H.J., Lea, D.W., Bijma, J., 2000. Temperature influence on the carbon isotopic composition of *Globigerina bulloides* and *Orbulina universa* (planktonic foraminifera). *Marine Micropaleontology* 38, 213-228.
- Berbery, E.H., Barros, V.R., 2002. The hydrologic cycle of the La Plata basin in South America. *Journal of Hydrometeorology* 3, 630-645.
- Berger, W.H., 1970. Planktonic foraminifera: differential production and expatriation off Baja California. *Limnology and Oceanography* 15, 183-204.
- Berger, W.H., Killingley, J.S., Vincent, E., 1978. Stable isotopes in deep-sea carbonates: Box Core ERDS-92 west equatorial Pacific. *Oceanologica Acta* 1, 203-216.
- Bianchi, C., Gersonde, R., 2004. Climate evolution at the last deglaciation: the role of the Southern Ocean. *Earth and Planetary Science Letters* 228, 407-424.
- Bijma, J., Faber, W.W., Hemleben, C., 1990. Temperature and salinity limits for growth and survival of some planktonic foraminifers in laboratory cultures. *Journal of Foraminiferal Research* 20, 95-116.

- Bleil, U., Cruise Participants, 1993. Report and preliminary results of Meteor Cruise M23/2, Rio de Janeiro–Recife, 27.02.–19.03.1993. Berichte, Fachbereich Geowissenschaften, Universität Bremen, Bremen 43, 133 pp.
- Bleil, U., Cruise Participants, 1994. Report and preliminary results of Meteor Cruise M29/2, Montevideo–Rio de Janeiro, 15.07.–08.08.1994. Berichte, Fachbereich Geowissenschaften, Universität Bremen, Bremen 59, 153 pp.
- Bleil, U., Cruise Participants, 2001a. Report and preliminary results of Meteor Cruise M46/3, Montevideo–Mar del Plata, 04.01.–07.02.2000. Berichte, Fachbereich Geowissenschaften, Universität Bremen, Bremen 172, 161 pp.
- Bleil, U., Cruise Participants, 2001b. Report and preliminary results of Meteor Cruise M49/3, Montevideo–Salvador, 09.03.–01.04.2001. Berichte, Fachbereich Geowissenschaften, Universität Bremen, Bremen 185, 99 pp.
- Blunier, T., Brook, J., 2001. Timing of millennial-scale change in Antarctica and Greenland during the last glacial period. *Science* 291, 109-112.
- Boddem, J., Schlitzer, R., 1995. Interocean exchange and meridional mass and heat fluxes in the South Atlantic. *Journal Geophysical Research* 100, 15 821-15 834.
- Boltovskoy, D., 1994. The sedimentary record of pelagic biogeography. *Progress in Oceanography* 34, 135-160.
- Boltovskoy, E., Boltovskoy, D., Brandini, F., 2000. Planktonic foraminifera from the south-western Atlantic epipelagic waters: abundance, distribution and year-to-year variations. *Journal of the Marine Biological Association of the United Kingdom* 79, 203-213.
- Boltovskoy, E., Boltovskoy, D., Correa, N., Brandini, F., 1996. Planktic foraminifera from the southwestern Atlantic (30°-60°S): species-specific patterns in the upper 50 m. *Marine Micropaleontology* 28, 53-72.
- Boltovskoy, E., Giussani, G., Watanabe, S., Wright, R., 1980. Atlas of benthic shelf foraminifera of the southwest Atlantic. Dr W. Junk bv Publishers, the Hague, 154 pp.
- Bond, G., Broecker, W., Johnsen, S., McManus, J., Labeyrie, L., Jouzel, J., Bonani, G., 1993. Correlations between climate records from North Atlantic sediments and Greenland ice. *Nature* 365, 143-147.
- Bond, G., Heinrich, H., Broecker, W., Labeyrie, L., McManus, J., Andrews, J., Huonparallel, S., Jantschik, R., Clasen, S., Simet, C., Tedesco, K., Klas, M., Bonani, G., Ivy, S., 1992. Evidence for massive discharges of icebergs into the North Atlantic ocean during the last glacial period. *Nature* 360, 245-249.
- Borowski, D., Gerdes, R., Olbers, D., 2002. Thermohaline and wind forcing of a circumpolar channel with blocked geostrophic contours. *Journal of Physical Oceanography* 32, 2520-2540.
- Boyle, E.A., Keigwin, L.D., 1985. Comparison of Atlantic and Pacific paleochemical records for the last 215,000 years: Changes in deep ocean circulation and chemical inventories. *Earth and Planetary Science Letters* 76, 135-150.
- Boyle, E.A., Keigwin, L.D., 1987. North Atlantic thermohaline circulation during the past 20,000 years linked to high-latitude surface temperature. *Nature* 330, 35-40.
- Brandini, F.P., Boltovskoy, D., Piola, A., Kocmur, S., Röttgers, R., Abreu, P.C., Lopes, R.M., 2000. Multiannual trends in fronts and distribution of nutrients and chlorophyll in the southwestern Atlantic (30-62°S). *Deep-Sea Research I* 47, 1015-1033.
- Brauer, A., Endres, C., Günter, C., Litt, T., Stebich, M., Negendank, J.F.W., 1999. High resolution sediment and vegetation responses to Younger Dryas climate change in varved lake sediments from Meerfelder Maar, Germany. *Quaternary Science Reviews* 18, 321-329.
- Broecker, W.S., 1986. Oxygen isotope constraints on surface temperatures. *Quaternary Research* 26, 121-134.
- Broecker, W.S., 1991. The great ocean conveyor. *Oceanography* 4, 79-89.
- Broecker, W.S., 1998. Paleocean circulation during the last deglaciation: A bipolar seesaw? *Paleoceanography* 13, 119-121.

- Broecker, W.S., Andree, M., Wolfli, W., Oeschger, H., Bonani, G., Kennett, J., Peteet, D., 1988. The chronology of the last deglaciation: Implications to the cause of the Younger Dryas event. *Paleoceanography* 3, 1-19.
- Broecker, W.S., Maier-Reimer, E., 1992. The influence of air and sea exchange on the carbon isotope distribution in the sea. *Global Biogeochemical Cycles* 6, 315-320.
- Broecker, W.S., Sutherland, S., Smethie, W., 1995. Oceanic radiocarbon: Separation of the natural and bomb components. *Global Biogeochemical Cycles* 9, 263-288.
- Bryden, H.L., Longworth, H.R., Cunningham, S.A., 2005. Slowing of the Atlantic meridional overturning circulation at 25°N. *Nature* 438, 655-657.
- Butzin, M., Prange, M., Lohmann, G., 2005. Radiocarbon simulations for the glacial ocean: the effects of wind stress, Southern Ocean sea ice and Heinrich events. *Earth and Planetary Science Letters* 235, 45-61.
- Campos, E.J.D., Velhote, D., Silveira, I.C.A., 2000. Shelf break upwelling driven by Brazil Current cyclonic meanders. *Geophysical Research Letters* 27, 751-754.
- Chave, K.E., 1954. Aspects of the biogeochemistry of magnesium 1: Calcareous marine organisms. *The Journal of Geology* 62, 266-283.
- Chiessi, C.M., Ulrich, S., Mulitza, S., Pätzold, J., Wefer, G., 2007. Signature of the Brazil-Malvinas Confluence (Argentine Basin) in the isotopic composition of planktonic foraminifera from surface sediments. *Marine Micropaleontology* 64, 52-66.
- Ciotti, A.M., Odebrecht, C., Fillmann, G., Möller Jr, O.O., 1995. Freshwater outflow and Subtropical Convergence influence on phytoplankton biomass on the southern Brazilian continental shelf. *Continental Shelf Research* 15, 1737-1756.
- Clark, P.U., Alley, R.B., Keigwin, L.D., Licciardi, J.M., Johnsen, S.J., Wang, H., 1996. Origin of the first global meltwater pulse following the last glacial maximum. *Paleoceanography* 11, 563-578.
- Clark, P.U., Pisias, N.G., Stocker, T.F., Weaver, A.J., 2002. The role of the thermohaline circulation in abrupt climate change. *Nature* 415, 863-869.
- Claussen, M., Mysak, L.A., Weaver, A.J., Crucifix, M., Fichefet, T., Loutre, M.-F., Weber, S.L., Alcamo, J., Alexeev, V.A., Berger, A., Calov, R., Ganopolski, A., Goosse, H., Lohmann, G., Lunkeit, F., Mokhov, I.I., Petoukhov, V., Stone, P., Wang, Z., 2002. Earth system models of intermediate complexity: closing the gap in the spectrum of climate system models. *Climate Dynamics* 18, 579-586.
- Cléroux, C., Cortijo, E., Duplessy, J.-C., Zahn, R., 2007. Deep-dwelling foraminifera as thermocline temperature recorders. *Geochemistry, Geophysics, Geosystems* 8, Q04N11, doi:10.1029/2006GC001474.
- Collischonn, W., Tucci, C.E.M., Clarke, R.T., 2001. Further evidence of changes in the hydrological regime of the River Paraguay: part of a wider phenomenon of climate change? *Journal of Hydrology* 245, 218-238.
- Conkright, M.E., Locarnini, R.A., Garcia, H.E., O'Brien, T.D., Boyer, T.P., Stephens, C., Antonov, J.I., 2002. *World Ocean Atlas 2001: Objective Analyses, Data Statistics, and Figures*, CD-ROM Documentation. National Oceanographic Data Center, Silver Spring, MD, 17 pp.
- Coplen, T.B., 1996. More uncertainty than necessary. *Paleoceanography* 11, 369-370
- Cox, P.M., 2001. Description of the 'TRIFFID' dynamic global vegetation model. Hadley Centre Technical Note 24, 17 pp.
- Cox, P.M., Betts, R.A., Bunton, C.B., Essery, R.L.H., Rowntree, P.R., Smith, J., 1999. The impact of new land surface physics on the GCM simulation of climate and climate sensitivity. *Climate Dynamics* 15, 183-203.
- Cronblad, H.G., Malmgren, B.A., 1981. Climatically controlled variation of Sr and Mg in Quaternary planktonic foraminifera. *Nature* 291, 61-64.
- Crowley, T.C., 1992. North Atlantic Deep Water cools the Southern Hemisphere. *Paleoceanography* 7, 489-497.

- Cruz Jr., F.W.C., Burns, S.J., Karmann, I., Sharp, W.D., Vuille, M., Cardoso, A.O., Ferrari, J.A., Dias, P.L.S., Viana Jr, O., 2005. Insolation-driven changes in atmospheric circulation over the past 116,000 years in subtropical Brazil. *Nature* 434, 63-66.
- Cubasch, U., Meehl, G.A., Boer, G.J., Stouffer, R.J., Dix, M., Noda, A., Senior, C.A., Raper, S., Yap, K.S., 2001. Projections of Future Climate Change. In: Houghton, J.T., Ding, Y., Griggs, D.J., Noguer, M., van der Linden, P.J., Dai, X., Maskell, K., Johnson, C.A., (Eds.), *Climate Change 2001: The Scientific Basis. Contribution of Working Group I to the Third Assessment Report of the Intergovernmental Panel on Climate Change*. Cambridge University Press, Cambridge, pp. 525-582.
- Cunningham, S.A., Kanzow, T., Rayner, D., Baringer, M.O., Johns, W.E., Marotzke, J., Longworth, H.R., Grant, E.M., Hirschi, J.J.-M., Beal, L.M., Meinen, C.S., Bryden, H.L., 2007. Temporal variability of the Atlantic meridional overturning circulation at 26.5°N. *Science* 317, 935-938.
- Curry, W.B., Oppo, D.W., 2005. Glacial water mass geometry and the distribution of $\delta^{13}\text{C}$ of ΣCO_2 in the western Atlantic Ocean. *Paleoceanography* 20, PA1017, doi:10.1029/2004PA001021.
- Damon, P.E., Lerman, J.C., Long, A., 1978. Temporal fluctuations of atmospheric ^{14}C : causal factors and implications. *Annual Review of earth and Planetary Science* 6, 457-494.
- Dansgaard, W., Johnsen, S.J., Clausen, H.B., Dahl-Jensen, D., Gundestrup, N.S., Hammer, C.U., Hvidberg, C.S., Steffensen, J.P., Sveinbjörnsdóttir, A.E., Jouzel, J., Bond, G., 1993. Evidence for general instability of past climate from a 250-kyr ice-core record. *Nature* 364, 218-220.
- Davis, K.J., Dove, P.M., Yoreo, J.J.D., 2000. The role of Mg^{2+} as an impurity in calcite growth, *Science* 290, 1134-1137.
- De Rijk, S., Jorissen, F.J., Rohling, E., Troelstra, S.R., 2000. Organic flux control on bathymetric zonation of Mediterranean benthic foraminifera. *Marine Micropaleontology* 40, 151-166.
- de Vargas, C., Renaud, S., Hilbrecht, H., Pawlowski, J., 2001. Pleistocene adaptive radiation in *Globorotalia truncatulinoides*: genetic, morphologic, and environmental evidence. *Paleobiology* 27, 104-125.
- Delworth, T. L., Mann, M.E., 2000. Observed and simulated multidecadal variability in the Northern Hemisphere. *Climate Dynamics* 16, 661-676.
- deMenocal, P.B., Arbuszewski, J.A., Kaplan, A., Bice, M., 2007. Fidelity of $\delta^{18}\text{O}$ seawater estimates using foraminiferal shell Mg/Ca and $\delta^{18}\text{O}$. *Eos Transactions AGU*, 88(52), Fall Meeting Supplement, Abstract PP41E-08.
- Depetris, P.J., Probst, J.-L., Pasquini, A.I., Gaiero, D.M., 2003. The geochemical characteristics of the Paraná River suspended sediment load: an initial assessment. *Hydrological Processes* 17, 1267-1277.
- Deuser, W.G., 1987. Seasonal variations in isotopic composition and deep-water fluxes of the tests of perennially abundant planktonic foraminifera of the Sargasso Sea: Results from sediment-trap collections and their paleoceanographic significance. *Journal of Foraminiferal Research* 17, 14-27.
- Deuser, W.G., Ross, E.H., 1989. Seasonally abundant planktonic foraminifera of the Sargasso Sea: Succession, deep-water fluxes, isotopic compositions, and paleoceanographic implications. *Journal of Foraminiferal Research* 19, 268-293.
- Díaz, A., Aceituno, P., 2003. Atmospheric circulation anomalies during episodes of enhanced and reduced convective cloudiness over Uruguay. *Journal of Climate* 16, 3171-3185.
- Doyle, M.E., Barros, V.R., 2002. Midsummer low-level circulation and precipitation in subtropical South America and related sea surface temperature anomalies in the South Atlantic. *Journal of Climate* 15, 3394-3410.
- Duckworth, D.L., 1977. Magnesium concentration in the tests of the planktonic foraminifer *Globorotalia truncatulinoides*. *Journal of Foraminiferal Research* 7, 304-312.

- Duplessy, J.C., Bé, A.W.H., Blanc, P.L., 1981. Oxygen and carbon isotopic composition and biogeographic distribution of planktonic foraminifera in the Indian Ocean. *Palaeogeography, Palaeoclimatology, Palaeoecology* 33, 9-46.
- Duplessy, J.C., Labeyrie, L., Juillet-Leclerc, A., Maitre, F., Duprat, J., Sarnthein, M., 1991. Surface salinity reconstruction of the North Atlantic Ocean during the last glacial maximum. *Oceanologica Acta* 14, 311-324.
- Durazzi, J.T., 1981. Stable-isotope studies of planktonic foraminifera in North Atlantic core tops. *Palaeogeography, Palaeoclimatology, Palaeoecology* 33, 157-172.
- Dürkoop, A., 1998. Der Brasil-Strom im Spätquartär: Rekonstruktion der oberflächennahen Hydrographie während der letzten 400 000 Jahre. *Berichte, Fachbereich Geowissenschaften, Universität Bremen, Bremen* 119, 121 pp.
- Elderfield, H., Bertram, C.J., Erez, J., 1996. A biomineralization model for the incorporation of trace elements into foraminiferal calcium carbonate. *Earth Planetary Science Letters* 142, 409-423.
- Emiliani, C., 1954. Depth habitat of some species of pelagic foraminifera as indicated by oxygen isotope ratio. *American Journal of Science* 252, 149-158.
- EPICA Community Members, 2006. One-to-one coupling of glacial climate variability in Greenland and Antarctica. *Nature* 444, 195-198.
- Eva, H.D., Miranda, E.E., Di Bella, C.M., Gond, C.M., Huber, O., Sgrenzaroli, M., Jones, S., Coutinho, A., Dorado, A., Guimarães, M., Elvidge, C., Achard, F., Belward, A.S., Bartholomé, E., Baraldi, A., De Grandi, G., Vogt, P., Fritz, S., Hartley, A., 2002. A vegetation map of South America. Office for Official Publications of the European Communities, Luxemburg, 34 pp.
- Ewing, M., Lonardi, A.G., 1971. Sediment transport and distribution in the Argentine Basin. 5. Sedimentary structure of the Argentine margin, basin and related provinces. In: Ahrens, L.H., Press, F., Runcorn, S.K., Urey, H.C., (Eds.), *Physics and Chemistry of the Earth*. Pergamon, Oxford, v. 8, pp. 123-251.
- Fairbanks, R.G., 1989. A 17,000-year glacio-eustatic sea level record: influence of glacial melting rates on Younger Dryas event and deep-ocean circulation. *Nature* 342, 637-642.
- Fairbanks, R.G., Charles, C.D., Wright, J.D., 1992. Origin of global meltwater pulses. In: Taylor, R.E. Long, A., Kra, R., (Eds.), *Radiocarbon after four decades: An interdisciplinary perspective*. Springer, New York, pp. 473-500.
- Fairbanks, R.G., Sverdrlove, M., Free, R., Wiebe, P.H., Bé, A.W.H., 1982. Vertical distribution and isotopic fractionation of living planktonic foraminifera from the Panama Basin. *Nature* 298, 841-844.
- Fairbanks, R.G., Wiebe, P.H., Bé, A.W.H., 1980. Vertical distribution and isotopic composition of living planktonic foraminifera in the western North Atlantic. *Science* 207, 61-63.
- Field, D.B., 2004. Variability in vertical distribution of planktonic foraminifera in the California Current: Relationships to vertical ocean structure. *Paleoceanography* 19, PA2014, doi:10.1029/2003PA000970.
- Folland, C.K., Palmer, T.N., Parker, D.E., 1986. Sahel rainfall and worldwide sea temperatures, 1901-85. *Nature* 320, 602-607.
- Ganssen, G.M., 1983. Dokumentation von küstennahem Auftrieb anhand stabiler Isotope in rezenten Foraminiferen vor Nordwest-Afrika. „Meteor“ Forschungs-Ergebnisse C 37, 1-46.
- Ganssen, G.M., Kroon, D., 2000. The isotopic signature of planktonic foraminifera from NE Atlantic surface sediments: implications for the reconstruction of past oceanic conditions. *Journal of the Geological Society* 157, 693-699.
- Ganssen, G.M., Sarnthein, M., 1983. Stable-isotopes compositions of foraminifers: The surface and bottom record of coastal upwelling. In: Suess, E., Thiede, J., (Eds.), *Coastal upwelling : Its Sediment Record (Part A)*. Plenum, New York, pp. 99-121.
- Garcia, C.A.E., Sarma, Y.V.B., Mata, M.M., Garcia, V.M.T., 2004. Chlorophyll variability and eddies in the Brazil-Malvinas Confluence region. *Deep-Sea Research II* 51, 159-172.

- Garcia, N.O., Vargas, W.M., 1996. The spatial variability of runoff and precipitation in the Rio de la Plata basin. *Hydrological Sciences Journal* 41, 279-299.
- Garzoli, S.L., Garraffo, Z., 1989. Transports, frontal motions and eddies at the Brazil-Malvinas Currents Confluence. *Deep-Sea Research A* 36, 681-703.
- Garzoli, S.L., Giulivi, C., 1994. What forces the variability of the southwestern Atlantic boundary currents? *Deep-Sea Research I* 41, 1527-1550.
- Godwin, H., 1962. Half-life of radiocarbon. *Nature* 195, 984.
- Goldenberg, S.B., Landsea, C.W., Mestas-Nuñez, A.M., Gray, W.M., 2001. The recent increase in Atlantic hurricane activity: Causes and implications. *Science* 293, 474-479.
- Gooday, A.J., 1988. A response by benthic foraminifera to the deposition of phytodetritus in the deep sea. *Nature* 332, 70-73.
- Gordon, A.L., 1981. South Atlantic thermocline ventilation. *Deep-Sea Research A* 28, 1239-1264.
- Gordon, A.L., Weiss, R.F., Smethie, W.M.Jr., Warner, M.J., 1992. Thermocline and intermediate water communication between the South Atlantic and Indian oceans. *Journal of Geophysical Research* 97, 7223-7240.
- Hall, M.M., Bryden, H.L., 1982. Direct estimates and mechanisms of ocean heat transport. *Deep-Sea Research* 29, 339-359.
- Hansen, J., Sato, M., Kharecha, P., Russell, G., Lea, D.W., Siddall, M., 2007. Climate change and trace gases. *Philosophical Transactions of the Royal Society A* 365, 1925-1954.
- Harloff, J., Mackensen, A., 1997. Recent benthic foraminiferal associations and ecology of the Scotia Sea and Argentine Basin. *Marine Micropaleontology* 31, 1-29.
- Haug, G.H., Hughen, K.A., Sigman, D.M., Peterson, L.C., Röhl, U., 2001. Southward migration of the Intertropical Convergence Zone through the Holocene. *Science* 293, 1304-1308.
- Heil, G.M.N., Arz, H.W., Behling, H., Wefer, G., *subm. to Quaternary Science Reviews*. Extent of high northern latitude temperature forcing on millennial-scale precipitation changes in eastern South America.
- Hemleben, C., Spindler, M., Anderson, O.R., 1989. *Modern Planktonic Foraminifera*. Springer-Verlag, New York, 363 pp.
- Hepp, D.A., Mörz, T., Grützner, J., 2006. Pliocene glacial cyclicity in a deep-sea sediment drift (Antarctic Peninsula Pacific Margin). *Palaeogeography, Palaeoclimatology, Palaeoecology* 231, 181-198.
- Hibler, W.D., 1979. A dynamic-thermodynamic sea-ice model. *Journal of Physical Oceanography* 9, 815-846.
- Hubbard, A., Hein, A.S., Kaplan, M.R., Hulton, N.R.J., Glasser, N., 2005. A modelling reconstruction of the Last Glacial Maximum ice sheet and its deglaciation in the vicinity of the Northern Patagonian Icefield, South America. *Geografiska Annaler Series A* 87, 375-391.
- Hughen, K.A., and 26 others, 2004. Marine04 marine radiocarbon age calibration, 0–26 cal kyr BP. *Radiocarbon* 46, 1059-1086.
- Hüls, M., 2000. Millennial-scale SST variability as inferred from planktonic foraminifera sensus counts in the western subtropical Atlantic. *GEOMAR Report, GEOMAR Research Center for Marine Geosciences, Christian Albrechts University in Kiel* 95, 118 pp.
- Hunke, E.C., Dukowicz, P.R., 1997. An elastic-viscous-plastic model for sea ice dynamics. *Journal of Physical Oceanography* 27, 1849-1867.
- Hut, G., 1987. Consultants group meeting on stable isotope reference samples for geochemical and hydrological investigations. Report to the Director General, International Atomic Energy Agency, Vienna, 42 pp.
- Iriarte, J., 2006. Vegetation and climate change since 14,810 ¹⁴C yr BP in southeastern Uruguay and implications for the rise of early Formative societies. *Quaternary Research* 65, 20-32.
- Jaeschke, A., Rühlemann, C., Arz, H., Heil, G., Lohmann, G., 2007., Coupling of millennial-scale changes in sea surface temperature and precipitation off northeastern Brazil with high-

- latitude climate shifts during the last glacial period. *Paleoceanography* 22, PA4206, doi:10.1029/2006PA001391.
- Jansen, J.H.F., Van der Gaast, S.J., Koster, B., Vaars, A.J., 1998. CORTEX, a shipboard XRF-scanner for element analyses in split sediment cores. *Marine Geology* 151, 143-153.
- Jennerjahn, T.C., Ittekkot, V., Arz, H.W., Behling, H., Pätzold, J., Wefer, G., 2004. Asynchronous terrestrial and marine signals of climate change during Heinrich events. *Science* 306, 2236-2239.
- Johns, W.E., Lee, T.N., Beardsley, R.C., Candela, J., Limeburner, R., Castro, B., 1998. Annual cycle and variability of the North Brazil Current. *Journal of Physical Oceanography* 28, 103-127.
- Jorissen, F.J., de Stitger, H.C., Widmark, J.G.V., 1995. A conceptual model explaining benthic foraminiferal microhabitats. *Marine Micropaleontology* 26, 3-15.
- Kalnay, E., Kanamitsu, M., Kistler, R., Collins, W., Deaven, D., Gandin, L., Iredell, M., Saha, S., White, G., Woolen, J., Zhu, Y., Leetmaa, A., Reynolds, B., Chelliah, M., Ebisuzaki, W., Higgins, W., Janowiak, J., Mo, K.C., Ropelewski, C., Wang, J., Jenne, R., Joseph, D., 1996. The NCEP/NCAR reanalysis project: Bulletin of the American Meteorological Society 77, 437-471.
- Kennett, J.P., 1970. Pleistocene paleoclimates and foraminiferal biostratigraphy in subantarctic deep-sea cores. *Deep-Sea Research* 17, 125-140.
- Kerr, R.A., 2000. A North Atlantic climate pacemaker for the centuries. *Science* 288, 1984-1985.
- King, A.L., Howard, W.R., 2001. Seasonality of foraminiferal flux in sediment traps at Chatham Rise, SW Pacific: implications for paleotemperature estimates. *Deep-Sea Research I* 48, 1687-1708.
- King, A.L., Howard, W.R., 2003. Planktonic foraminiferal flux seasonality in Subantarctic sediment traps: A test for paleoclimate reconstructions. *Paleoceanography* 18, 1019, doi:10.1029/2002PA000839.
- King, A.L., Howard, W.R., 2005. $\delta^{18}\text{O}$ seasonality of planktonic foraminifera from Southern Ocean sediment traps: Latitudinal gradients and implications for paleoclimate reconstructions. *Marine Micropaleontology* 56, 1-24.
- Knight, J.R., Allan, R.J., Folland, C.K., Vellinga, M., Mann, M.E., 2005. A signature of persistent natural thermohaline circulation cycles in observed climate. *Geophysical Research Letters* 32, L20798, doi:10.1029/2005GL024233.
- Knorr, G., Lohmann, G., 2003. Southern Ocean origin for the resumption of Atlantic thermohaline circulation during deglaciation. *Nature* 424, 532-536.
- Kroopnick, P., 1980. The distribution of ^{13}C in the Atlantic Ocean. *Earth and Planetary Science Letters* 49, 469-484.
- Kroopnick, P.M., 1985. The distribution of ^{13}C of ΣCO_2 in the world oceans. *Deep-Sea Research A* 32, 57-84.
- Kuhlmann, H., Meggers, H., Freudenthal, T., Wefer, G., 2004. The transition of the monsoonal and the N Atlantic climate system off NW Africa during the Holocene. *Geophysical Research Letters* 31, L22204, doi:10.1029/2004GL021267.
- Lambeck, K., Chappell, J., 2001. Sea level change through the last glacial cycle. *Science* 292, 679-686.
- Lea, D.W., Pak, D.K., Spero, H.J., 2000. Climate impact of late Quaternary equatorial Pacific sea surface temperature variations. *Science* 289, 1719-1724.
- Lear, C.H., Rosenthal, Y., Slowey, N., 2002. Benthic foraminiferal Mg/Ca-paleothermometry: A revised core-top calibration. *Geochimica et Cosmochimica Acta* 66, 3375-3387.
- LeGrande, A.N., Lynch-Stieglitz, J., Farmer, E.C., 2004. Oxygen isotopic composition of *Globorotalia truncatulinoides* as a proxy for intermediate depth density. *Paleoceanography* 19, PA4025, doi:10.1029/2004PA001045.
- LeGrande, A.N., Schmidt, G. A., 2006. Global gridded data set of the oxygen isotopic composition in seawater. *Geophysical Research Letters* 33, L12604, doi:10.1029/2006GL026011.

- Lenton, T.M., Held, H., Kriegler, E., Hall, J.W., Lucht, W., Rahmstorf, S., Schellnhuber, H.J., 2008. Tipping elements in the Earth's climate system. *Proceedings of the National Academy of Sciences* 105, 1786-1793.
- Levi, C., Labeyrie, L., Bassinot, F., Guichard, F., Cortijo, E., Waelbroeck, C., Caillon, N., Duprat, J., Garidel-Thoron, T., Elderfield, H., 2007. Low-latitude hydrological cycle and rapid climate changes during the last deglaciation. *Geochemistry, Geophysics, Geosystems* 8, Q05N12, doi:10.1029/2006GC001514.
- Libby, W.F., 1955. Radiocarbon dating. University of Chicago Press, Chicago, 205 pp.
- Liu, Z., Philander, S.G.H., 2001. Tropical-extratropical oceanic exchange pathways. In: Siedler, G., Church, J., Gould, J., (Eds.), *Ocean circulation and climate: Observing and modeling the global ocean*. Elsevier, New York, pp. 247- 257.
- Lockwood, J.G., 2001. Abrupt and sudden climatic transitions and fluctuations: A review. *International Journal of Climatology* 21, 1153-1179.
- Lohmann, G.P., 1995. A model for variation in the chemistry of planktonic foraminifera due to secondary calcification and selective dissolution. *Paleoceanography* 10, 445-457.
- Lohmann, G.P., Schweitzer, P.N., 1990. *Globorotalia truncatulinoides*' growth and chemistry as probes of the past thermocline: 1. Shell size. *Paleoceanography* 5, 55-75.
- Lonardi, A.G., Ewing, M., 1971. Sediment transport and distribution in the Argentine Basin. 4. Bathymetry of the continental margin, Argentine Basin and other related provinces, canyons and sources of sediments. In: Ahrens, L.H., Press, F., Runcorn, S.K., Urey, H.C., (Eds.), *Physics and Chemistry of the Earth*. Pergamon, Oxford, v. 8, pp. 79-121.
- Longhurst, A., 1998. *Ecological Geography of the Sea*. Elsevier, New York, 398 pp.
- Loubere, P., 1991. Deep-sea benthic foraminiferal assemblage response to a surface ocean productivity gradient: a test. *Paleoceanography* 6, 193-204.
- Lu, R., Dong, B., Ding, H., 2006. Impact of the Atlantic Multidecadal Oscillation on the Asian summer monsoon. *Geophysical Research Letters* 33, L24701, doi:10.1029/2006GL027655.
- Lutze, G., 1986. *Uvigerina* species of the eastern North Atlantic. *Utrecht Micropaleontological Bulletins* 35, 21-46.
- Lynch-Stieglitz, J., Curry, W.B., Oppo, D.W., Ninneman, U.S., Charles, C.D., Munson, J., 2006. Meridional overturning circulation in the South Atlantic at the last glacial maximum. *Geochemistry, Geophysics, Geosystems* 7, Q10N03, doi:10.1029/2005GC001226.
- Lynch-Stieglitz, J., Curry, W.B., Slowey, N., 1999. Weaker Gulf Stream in the Florida Straits during the Last Glacial Maximum. *Nature* 402, 644-648.
- Mahowald, N.M., Muhs, D.R., Levis, S., Rasch, P.J., Yoshioka, M., Zender, C.S., Luo, C., 2006. Change in atmospheric mineral aerosols in response to climate: Last glacial period, preindustrial, modern, and doubled carbon dioxide climates. *Journal of Geophysical Research* 111, D10202, doi:10.1029/2005JD006653.
- Manabe, S., Stouffer, R.J., 1988. Two stable equilibria of a coupled ocean-atmosphere model. *Journal of Climate* 1, 841-866.
- Manabe, S., Stouffer, R.J., 1997. Coupled ocean-atmosphere model response to fresh-water input: Comparison to Younger Dryas event. *Paleoceanography* 12, 321-336.
- Martinson, D.G., Pisias, N.G., Hays, J.D., Imbrie, J., Moore, T.C., Shackleton, N.J., 1987. Age dating and the orbital theory of the Ice Ages: development of a high-resolution 0 to 300,000-year chronostratigraphy. *Quaternary Research* 27, 1-29.
- Mashiotta, T.A., Lea, D.W., Spero, H.J., 1999. Glacial-interglacial changes in Subantarctic sea surface temperature and $\delta^{18}\text{O}$ -water using foraminiferal Mg. *Earth and Planetary Science Letters* 170, 417-432.
- Maslin, M.A., Durham, E., Burns, S.J., Platzman, E., Grootes, P., Greig, S.E.J., Nadeau, M.-J., Schleicher, M., Plafmann, U., Lomax, B., Rimington, N., 2000. Palaeo-reconstruction of the River Amazon freshwater and sediment discharge using sediments recovered at Site 942 on the Amazon Fan. *Journal of Quaternary Science* 15, 419-434.

- Matano, R.P., Schlax, M.G., Chelton, D.B., 1993. Seasonal variability in the southwestern Atlantic. *Journal of Geophysical Research* 98, 18 027-18 035.
- Matsumoto, K., Lynch-Stieglitz, J., 2003. Persistence of Gulf Stream separation during the Last Glacial Period: Implications for current separation theories. *Journal of Geophysical Research* 108, 3174, doi:10.1029/2001JC000861.
- McManus, J.F., Francois, R., Gherardi, J.-M., Keigwin, L.D., Brown-Leger, S., 2004. Collapse and rapid resumption of Atlantic meridional circulation linked to deglacial climate changes. *Nature* 428, 834-837.
- Meehl, G.A., Stocker, T.F., Collins, W.D., Friedlingstein, P., Gaye, A.T., Gregory, J.M., Kitoh, A., Knutti, R., Murphy, J.M., Noda, A., Raper, S.C.B., Watterson, I.G., Weaver, A.J., Zhao, Z.-C., 2007. Global Climate Projections. In: Solomon, S., Qin, D., Manning, M., Chen, Z., Marquis, M., Averyt, K.B., Tignor M., Miller, H.L., (Eds.), *Climate Change 2007: The Physical Science Basis. Contribution of Working Group I to the Fourth Assessment Report of the Intergovernmental Panel on Climate Change*. Cambridge University Press, Cambridge, pp. 747-845.
- Meissner, K.J., Weaver, A.J., Matthews, H.D., Cox, P.M., 2003. The role of land surface dynamics in glacial inception: a study with the UVic Earth System Model. *Climate Dynamics* 21, 515-527.
- Milani, E.J., Thomaz Filho, A., 2000. Sedimentary basins of South America. In: Cordani, U.G., Milani, E.J., Thomaz Filho, A., Campos, D.A., (Eds.), *Tectonic evolution of South America*. Rio de Janeiro, pp.389-449.
- Mollenhauer, G., McManus, J.F., Benthien, A., Müller, P.J., Eglinton, T.I., 2006. Rapid lateral particle transport in the Argentine Basin: Molecular ^{14}C and $^{230}\text{Th}_{\text{xs}}$ evidence. *Deep-Sea Research I* 53, 1224-1243.
- Mortlock, R.A., Charles, C.D., Froelich, P.N., Zibello, M.A., Salzmann, J., Hayes, J.D., Burckle, L.H., 1991. Evidence for lower productivity in the Antarctic Ocean during the last glaciation. *Nature* 351, 220-223.
- Mortyn, P.G., Charles, C.D., 2003. Planktonic foraminiferal depth habitat and $\delta^{18}\text{O}$ calibrations: Plankton tow results from the Atlantic sector of the Southern Ocean. *Paleoceanography* 18, 1037, doi:10.1029/2001PA000637.
- Mulitza, S., Boltovskoy, D., Donner, B., Meggers, H., Paul, A., Wefer, G., 2003. Temperature: $\delta^{18}\text{O}$ relationships of planktonic foraminifera collected from surface waters. *Palaeogeography, Palaeoclimatology, Palaeoecology* 202, 143-152.
- Mulitza, S., Dürkoop, A., Hale, W., Wefer, G., Niebler, H.-S., 1997. Planktonic foraminifera as recorders of past surface-water stratification. *Geology* 25, 335-338.
- Müller, P., 2004. Carbon and nitrogen data of sediment core GeoB6211-2, #137054, PANGAEA, Department of Geosciences, Bremen University, Bremen.
- NGRIP members, 2004. High-resolution record of Northern Hemisphere climate extending into the last interglacial period. *Nature* 431, 147-151.
- Niebler, H.-S., Hubberten, H.-W., Gersonde, R., 1999. Oxygen Isotope Values of Planktic Foraminifera: A Tool for the Reconstruction of Surface Water Stratification. In: Fischer, G., Wefer, G., (Eds.), *Use of Proxies in Paleoclimatology: Examples from the South Atlantic*. Springer-Verlag, Berlin Heidelberg, pp. 165-189.
- Nürnberg, D., Bijma, B., Hemleben, C., 1996. Assessing the reliability of magnesium in foraminiferal calcite as a proxy for water mass temperatures. *Geochimica et Cosmochimica Acta* 60, 803-814.
- Olson, D.B., Podestá, G.P., Evans, R.H., Brown, O.B., 1988. Temporal variations in the separation of Brazil and Malvinas Currents. *Deep-Sea Research A* 35, 1971-1990.
- Oppo, D.W., Fairbanks, R.G., 1987. Variability in the deep and intermediate water circulation of the Atlantic Ocean during the past 25,000 years: Northern Hemisphere modulation of the Southern Ocean. *Earth and Planetary Science Letters* 86, 1-15.

- Oppo, D.W., Fairbanks, R.G., 1989. Carbon isotope composition of tropical surface water during the past 22,000 years. *Paleoceanography* 4, 333-351.
- Pacanowski, R.C., 1996. MOM 2. Documentation, user's guide and reference manual. GFDL Ocean Group Technical Report 3.2, 328 pp.
- Pätzold, J., Cruise Participants, 1996. Report and preliminary results of RV Victor Hensen Cruise JOPS II, Leg 6, Fortaleza–Recife, 13.03.–26.03.1995 and Leg 8, Vitória-Vitória, 10.04.–23.04.1995. Berichte, Fachbereich Geowissenschaften, Universität Bremen, Bremen 76, 87 pp.
- Paul, A., Schäfer-Neth, C., 2003. Modeling the water masses of the Atlantic Ocean at the Last Glacial Maximum. *Paleoceanography* 18, PA1058, doi:10.1029/2002PA000783.
- Paul, A., Schäfer-Neth, C., 2004. The Atlantic Ocean at the Last Glacial Maximum: 2. Reconstructing the current systems with a global ocean model. In: Wefer, G., Mulitza, S., Ratmeyer, V., (Eds.), *The South Atlantic in the Late Quaternary: Reconstruction of material budgets and current systems*. Springer-Verlag, Berlin, pp. 549-583.
- Peeters, F.J.C., Acheson, R., Brummer, G.-J.A., de Ruijter, W.P.M., Schneider, R.R., Ganssen, G.M., Ufkes, E., Kroon, D., 2004. Vigorous exchange between the Indian and Atlantic oceans at the end of the past five glacial periods. *Nature* 430, 661-665.
- Peeters, F.J.C., Brummer, G.J.A., Ganssen, G., 2002. The effect of upwelling on the distribution and stable isotope composition of *Globigerina bulloides* and *Globigerinoides ruber* (planktic foraminifera) in modern surface waters of the NW Arabian Sea. *Global and Planetary Change* 34, 269-291.
- Peltier, W.R., Fairbanks, R.G., 2006. Global glacial ice volume and Last Glacial Maximum duration from an extended Barbados sea level record. *Quaternary Science Reviews* 25, 3322-3337.
- Peterson, L.C., Haug, G.H., Hughen, K.A., Röhl, U., 2000. Rapid changes in the hydrologic cycle of the tropical Atlantic during the last glacial. *Science* 290, 1947-1951.
- Peterson, R.G., Johnson, C.S., Krauss, W., Davis, R.E., 1996. Lagrangian Measurements in the Malvinas Current. In: Wefer, G., Berger, W., Siedler, G., Webb, D.J., (Eds.), *The South Atlantic: Present and Past Circulation*. Springer-Verlag, Berlin Heidelberg, pp. 239-247.
- Peterson, R.G., Stramma, L., 1991. Upper-level circulation in the South Atlantic Ocean. *Progress in Oceanography* 26, 1-73.
- Pether, J., 1994. Molluscan evidence for enhanced deglacial advection of Agulhas water in the Benguela current, off southwestern Africa. *Palaeogeography, Palaeoclimatology, Palaeoecology* 111, 99-117.
- Piola, A.R., Gordon, A.L., 1989. Intermediate waters in the southwest South Atlantic. *Deep Sea Research I* 36, 1-16.
- Piola, A.R., Matano, R.P., Palma, E.D., Möller Jr., O.O., Campos, E.J.D., 2005. The influence of the PlataRiver discharge on the western South Atlantic shelf. *Geophysical Research Letters* 32, L01603, doi:10.1029/2004GL021638.
- Poole, R., Tomczak, M., 1999. Optimum multiparameter analysis of the water mass structure in the Atlantic Ocean thermocline. *Deep-Sea Research I* 46, 1895-1921.
- Provost, C., Garcia, O., Garçon, V., 1992. Analysis of satellite sea surface temperature time series in the Brazil-Malvinas Current confluence region: Dominance of the annual and semiannual periods. *Journal of Geophysical Research* 97, 17 841-17 858.
- Rahmstorf, S., 2002. Ocean circulation and climate during the past 120,000 years. *Nature* 419, 207-214.
- Randall, D.A., Wood, R.A., Bony, S., Colman, R., Fichefet, T., Fyfe, J., Kattsov, V., Pitman, A., Shukla, J., Srinivasan, J., Stouffer, R.J., Sumi, A., Taylor, K.E., 2007. Climate Models and Their Evaluation. In: Solomon, S., Qin, D., Manning, M., Chen, Z., Marquis, M., Averyt, K.B., Tignor, M., Miller, H.L., (Eds.), *Climate Change 2007: The Physical Science Basis. Contribution of Working Group I to the Fourth Assessment Report of the Intergovernmental Panel on Climate Change*. Cambridge University Press, Cambridge, pp. 589-662.

- Rao, V.B., Cavalcanti, I.F.A., Hada, K., 1996. Annual variation of rainfall over Brazil and water vapor characteristics over South America. *Journal of Geophysical Research* 101, 26,539-26,551.
- Rasmussen, S.O., Andersen, K.K., Svensson, A.M., Steffensen, J.P., Vinther, B.M., Clausen, H.B., Siggaard-Andersen, M.-L., Johnsen, S.J., Larsen, L.B., Dahl-Jensen, D., Bigler, M., Röthlisberger, R., Fischer, H., Goto-Azuma, K., Hansson, M.E., Ruth, U., 2006. A new Greenland ice core chronology for the last glacial termination. *Journal of Geophysical Research* 111, D06102, doi:10.1029/2005JD006079.
- Ravelo, A.C., Fairbanks, R.G., 1995. Carbon isotopic fractionation in multiple species of planktonic foraminifera from core-tops in the tropical Atlantic. *Journal of Foraminiferal Research* 25, 53-74.
- Reimer, P.J., and 28 others, 2004. IntCal04 terrestrial radiocarbon age calibration, 0-26 cal kyr bp. *Radiocarbon* 46, 1029-1058.
- Reimer, P.J., Reimer, R.W., 2001. A marine reservoir correction database and on-line interface. *Radiocarbon* 43, 461-463.
- Renssen, H., Isarin, R.F.B., 2001. The two major warming phases of the last deglaciation at ~14.7 and ~11.5 ka cal BP in Europe: climate reconstructions and AGCM experiments. *Global and Planetary Change* 30, 117-153.
- Rial, J.A., Pielke Jr., R.A., Beniston, M., Claussen, M., Canadel, J., Cox, P., Held, H., De Noblet-Ducoudre, N., Prinn, R., Reynolds, J.F., Salas, J.D., 2004. Nonlinearities, feedbacks and critical thresholds within the Earth's climate system. *Climatic Change* 65, 11-38.
- Robertson, A.W., Farrara, J.D., Mechoso, C.R., 2003. Simulations of the atmospheric response to South Atlantic sea surface temperatures anomalies. *Journal of Climate* 16, 2540-2551.
- Robertson, A.W., Mechoso, C.R., 2000. Interannual and interdecadal variability in the South Atlantic convergence zone. *Monthly Weather Review* 128, 2947-2957.
- Röhl, U., Abrams, L.J., 2000. High resolution, downhole, and non-destructive core measurements from sites 999 and 1001 in the Caribbean Sea: application to the Late Paleocene Thermal Maximum. *Proceedings of the Integrated Ocean Drilling Program Scientific Results* 165, 191-204.
- Rühlemann, C., Dickmann, B., Mulitza, S., Frank, M., 2001. Late Quaternary changes of western equatorial Atlantic surface circulation and Amazon lowland climate recorded in Ceara Rise deep-sea sediments. *Paleoceanography* 16, 293-305.
- Rühlemann, C., Mulitza, S., Lohmann, G., Paul, A., Prange, M., Wefer, G., 2004. Intermediate depth warming in the tropical Atlantic related to weakened thermohaline circulation: Combining paleoclimatic data and modelling results for the last deglaciation. *Paleoceanography* 19, PA1025, doi:10.1029/2003PA000948.
- Rühlemann, C., Mulitza, S., Müller, P.J., Wefer, G., Zahn, R., 1999. Warming of the tropical Atlantic Ocean and slowdown of thermohaline circulation during the last deglaciation. *Nature* 402, 511-514.
- Rushdi, A.I., Chen-Tung, A.C., Suess, E. 1998. The solubility of calcite in seawater solution of different magnesium concentrations at 25°C and 1 atm total pressure: A laboratory reexamination. *La Mer* 36, 9-22.
- Saraceno, M., Provost, C., Piola, A.R., 2005. On the relationship between satellite-retrieved surface temperature fronts and chlorophyll *a* in the western South Atlantic. *Journal of Geophysical Research* 110, C11016, doi:10.1029/2004JC002736.
- Sarnthein, M., Stategger, K., Dreger, D., Erlenkeuser, H., Grootes, P., Haupt, B., Jung, S., Kiefer, T., Kuhnt, W., Pflaumann, U., Schäfer-Neth, V., Schulz, H., Schulz, M., Seidov, D., Simstich, J., van Kreveld, S., Vogelsang, E., Völker, A., Weinelt, M., 2001. Fundamental modes and abrupt changes in North Atlantic circulation and climate over the last 60 ky - Concepts, reconstruction and numerical modeling. In: Schäfer, P., Ritzrau, W., Schlüter, M., Thiede, J., (Eds.) *The Northern North Atlantic: A Changing Environment*. Pergamon, Berlin, pp. 365-410.

- Schenk, C.J., Viger, R.J., Anderson, C.P., 1997. Maps showing geology, oil and gas fields, and geologic provinces of the South America region. Open file report 97-470D, U.S. Geological Survey, Denver, 12 pp.
- Schmidt, G.A., 1999. Error analysis of paleosalinity calculations. *Paleoceanography* 14, 422-429.
- Schmidt, M.W., Spero, H.J., Lea, D.W., 2004. Links between salinity variation in the Caribbean and North Atlantic thermohaline circulation. *Nature* 428, 160-163.
- Schobbenhaus, C., Campos, D.A.C., Derze, G.R., Asmus, H.E., 1981. Geologic map of Brazil and adjoining ocean floor including mineral deposits. Scale 1:2,500,000. Departamento Nacional da Produção Mineral, Brasília.
- Schott, F., Stramma, L., Fischer, J., 1995. The warm water inflow into the western tropical Atlantic boundary regime, spring 1994. *Journal of Geophysical Research* 100, 24 745-24 760.
- Schrag, D.P., Adkins, J.F., McIntyre, K., Alexander, J.L., Hodell, D.A., Charles, C.D., McManus, J.F., 2002. The oxygen isotopic composition of seawater during the Last Glacial Maximum. *Quaternary Science Reviews* 21, 331-342.
- Schulz, H.D., Cruise Participants, 2001. Report and preliminary results of Meteor Cruise M46/2, Recife–Montevideo, 02.12.–29.12.1999. Berichte, Fachbereich Geowissenschaften, Universität Bremen, Bremen 174, 107 pp.
- Schulz, M., Mudelsee, K., 2002. REDFIT: estimating red-noise spectra directly from unevenly spaced paleoclimatic time series. *Computers & Geosciences* 28, 421-426.
- Segl, M., Cruise Participants, 1994. Report and preliminary results of Meteor Cruise M29/1, Buenos Aires–Montevideo, 17.06.–13.07.1994. Berichte, Fachbereich Geowissenschaften, Universität Bremen, Bremen 58, 94 pp.
- Semtner, A.J., 1976. A model for the thermodynamic growth of sea ice in numerical investigations of climate. *Journal of Physical Oceanography* 6, 379-389.
- Severinghaus, J.P., Brook, E.J., 1999. Abrupt climate change at the end of the last glacial period inferred from trapped air in polar ice. *Science* 286, 930-934.
- Shackleton, N.J., 1974. Attainment of isotopic equilibrium between ocean water and the benthonic foraminifera genus *Uvigerina*: Isotopic changes in the ocean during the last glacial. *Colloques Internationaux C.N.R.S.* 219, 203-209.
- Shackleton, N.J., 1977. ^{13}C in *Uvigerina*: Tropical rainforest history and the equatorial Pacific carbonate dissolution cycles. In: Anderson, N., Malahof, A., (Eds.), *Fate of fossil fuel CO₂ in the oceans*. Plenum, New York, pp. 401-427.
- Shackleton, N.J., Opdyke, N.D., 1973. Oxygen isotope and paleomagnetic stratigraphy of equatorial Pacific core V28-238: Oxygen isotope temperatures and ice volumes on a 10⁵ year scale. *Quaternary Research* 3, 39-55.
- Shemesh, A., Hodell, D., Crosta, X., Kanfoush, S., Charles, C., Guilderson, T., 2002. Sequence of events during the last deglaciation in Southern Ocean sediments and Antarctic ice cores. *Paleoceanography* 17, PA1056, doi:10.1029/2000PA000599.
- Shin, S.-I., Liu, Z., Otto-Bliesner, B.L., Kutzbach, J.E., Vavrus, S.J., 2003. Southern Ocean sea-ice control of the glacial North Atlantic thermohaline circulation. *Geophysical Research Letters* 30, 1096, doi:10.1029/2002GL015513.
- Shukla, J., DelSole, T., Fennessy, M., Kinter, J., Paolino, D., 2006. Climate model fidelity and projections of climate change. *Geophysical Research Letters* 33, L07702, doi:10.1029/2005GL025579.
- Siddall, M., Rohling, E.J., Almogi-Labin, A., Hemleben, C., Meischner, D., Schmelzer, I., Smeed, D.A., 2003. Sea-level fluctuations during the last glacial cycle. *Nature* 423, 853-858
- Silveira, I.C.A., Miranda, L.B., Brown, W.S., 1994. On the origins of the North Brazil Current. *Journal of Geophysical Research* 99, 22501-22512.
- Soubiès, F., Seidel, A., Mangin, A., Genty, D., Ronchail, J., Plagnes, V., Hirooka, S., Santos, R., 2005. A fifty-year climatic signal in three Holocene stalagmite records from Mato Grosso, Brazil. *Quaternary International* 135, 115-129.
- Spero, H.J., Bijma, J., Lea, D.W., Bemis, B.E., 1997. Effect of seawater carbonate concentration on foraminiferal carbon and oxygen isotopes. *Nature* 390, 497-500.

- Spero, H.J., Lea, D.W., 1993. Intraspecific stable isotope variability in the planktic foraminifera *Globigerinoides sacculifer*: Results from laboratory experiments. *Marine Micropaleontology* 22, 221-234.
- Spero, H.J., Lea, D.W., 1996. Experimental determination of stable isotope variability in *Globigerina bulloides*: implications for paleoceanographic reconstructions. *Marine Micropaleontology* 28, 231-246.
- Stramma, L., England, M., 1999. On the water masses and mean circulation of the South Atlantic Ocean. *Journal of Geophysical Research* 104, 20 863-20 883.
- Stuiver, M., Östlund, H.G., 1980. GEOSECS Atlantic radiocarbon. *Radiocarbon* 22, 1-24.
- Stuiver, M., Polach, H.A., 1977. Discussion reporting of ^{14}C data. *Radiocarbon* 19, 355-363.
- Stuiver, M., Reimer, P.J., 1993. Extended ^{14}C database and revised CALIB 3.0 ^{14}C age calibration program. *Radiocarbon* 35, 215-230.
- Sutton, R.T., Hodson, D.L.R., 2005. Atlantic Ocean forcing of North American and European summer climate. *Science* 309, 115-118.
- Tjallingii, R., Röhl, U., Kölling, M., Bickert, T., 2007. Influence of the water content on X-ray fluorescence core-scanning measurements in soft marine sediments. *Geochemistry, Geophysics, Geosystems* 8, Q02004, doi:10.1029/2006GC001393.
- Tomczak, M., Godfrey, J.S., 1994. *Regional Oceanography: An Introduction*. Pergamon, Oxford.
- Torrence, C., Compo, G.P., 1998. A practical guide to wavelet analysis. *Bulletin of the American Meteorological Society* 79, 61-78.
- Tsuchiya, M., Talley, L.D., McCartney, M.S., 1994. Water-mass distributions in the western South Atlantic; A section from South Georgia Island (54°S) northward across the equator. *Journal of Marine Research* 52, 55-81.
- Turner, K.J., Fogwell, C.J., McCulloch, R.D., Sugden, D.E., 2005. Deglaciation of the eastern flank of the NPI and associated continental-scale lake diversions. *Geografiska Annaler Series A* 87, 363-374.
- Urey, H.C., 1947. The thermodynamic properties of isotopic substances. *Journal of the Chemical Society* 562-581.
- Venegas, S.A., Mysak, L.A., Straub, D.N., 1997. Atmosphere-ocean coupled variability in the South Atlantic. *Journal of Climate* 10, 2904-2920.
- Vera, C.S., Vighiarolo, P.K., Berbery, E.H., 2002. Cold season synoptic-scale waves over subtropical South America. *Monthly Weather Review* 130, 684-699.
- Vidal, L., Labeyrie, L., Cortijo, E., Arnold, M., Duplessy, J.C., Michel, E., Becque, S., van Weering, T.C.E., 1997. Evidence for changes in the North Atlantic Deep Water linked to meltwater surges during the Heinrich events. *Earth and Planetary Science Letters* 146, 13-27.
- Waelbroeck, C., Labeyrie, L., Michel, E., Duplessy, J.C., McManus, J.F., Lambeck, K., Balbon, E., Labracherie, M., 2002. Sea-level and deep water temperature changes derived from benthic foraminifera isotopic records. *Quaternary Science Reviews* 21, 295-305.
- Wainer, I., Gent, P., Goni, G., 2000. Annual cycle of the Brazil-Malvinas confluence region in the National Center for Atmospheric Research Climate System Model. *Journal of Geophysical Research* 105, 26 167-26 177.
- Wang, X., Auler, A.S., Edwards, R.L., Cheng, H., Cristalli, P.S., Smart, P.L., Richards, D.A., Shen, C.-C., 2004. Wet periods in northeastern Brazil over the past 210 kyr linked to distant climate anomalies. *Nature* 432, 740-743.
- Wang, X., Auler, A.S., Edwards, R.L., Cheng, H., Ito, E., Wang, Y., Kong, X., Solheid, M., 2007. Millennial-scale precipitation changes in southern Brazil over the past 90,000 years. *Geophysical Research Letters* 34, L23701, doi:10.1029/2007GL031149.
- Weaver, A.J., Eby, M., Kienast, M., Saenko, O.A., 2007a. Response of the Atlantic meridional overturning circulation to increasing atmospheric CO_2 : Sensitivity to mean climate state. *Geophysical Research Letters* 34, L05708, doi:10.1029/2006GL028756.
- Weaver, A.J., Eby, M., Wiebe, E.C., Bitz, C.M., Duffy, P.B., Ewen, T.L., Fanning, A.F., Holland, M.M., MacFadyen, A., Matthews, H.D., Meissner, K.J., Saenko, O., Schmittner, A.,

- Wang, H., Yoshimori, M., 2001. The UVic Earth System Climate Model: Model description, climatology, and applications to past, present and future climates. *Atmosphere-Ocean* 39, 361-428.
- Weaver, A.J., Saenko, O.A., Clark, P.U., Mitrovica, J.X., 2003. Meltwater pulse 1A from Antarctica as a trigger of the Bølling-Allerød warm interval. *Science* 299, 1709-1713.
- Weaver, A.J., Zickfeld, K., Montenegro, A., Eby, M., 2007b. Long term climate implications of 2050 emission reduction targets. *Geophysical Research Letters* 34, L19703, doi:10.1029/2007GL031018.
- Weber, S.L., Drijfhout, S.S., 2007. Stability of the Atlantic Meridional Overturning Circulation in the Last Glacial Maximum climate. *Geophysical Research Letters* 34, L22706, doi:10.1029/2007GL031437.
- Wefer, G., Cruise Participants, 2001. Report and preliminary results of Meteor Cruise M46/4, Mar del Plata (Argentina)-Salvador (Brazil), 10.02.-13.03.2000. With partial results of Meteor cruise M46/2, Recife-Montevideo, 2.-29.12.1999. *Berichte, Fachbereich Geowissenschaften, Universität Bremen, Bremen* 173, 136 pp.
- Weijer, W., de Ruijter, W.P.M., Sterl, A., Drijfhout, S.S., 2002. Response of the Atlantic overturning circulation to South Atlantic sources of buoyancy. *Global and Planetary Change* 34, 293- 311.
- Weldeab, S., Schneider, R.R., Kölling, M., 2006. Deglacial sea surface temperature and salinity increase in the western tropical Atlantic in synchrony with high latitude climate instabilities. *Earth and Planetary Science Letters* 241, 699-706.
- Westerhold, T., Bickert, T., Röhl, U., 2005. Middle to late Miocene oxygen isotope stratigraphy of ODP site 1085 (SE Atlantic): new constraints on Miocene climate variability and sea-level fluctuations. *Palaeogeography, Palaeoclimatology, Palaeoecology* 217, 205-222
- White, W.B., Peterson, R.G., 1996. An Antarctic circumpolar wave in surface pressure, wind, temperature and sea-ice extent. *Nature* 380, 699-702.
- Wilke, I., Bickert, T., Peeters, F.J.C., 2006. The influence of seawater carbonate ion concentration [CO_3^{2-}] on the stable carbon isotope composition of the planktic foraminifera species *Globorotalia inflata*. *Marine Micropaleontology* 58, 243-258.
- Williams, D.F., Healy-Williams, N., 1980. Oxygen isotopic-hydrographic relationships among recent planktonic foraminifera from the Indian Ocean. *Nature* 283, 848-852.
- Wohlfarth, B., 1996. The chronology of the Last Termination: A review of radiocarbon-dated, high-resolution terrestrial stratigraphies. *Quaternary Science Reviews* 15, 267-284.
- Wu, G., Berger, W.H., 1989. Planktonic foraminifera: Differential dissolution and the Quaternary stable isotope record in the West Equatorial Pacific. *Paleoceanography* 4, 181-198.
- Xie, P., Arkin, P.A., 1997. Global precipitation: A 17-year monthly analysis based on gauge observations, satellite estimates, and numerical model outputs. *Bulletin of the American Meteorological Society* 78, 2539-2558.
- Yokoyama, Y., Lambeck, K., De Deckker, P., Johnston, P., Fifield L.K., 2000. Timing of the Last Glacial Maximum from observed sea-level minima. *Nature* 406, 713-716.
- You, Y., Lutjeharms, J.R.E., Boebel, O., de Ruijter, W.P.M., 2003. Quantification of the interocean exchange of intermediate water masses around southern Africa. *Deep-Sea Research II* 50, 197-228.
- Zaric, S., Donner, B., Fischer, G., Mulitza, S., Wefer, G., 2005. Sensitivity of planktic foraminifera to sea surface temperature and export production as derived from sediment trap data. *Marine Micropaleontology* 55, 75-105.
- Zhang, R., Delworth, T.L., 2005. Simulated tropical response to a substantial weakening of the Atlantic thermohaline circulation. *Journal of Climate* 18, 1853-1860.
- Zhou, J., Lau, K.-M., 1998. Does a monsoon climate exist over South America? *Journal of Climate* 11, 1020-1040.